A STUDY OF ORBIT DEVELOPMENT AND ITS RELATIONSHIP TO EYE SIZE IN MYOPIA USING MAGNETIC RESONANCE IMAGING

CHAU CHEUK MAN, ANSON

M.PHIL.

THE HONG KONG POLYTECHNIC UNIVERSITY

2003

Certificate of Originality

I hereby declare that this thesis is my own work and that, to the best of my knowledge and belief, it reproduces no material previously published or written nor material which has been accepted for the award of any other degree or diploma, except where due acknowledgement has been made in the text.

_____ (Signed)

CHAU CHEUK MAN (Name of student)

Abstract

This study covers three aspects: the first is a calibration study performed on phantoms simulating the orbit and eyeball to evaluate the accuracy of volumetric determination using MRI DICOM (Digital Imaging and Communication in Medicine) images; the second is a study on the orbit development in Hong Kong Chinese and the third is a study to demonstrate the relationship between eye size and the volume of the orbit in adult subjects with varying degrees of myopia.

Calibration was conducted using ten tailor-made spherical silicon balls ranging from 5 to 14 cm^3 and 10 silicon moulds of orbits from 10 human dry skulls. These were used to simulate the eyes and orbits respectively. The phantoms were subjected to MRI scanning. A T2-weighted sequence was used. The volume of each phantom was computed and compared with the known physical volumes. The computed and physical volumes were highly correlated for both eyeball and the orbit phantoms. Coefficient of variations of the computed and physical volumes were low. Consequently, it is possible to apply a calibration value to the computed volume to estimate the physical volume with a high level of confidence.

The study on orbit development involved a cross-sectional MRI study of 81 Hong Kong Chinese subjects aged from 1 to 42 years. A linear growth rate was

found in the first 15 years of life. The orbit grew from around 11.56 cm^3 to 25.50 cm^3 in 42 years. The orbit reached maturity at around the age of 16 years.

To study the relationship between eye size and the volume of the orbit 33 adult subjects with varying degrees of ametropia (+1.00D to -12.75D) underwent MRI of the orbit. Results show that the larger myopic eye was not associated with a larger orbit.

Publication arising from the thesis

"Is eye size related to orbit size in human subjects?" (in press)

Anson Chau, Karl Fung, Karen Pak, Maurice Yap

Ophthalmic Physiol Opt

Acknowledgement

I am indebted to my supervisors who went through this study with me over the past two years. I thank Prof. Maurice Yap for his wisdom which helped me to see things from different perspectives and for his patience. I wish to thank my co-supervisor, Dr. Karl Fung, for his enormous support in the data collection, for his special kindness and precious time. Their guidance has made such a difference in my life and I shall always be grateful for them.

I would like to express my sincere gratitude to Mr. Lawrance Yip, Senior Radiographer at QMH, Dr. Karen Pak, Mr. K.K. Chan, and the MRI team at QEH for their help in data collection. Without them, this study could not be realized.

I want to thank, from the bottom of my heart, all the staff in OR. They have given me comfort and understanding and have enriched my life. My fellow research students have given me warm friendship which I shall always treasure.

Last but not least, I would like to dedicate this thesis to my parents. Their discipline, respect and endless love for me drove me to fly high.

Content

Chapter 2 Instrumentation

Chapter 3 Calibration

List of figures and tables

Chapter 1

Chapter 2

Chapter 3

Chapter 4

Chapter 5

Appendix 6

Chapter 1 Literature Review

1.1 Prevalence of myopia in Hong Kong

There have been many cross-sectional or longitudinal studies reporting the prevalence of myopia and the development of refractive error among Chinese people in Hong Kong. These investigations covered a range of ages from childhood to adulthood.

Early infancy

Using retinoscopy, Edwards (1991) refracted 158 full-term infants and found a refractive error spread similar to those reported in Caucasian infants. However, in a subset of children refracted at three subsequent occasions at 10 weekly intervals, a sharp decrease in hyperopia was found which was not noted in Caucasian studies. In a follow up study, Edwards and Shing (1999) examined thirty-two children with mean age of 11 weeks and found that their mean spherical equivalent refraction (SER) was +2.81D. Hyperopic power decreased rapidly to about +0.80D at 36 weeks. Subjects were refracted again at the age of 94 weeks, and the mean SER changed to –0.31D.

Aged 3 to 5.5 years

Ninety-five percent of 570 Hong Kong children aged 3 to 5.5 years were found to have refractive errors with mean SER of +0.45D (Chan and Edwards, 1994).

Aged 6 to 17 years

The prevalence of myopia increased from 30% at the age of 6 to 7 years to 70% at the age of 16 to 17 years among 383 school children. The SER was –0.90D at the age of 6 years, -1.77D at the age of 10 years and –2.00D at the age of 16 to 17 years (Lam and Goh, 1991). In both cross-sectional and longitudinal studies of this age group, the mean SER was shown to become more myopic with increasing age. There were also negative correlations between change in SER and change in vitreous chamber depth, and between change in SER and change in axial length. The incidence rate was 11.8%, and the rate of myopia progression was greatest between ages of 6 and 10 years (Lam et al., 1999).

In 1993, Goh and Lam (1993) conducted another survey on 1247 children aged from 6 to 17 years. Twenty percent of the children at the age of 6 years were myopic, and this percentage increased with increasing age, and reached 74% for those subjects who aged 17 years. More girls were found to be myopic than boys before the age of 12 years. This situation was reversed after 13 years old. It was

suggested that these results correlated with the age of puberty, as girls reach puberty earlier than boys.

Another longitudinal study carried out by Edwards (1999) from 1991 to 1996 showed that the mean SER became more negative with increasing age. Among 123 subjects who were aged 7 years, the mean SER was found to be +0.32D becoming –1.09D at the age of 12 years. At the age of 7 years, the prevalence of myopia was 11%, and by the age of 12 years, this increased to 55%. In the study, the researcher also suggested that myopia first appeared at about the age of 6 years.

Goldschmidt et al. (2001) followed a group of 128 six year old school children over a two and one-half year period and found that. the prevalence of myopia increased throughout the study from less than 8% to 30% by the end of the study. In addition, the mean SER shifted from hyperopia to myopia, from +0.5D to –0.5D.

Aged 19 to 22 years

Lam and Yap (1990) reported that 69% of the 109 university students recruited were myopic, with mean SER around –3.00D. In a larger scale study, among 2000 university students, 87.5% were myopic, with 22.3% of them having myopia of –6.00D or more (Ho et al., 1995). Another study performed in 1996 on 1534 university students aged 17 to 23 years found that, the prevalence of myopia

was up to 91.7%. The mean refraction among the students was –4.00D (Lo et al., 1996).

Aged 19 to 39 years

In a study consisting of 105 subjects aged between 19 and 39 years, 71.5% of them were myopic, 27% were emmetropic and only 1.5% were hyperopic. They had a mean SER of about –3.00D (Goh and Lam, 1994).

Aged over 40 years

A study of 120 subjects aged over 40 years showed that only 29% of them were myopic (Lam et al., 1994). The majority of this group was emmetropic. Breaking them into smaller groups, revealed a trend of refractive status change related to age. At ages 40 to 44 years, half of them were myopic, and the remaining half were emmetropic. When age increased, the percentage of myopia decreased gradually, and the percentage of emmetropia also diminished markedly at the age of 55, whereas hyperopia rose gradually to 65% in the over 65 age group. The researchers also claimed that Hong Kong Chinese had a tendency towards an increase in hyperopia from the age of 40. Myopia peaked at between 21 and 40 years old.

Summary

From the above review, we find that the SER distribution is bell shaped at birth with a large variance. The degree of variance decreases with age and approaches the adult value at close to one year of age. Refractive errors tend to be more myopic during school age. Hong Kong Chinese reach their most myopic state in the age range of young adult to pre-presbyopic. At about 40 years of age, there is an overall tendency to shift towards hyperopia. Figure 1.1 shows the summary of the prevalence of myopia in Hong Kong at different ages.

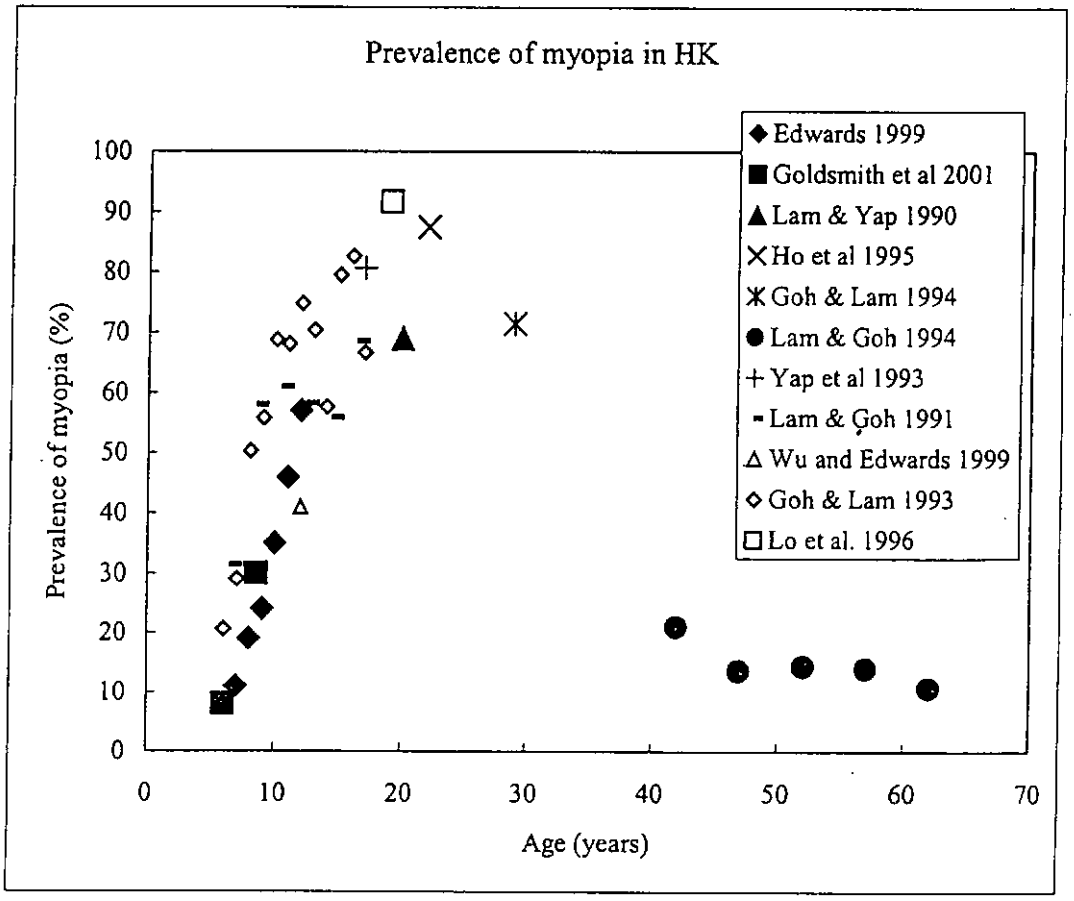

Fig. 1.1 Summary of the prevalence of myopia in the HK population

1.2 Age of onset of myopia

There are different systems for myopia classification; one is based on the age of onset. Commonly used terms include youth-onset or early-onset myopia (EOM), and adult-onset or late-onset myopia (LOM). Different researchers define EOM and LOM differently. Many researchers have suggested that EOM is myopia which occurs from about 6 years of age to the mid-teenage years (e.g. 13 years of age), while LOM begins at age 15 years or later (Bullimore et al., 1992, Gossman et al., 1999, Jiang and Woessner, 1996, McBrien and Millodot, 1987, Osborne et al., 1974, Wilson et al., 1997, Woung et al., 1993). They used 15 years of age to distinguish between EOM and LOM because they thought that childhood myopia progression generally ceases between 15 and 17 years of age, which is the same time as the cessation of general body growth. This is supported by many studies carried out on biometric measurement (e.g. corneal curvature, anterior chamber depth and lens thickness). All of these studies show that ocular growth is completed at the age of 13 to 15 years (Larsen, 1971, Larsen, 1971, Sorsby et al., 1961, Sorsby and Leary, 1969).

Grosvenor (1987) and Grosvenor and Scott (1991) defined EOM as myopia which occurs during the period between age 6 years to 16 years. However, they further divided LOM into early and late categories. Early adult-onset myopia takes place during the period from the age of 20 years to about the age of 40 years. Late adult-onset myopia occurs after 40 years of age.

From the above description, we found that there is an age gap (16-20) between EOM and LOM. The terms 'juvenile-onset' and 'adolescent-onset' have also been used to describe myopia that starts before the age of about 18 years.

Although ocular growth and the co-ordinated growth are sometimes thought to be completed at the age of 15 years, studies of LOM have shown that an increase in axial length of the eyeball is responsible for LOM. This means the eye still has the ability to grow after so called "maturity" (15 to 18 years of age) (Adams, 1987, Fledelius, 1995, McBrien and Adams, 1997, McBrien and Millodot, 1987).

In the case of LOM, the prevalence does not increase as rapidly, nor does the average refractive error change as markedly as in EOM (Jiang and Woessner, 1996). The degree of myopia is significantly higher in EOM than LOM. However, both EOM and LOM can progress to a high myopia degree (-8D or above) (Bullimore et al., 1992, Fledelius, 1995). Figure 1.2 shows a summary chart of the classification of the onset of myopia.

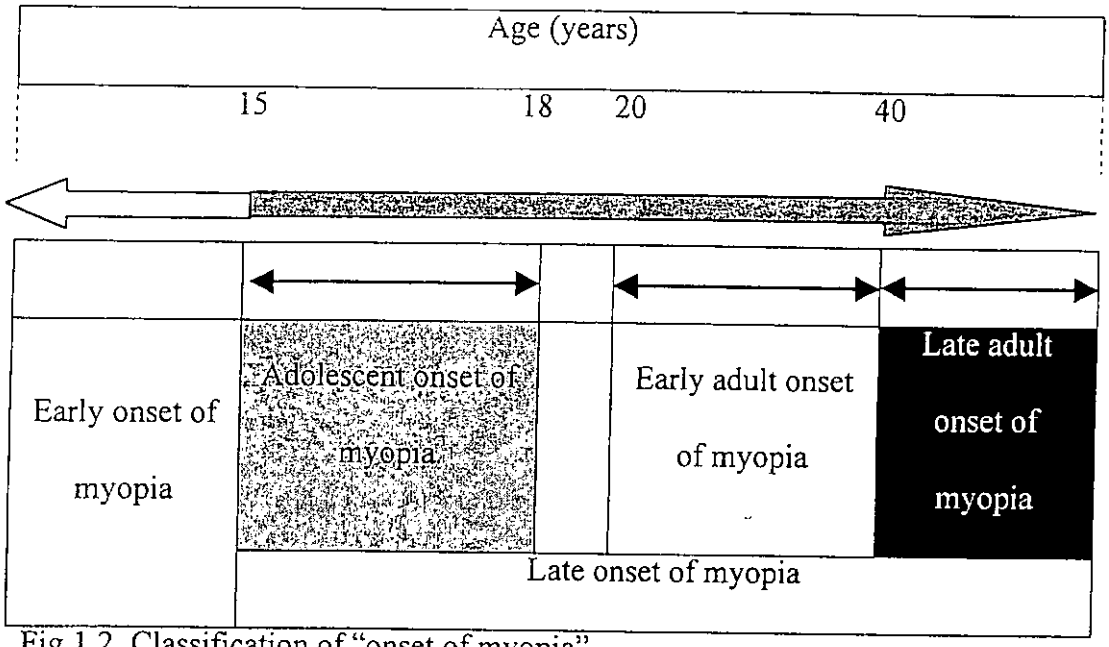

Fig 1.2. Classification of "onset of myopia"

Age of onset of myopia in Hong Kong

The age of onset of myopia in Hong Kong usually occurs in childhood. Some of the longitudinal studies showed that the age of onset of myopia ranged from 6 to 16 years (Lam et al., 1999). In a study done by Edwards (1999), the age of onset among Hong Kong children was reported to be at about the age of 6 years.

Ocular structural differences induced by EOM and LOM

It is generally understood that EOM and LOM progression are caused by axial elongation (Grosvenor and Scott, 1991, Jiang and Woessner, 1996, McBrien and Adams, 1997). However, axial length has been found to be significantly greater in EOM than in LOM (Grosvenor and Scott, 1991, McBrien and Adams,

1997). Corneal steepening may be a feature found in the early development of myopia, but insignificant in the whole development (Jiang and Woessner, 1996, McBrien and Adams, 1997). McBrien and Adams (1997) observed a thinning of the crystalline lens in LOM. They suggested that this might be caused by stretching of the lens due to axial and equatorial growth in the myopic eye.

1.3 Factors affecting ocular parameters

1.3.1 Gender differences

Gender shows significant effect on ocular components data such as corneal power in both vertical and horizontal meridians, anterior chamber depth, both Gullstrand lens power and calculated lens power, vitreous chamber depth and axial length of eyeball. Gender differences have been observed for parameters such as the corneal radii, vitreous depth and axial length. Males have flatter corneal radii and thinner lenses but longer axial lengths due to a longer anterior segment distance and vitreous depth. Females usually have smaller ocular dimensions than men, but stronger Gullstrand lens powers and calculated lens powers (Curtin, 1985, Goh and Lam, 1994, Grosvenor and Goss, 1999, Lam et al., 1994, Lam and Goh, 1991, Wong et al., 2001). In general, there is a conspicuous gender difference in ocular volume between males and females. Males had 0.5 cm^3 larger ocular volume than females during the entire growth period (Hahn and Chu, 1984).

Apart from the ocular components mentioned above, orbital volume is also gender dependent. Schuknecht et al. (1996) and Bite et al. (1985) found that orbital cavity volumes in males were larger than those in females. On the other hand, Forbes et al. (1985) found that females appeared to have larger orbits than males.

1.3.2 Body habitus

Ocular components also show differences in different body habitus. Wong et al. (2001) found that taller persons tended to have longer axial lengths, deeper anterior chamber distances and longer vitreous chamber distances but thinner lenses and flatter corneas than shorter subjects.

1.3.3 Race

Zadnik et al. (2003) compared ocular components such as corneal power and anterior chamber depths found in different races. They found that the corneal power of Melanesian children appeared to be slightly flatter than American children. The anterior chambers of Melanesian children were slightly shallower than American children while the Malay children were markedly shallower than either White or American children.

Barretto and Mathog (1999) measured the globe projection, the intercanthal distance, interpupillary distance, palpebral fissure width and palpebral fissure height of 126 adult black and white subjects. They found significant differences between globe projection, interpupillary distance and palpebral fissure width between black and white subjects. They speculated that the increased degree of projection in black adults was because of a difference in the shape of the orbits between races. Black subjects usually have more orbital soft tissue protrusion, shallower orbit and more obtuse angle between the longitudinal axes

of the orbits comparing with white ones. Black subjects had larger interpupillary distance compared with white ones. The increase in interpupillary distance was due to the increased angle between the longitudinal axes of the orbits.

Quant and Woo (1993) reported the normal values of eye position and head size in 232 Hong Kong Chinese children with a mean age of 8.93 years. They found that values of eye projection, interpupillary distance, interorbital distance, distance between medial canthi and head dimensions for the Hong Kong children were larger than those of Caucasian children from Britain and American Black subjects. However, comparing with the data found by Waitzman et al. (1992), the eye projection between Hong Kong and Canadian children aged from 7 to 11 years, the value of eye projection of Canadian children was larger than Hong Kong children.

1.4 Growth and dimensions of the orbit

Throughout human life the orbital breadth and height increases by about 52% and 76% respectively (Ranly, 2000). The growth of the orbital volume increases dramatically during the first year of life (Taylor and Day, 1997). Lo et al. (1990) suggested that the majority of orbital growth occurs by 2 to 3 years of age. By the age of 3 years, nearly 80% of adult size has been attained, and by the age of 7 years, the orbit is 94% of adult size (Fountain et al., 1999). Orbital growth is completed between 7 years of age and puberty (Goose and Appleton, 1982, Heinz et al., 1998, Rootman, 1988). The bony orbit expands by both sutural growth and bone deposition in response to the primary growth of its contents. The degree of expansion of the orbit depends on the growth of the eye, which also expands (Ranly, 2000). The growth pattern of the orbit seems to mirror the growth pattern of the whole body skeleton. Bishara (2000) found that 40% of total skeletal change occurs between the age of 5 and 10 years, another 40% occurs between the age of 10 and 15 years, and the balance occurs after 15 years. As suggested by Forbes et al. (1985), adult status is established at the age of 25 years as far as complete stabilization of orbitofacial growth is concerned. The orbital volume is about 30 ml and the orbital depth is approximately 4.5 cm at adulthood (Rootman, 1988, Wojno, 1991).

Using computed tomography (CT) images to calculate orbit volume, Bite et al. (1985) found that the mean orbit volume of 6 female subjects was

22.77 cm^3 while that of 4 male subjects was 23.81 cm^3. All subjects were aged from 13 to 53 years. Another study performed by Forbes et al. (1985) reported volume differences between left and right orbits. In 29 normal subjects with ages ranging from 6 months to 76 years, they found that the volumes of the bony orbit varied from 0% to 8% between the right and left orbits in the same person. This intra-individual side-to-side difference deviation is quite large compared with the results reported from Schuknecht et al. (1996), which was only 2.3%. When a person reaches the mature state, the normal volume of adult male and female bony orbit is widely accepted between 25 to 30cm^3 (Furuta, 2001).

Furuta (2001) studied CT images of the orbit of 109 Japanese subjects with age ranging from 0.2 to 66.8 years and found that the rapid growth of orbital volume from birth stopped at the age of 14.9 and 10.9 years in boys and girls respectively. The mature orbital volume was found to lie within a range of 20.1 to 23.2 cm^3. The author suggested that the orbital growth pattern was similar to that of the interpupillary distance and intermedial canthal distance and body height.

Bentley et al. (2002) conducted a magnetic resonance imaging (MRI) study which included 67 subjects of different ages aged from 1 month to around 15 years old to determine the orbit volume at different ages. They found that the orbits grew from 14 cm^3 to 25 cm^3 within the first 15-year growth in humans. Comparing their findings with others, it would seem that

the orbital volume reached maturity at the age of 15 years. Bentley et al's study also showed that there was no statistical difference between the orbital development of boys and girls and also between left and right orbits. During the first 15 years, orbital growth showed a linear increase with advancing age, and the rate of growth was constant throughout these years.

1.5 Growth and dimensions of the eyeball

At birth, the antero-posterior diameter of the infant's eye is 70% that of an adult's, while the volume of the infant's eye is only 50% that of an adult's (Curtin, 1985, Day, 1997, Gossman et al., 1999). The eye exhibits rapid growth during the first few years of life resulting in a threefold increase in volume by adolescence (age 13 years), of which 70% is attained by the age of 4 years and 90% by the age of 7 years. Ocular growth is minimal beyond age 13 years (Curtin, 1985, Eppley et al., 1993, Moller, 1997).

Goss et al. (1990) found that the cessation of axial elongation of eyeball was strongly correlated with the cessation of myopia progression. For those myopic children, the cessation of ocular growth was the same as that of body growth in terms of height. The study suggested that the developing eye has a profound post-natal growth influence on the size and morphology of the bony orbit as well as numerous surrounding skeletal structures

The average adult eye is 7 cm^3 in volume (Fountain et al., 1999). The adult globe measures 24 mm in length and weighs 7.5 g (Gentry, 1998). The neonatal globe is only 17 mm to 18.5 mm in length and 15 mm to 19 mm in diameter (Curtin, 1985, Day, 1997, Gossman et al., 1999, Morris, 1997); and the average length being 20.3 mm at the age of 6 months and 22.8 mm at the age of 20 months (Taylor and Day, 1997).

A study performed by Hendicott and Lam (1991) on 60 Hong Kong Chinese aged between 19-25 showed that the mean axial length of the eye was 24.75 mm, with a range of 21.98 to 28.21 mm. Another study on a similar age group found similar axial length (i.e. 22.00 to 28.00mm) (Goh and Lam, 1994)

Using CT imaging, Bite et al. (1985) found that the mean eyeball volume of 6 female subjects was 9.67 cm^3 while that of 4 male subjects was 8.94 cm^3. Subjects were aged 13 to 53 years. Hahn and Chu (1984) examined 100 CT head scans of subjects from age group of 0 - 1 to 65 - 99 years. They determined ocular volume by assuming the eyeballs were spherical and antero-posterior and coronal diameters of the eyeball were used to calculate the total volume of the eyeball. They found that the mean ocular volumes ranged from 4.24 ± 1.16 to 8.86 ± 0.73 cm^3. They claimed that the eyeball doubled its volume in the first year of growth, and males always had larger eyeballs than female by $0.5cm^3$ during the entire growth period.

1.6 The relationship between the eyeball and the orbit

Normal orbital bony growth is dependent on the presence of orbital soft tissue (Heinz et al., 1998, Taylor and Day, 1997). Many studies have shown that the increase and decrease in the size of the eye stimulates an orbital response in terms of bone growth and bone remodeling, for example congenital anophthalmos (Eppley et al., 1993, Reedy et al., 1999, Taylor and Day, 1997), microphthalmos (Eppley et al., 1993, Taylor and Day, 1997), enophthalmos (Bite et al., 1985, Fountain et al., 1999, Rootman, 1988, Schuknecht et al., 1996), and enucleation will result in orbital hypoplasia and deformity (Kennedy, 1997, Yago and Furuta, 2001). On the other hand, buphthalmos will result in an enlarged orbit (Heinz et al., 1998). Some studies have also shown that orbital growth can be stimulated by the use of expandable implants for patients who have undergone enucleation (Cepela et al., 1992, Eppley et al., 1993, Gossman et al., 1999, Yago and Furuta, 2001). The effect on orbital growth is more significant during childhood.

Kennedy (1997) observed in a skull X-ray of a child that the orbit on the side of a unilateral congenital anophthalmos was smaller compared to the fellow orbit. He also found that from the linear measurements on the X-ray, 15% to 30% reduction in orbit size were due to the loss or removal of an eye and congenital anophthalmos. Ten percent difference was also found in the reduction in orbit volume when there was enucleation with and without implant. This paper also demonstrated significant bony changes took place in adulthood by using an X-ray which was obtained 38 years after encleation of a 83-year-old woman. Changes in

optic foramina, walls of the orbit, orbital rims, superior orbital fissure and neighboring sinuses could be seen. Orbit volume was estimated to at least 20% reduction from the radiographs.

Yago and Furuta (2001) measured the orbital volume of 5 adults who had an eye removed in childhood. They found that the difference in volume between the anophthalmic and normal orbit was up to 7.1 cm^3, which is nearly 40% in the normal orbital volume. When compared the orbital volume difference between those subjects who had an orbital implant after enucleation with those who had not, the authors found marked differences between the anophthalmic and normal orbits.

Hintschich et al. (2001) also studied bony orbital development after early enucleation in early childhood and results from 29 subjects confirmed a reduction of the anophthalmic bony orbit. However, the reduction was only around 10%, which was less than those found by Yago and Furuta (2001). This study also found a significant reduction of the orbital volume in subjects who had an eye enucleated at adulthood, suggesting that the orbit can still change shape at maturity.

Heniz et al. (1998) studied the effect of buphthalmos on orbital volume using CT imaging. They recruited 8 buphthalmic children subjects whose axial length difference between the buphthalmic and normal eyes was around 23%.

They found an 11% mean difference between the buphthalmic and the nonbuphthalmic orbit volumes.

Schuknecht et al. (1996) assessed 11 patients who had post-traumatic enophthalmos and found that there was increased orbital and fat volume. In enophthalmic orbits, the mean orbital volume increase was 17.9% while the fat volume increase was 13.9%. These two percentages corresponded to 4.4 cm^3 and 1.4 cm^3 in total orbital and fat volumes respectively.

Bite et al. (1985) measured orbital volume in 11 enophthalmic subjects and found a statistically significant increase in bony orbital volume in the enophthalmic eye but the total volume for soft-tissue, fat, neuromuscular tissue and eyeball remained unchanged compared with the normal eye. The range of the increase in volume was 6 to 13% in enophthalmic orbits when compared with the normal orbits.

Gossman et al. (1999) compared the bone and eyelid growth in 5 microphthalmic children, aged from 10 months to 6 years old, before and after using an orbital tissue expander. The eyelid length deficit and orbital dimension deficit were greatly reduced after using the expander for 12% to 21% and 7% to 17% respectively. Also, the development of the frontal, maxillary, and zygomatic bone was significantly improved. The anterior orbital aperture was symmetric with the normal orbit with the eyelid length nearly equal to the contralateral side.

The study also claimed that the age of the subject at the time of implantation and the severity of the deformity did not affect the degree of eyelid and orbital growth.

Osborne et al. (1974) conducted a study on 65 patients who had had enucleation of the eye in order to find the percentage difference in the size of orbits with and without implant after enucleation. They found that the difference in orbit size was most marked when enucleation occurred before the age of 13 years. The highest mean percentage difference in orbital size was found in patients who had the enucleation done from birth to 2 years old. Those with implants had a mean percentage difference around 6% while for those without implants, the mean percentage difference was up to 16%. Based on observation of the radiographs, the decrease in orbit size was caused by enlargement of the maxillary antrum and the ethmoidal air cells.

Many studies have been performed to find out the factors affecting orbital growth. The studies done by Cepela et al. (1992), Eppley et al. (1993), Heinz et al. (1998) and Lo et al. (1990), support the view that the increase in orbital volume is independent of hormonal, hemodynamic, or epigenetic factors provided by the growth of the eye. Goose and Appleton (1982) applied the "functional matrices" theory to explain orbital growth. They claimed that the enlarging eye creates tensional forces within the orbit, resulting in sutural separation and subsequent orbital bony growth at the sutures. The orbit continues to grow until the globe ceases its growth. Orbital growth at the sutures then ceases, synostosis occurs, and growth of the orbit is no longer possible. Beyond this, only bony remodeling is

possible. This theory is supported by studies done on orbit implants. According to the findings from those studies, pressure is the main factor in the alteration and reshaping the facial skeleton, including partial correction of orbital deformities following orbital evisceration in both humans and animals (Buchman et al., 1994, Reedy et al., 1999). This implies that pressure has a regulatory role on bone growth. There are a few possible findings that explain the orbital changes, such as pressure and growth factors. Pressure is caused by eye growth while growth factors are those released from the retina (Cepela et al., 1992, Wilson et al., 1997).

Whereas there is a wealth of evidence to show that the eyeball plays a role in the development of the orbit, is there any evidence that the orbit may also affect the development of the eyeball? Some studies have shown that a change of intraorbital volume due to orbit wall movements also affects the eyeball forward and backward position. The study by Parsons and Mathog (1988) revealed that 2.8% of orbit volume change resulted in 1mm change of globe forward and backward position. The change in orbit volume is due to subtle movements of either the inferior or medial wall. A mere 3 mm displacement of the inferior or medial orbital walls resulted in a 7.1 % and 11.8 % orbit volume change. However, the study of Schuknecht et al. (1996) showed that 5.6% of orbit volume change was necessary for 1 mm eye position change.

1.7 Ocular optical component changes in myopia

Many studies showed that increase of myopia is related with the increase of axial length (e.g. Adams et al, 1989). The majority of the change in axial length was in the vitreous chamber. The increase in vitreous depth was usually paralleled with that of the axial length (Lam and Goh, 1991). Leung and Brown (1999) found that the mean increase in axial length was 0.74 mm when the subjects had –1.23D change in the refraction. Those subjects also had 0.63 mm increase in the vitreous chamber depth.

For other components such as anterior segment depth and corneal curvature, there is no correlation found with the refraction (Lam and Goh, 1991).

Cheng et al. (1992) studied the shape of myopic eye by high-resolution MR images and found that myopic eyes showed an overall enlargement. They compared axial and coronal T1-weighted MR images from 21 subjects (8 were hyperopes, 6 were emmetropes and 7 were myopes) by measuring the axial diameter, equatorial diameter, and vertical diameter of the eyeballs. They found that there was no significant difference for all dimensions between hyperopic and emmetropic eyes, but significance difference was found between myopic and hyperopic eyes.

Some researchers believe that orbital anatomy could be a factor in producing myopia. For example, a skull with low orbits would place the superior

oblique muscle in a position to compress the eye when it is in the reading position, while a large interorbital distance would result in increased convergence. Deep orbits was believed to be conducive to axial elongation of the eye (Curtin, 1985, Cutin, 1985).

The ocular components change in different ways at different ages. The ocular component change that produces the increase in myopia in childhood is axial elongation of the vitreous chamber. In young adulthood, the same change is due to greater anterior chamber depth, lesser crystalline lens thickness, more powerful cornea, and a greater vitreous depth (Grosvenor and Goss, 1999).

1.8 Research showing the effects of myopia on the eyeball and orbit

A study by Wilson et al. (1997) demonstrated the linkage between eye and orbital growth, and showed that ocular development also has an extraocular influence. They used defocusing lenses to induce myopia (-15D) and hyperopia (+15D) in chicks. Intraocular dimensions, orbital dimensions, and histological analysis of frontal bone were carried out to evaluate the differences between eyeball, orbit and frontal bone before and after depriving the developing eyes of clear form vision. They found that myopic eyes were longer with longer orbital axes while hyperopic eyes were shorter with shorter orbital axes. As far as the changes to the frontal bone was concerned, myopic eyes pushed the posterior frontal bone caudally and superiorly. The interorbital septum was pushed medially, and the floor of the orbit was lowered. The suggested reason for the larger orbit in myopic eyes was that the larger myopic eye needs more room and the orbit adjusts its growth to compensate for this need. The orbit remodels itself to make the opening as large as is necessary to encircle the eye. In order to do so, the frontal bone in myopic eyes is higher in mesenchymal tissue, and more mineralized bone tissue is present, which suggests that the bone has undergone growth, resorption and reshaping. It was suggested that these remodeling processes of orbital bone were induced by growth factors released by the retina due to myopia. Therefore, the question was raised as to whether growth factors were having both an intra and extraocular effect.

1.9 Imaging modalities of the orbit and eyeball

The imaging technologies in evaluating the eye and orbits are changing. Traditionally examination of these structures was restricted to survey radiography and a variety of contrast procedures (dacryocystorhinography, zygomatic sialography, orbital angiography, orbital venography, cavernous sinus venography, and cerebral angiography). Conventional radiographic studies are limited by the superimposition of overlying bone and the inability to differentiate between the various intraocular structures, soft tissues and fat opacities in the retrobulbar region, while vascular contrast examinations are limited to the extraocular tissues and often do not completely identify the extent of disease (Johnston and Feeney, 1980). Today, there are two main imaging modalities that can be used to obtain ocular images. They are computed tomography (CT), and magnetic resonance imaging (MRI). The major advantage of these two modalities is that the two-dimensional images of orbits and eyes are free of superimposing structures (Duvoisin et al., 1998). Each imaging modality has its unique strength and application in ocular scans. The use of each imaging modality is indicated by the pathological history of the patient.

1.9.1 CT orbit scan

CT has been widely used in clinical diagnosis since the late 1970s and until now, it is still the most widely available and cost-effective modality in orbital diseases evaluation. CT shows different anatomical structures by using different Hounsfield Units[1] (HU). For the orbit, the orbital fat has –100 HU, while the nerve and muscles are about 30-35 HU and the bone has the highest HU (Weber and Sabates, 1996). Therefore, orbital walls can be clearly delineated in images from ocular soft tissue; and the retrobulbar fat provides excellent image contrast that allows the extraocular structures (e.g. nerves and muscles) and cortical bone to be easily observed due to their large difference in Hounsfield Units (Duvoisin et al., 1998, Weber and Sabates, 1996).

In general practice, axial and coronal images are taken. CT has a great advantage in lesion detectability especially on the bony structures and areas of calcification (Weber and Sabates, 1996).

In basic scanning, axial scan can access some specific structures, such as delicate osseous structures of the lateral orbital wall in fronto-occipital extension, the infraorbital foramen and the infraorbital canal, the groove of the lacrimal sac, the Haller's cells and the ethmoidal foramina in great detail. In coronal scan, the cranio-caudal extension can be examined precisely (Hass et al., 1994).

---

[1] Hounsfield Units (HU) is an expression of the quantified measurement of the degree of X-ray attenuatin on a CT images. HU are also referred to as CT numbers. The equation of CT number = $(\mu_t - \mu_w / \mu_w)$X1000HU, where μ_t is the linear attenuation coefficient of the measured tissue, μ_w is the attenuation coefficient of water (Romans, 1995, Seeram, 2001, Willi, 2000)

In general, 3D reconstructions of the whole facial skull, or of parts of it can, deliver a radio-anatomical survey of the bony walls of the orbit and demonstrate their relationship to each other (Hass et al., 1994).

However radiation dose is the major disadvantage of CT. Aside from that, CT also has a lower contrast resolution when compared with MRI. CT cannot differentiate the different layers of the globe (the retina, uvea and sclera), and only the largest orbital nerve can be identified on CT images (Maya and Heier, 1998). CT cannot delineate intracanalicular optic nerve and orbital apex structures clearly due to partial volume averaging of bone and dental artefacts in these regions (Dorfman and Spickler, 1990).

1.9.2 MRI orbit scan

MRI has been used clinically since the 1980s. MRI utilises the electromagnetic properties of the hydrogen nuclei in free water to produce images. Due to the electromagnetic properties, hydrogen nucleus spins on its own axis and precesses around an externally applied magnetic field (Bo) that is applied during MRI scan. Apart from precession, when there is a Bo applied, hydrogen nuclei align themselves either parallel or anti-parallel to the Bo. The difference in the number of nuclei between different alignment to the Bo generates net magnetization vector (NMV) (Westbrook, 2002). When consider this concept in a 3D model, NMV is now at the longitudinal plane.

It is important to induce resonance in MRI scan. Resonance in MRI is produced by applying a radiofrequency (RF) pulse to the nuclei. The RF pulse must have the same frequency as the precessing hydrogen nuclei, while the precessional frequency of each element is unique.

Two things happen in the scanned medium when applying a RF pulse to a Bo: energy absorption and phase coherence. In energy absorption, NMV moves from the longitudinal plane to the transverse plane where the receiving coil is placed. The increased NMV in the transverse plane causes the precession of hydrogen nuclei in phase to each other. Once the RF pulse is removed, free induction decay (FID) begins (Westbrook, 2002). During FID, the NMV in the

transverse plane decrease due to the relaxation processes. There are two relaxation processes: T1 recovery and T2 decay.

T1 recovery described the restoration of NMV in the longitudinal plane. When the RF pulse removed, the nuclei dissipate their energy to the surrounding environment, and return to Bo. Therefore, NMV moves from the transverse plane to the longitudinal plane. The rate at which this occurs is an exponential process (Fig. 1.3) and the T1 time of each tissue is different. T1 time is defined as the time for 63% longitudinal magnetization recovery. In addition, T2 decay focuses on the decay of NMV in the transverse plane due to the loss of phase coherence of hydrogen nuclei precession. Again, T2 decay happens in an exponential process (Fig. 1.4), and is defined as the time when 63% of transverse magnetization has decayed. Different tissue has specific T2 time (Westbrook, 2002).

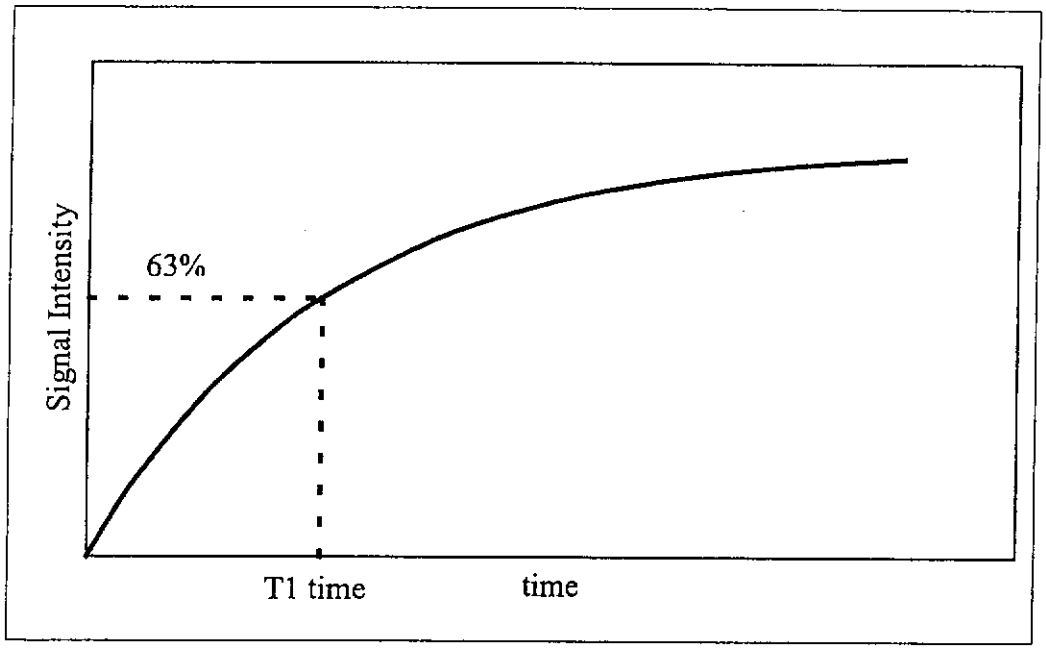

Fig. 1.3. The T1 recovery curve

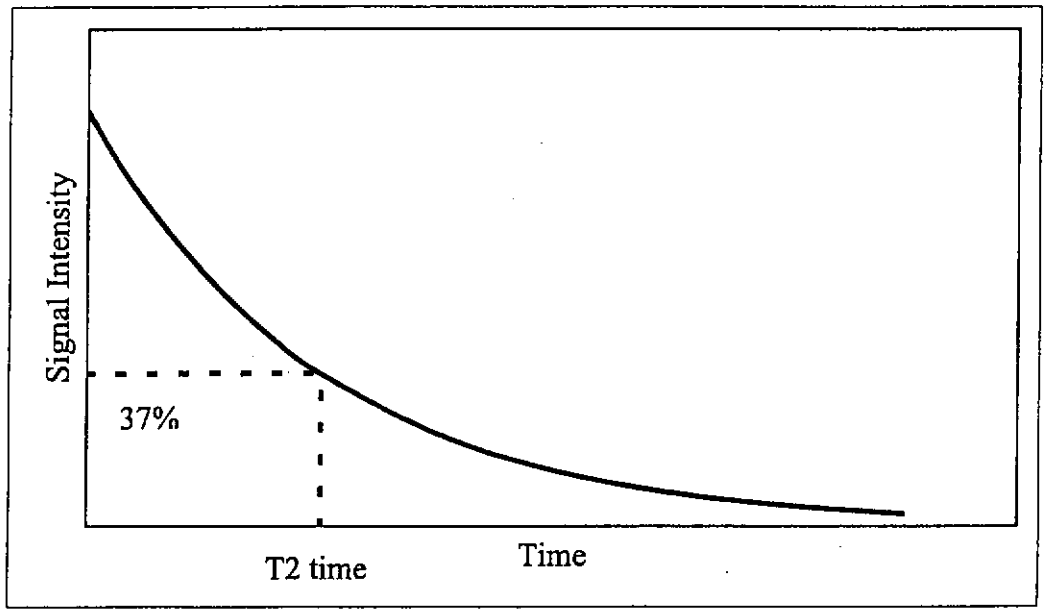

Fig. 1.4. The T2 decay curve

In order to produce contrast that indicates tissue differentiation on images, the manipulation of several extrinsic contrast parameters, for example, repetition time (TR) and echo time (TE) are needed. TR indicates the time interval between 2 RF pulses. TE shows the time interval between the delivery of RF pulse and the collection of the signal (Westbrook, 2002).

Two types of MR images called T1 and T2-weighted images are commonly used in showing the anatomical and pathological details of orbit and eyeball. T1-weighted image means that the image contrast is demonstrated by showing the difference in T1 times of tissues which T2-weighted image aims to demonstrate the difference in T2 times of tissues. Using fat and water as an example, it is easy to know that in order to produce a T1-weighted image, short TR and TE should be used. Short TR and TE exaggerated the difference between

the T1 times of tissues but diminish the T2 effect (Figures 1.5 & 1.6). The principle in producing T2-weighted image is vice versa (Figures 1.7 & 1.8). Therefore, T2-weighted image has long TR and TE.

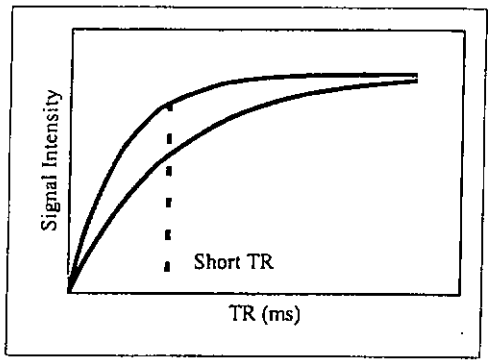

Fig. 1.5 Large T1 difference between tissues shown using short TR.

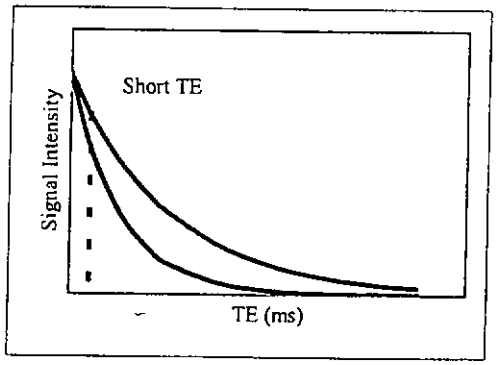

Fig. 1.6 Small T2 difference between tissues shown using short TE.

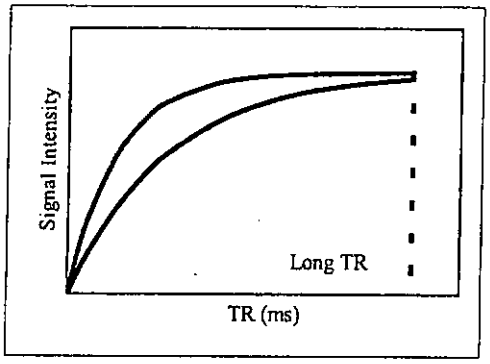

Fig. 1.7 Small T1 difference between tissues shown using long TR.

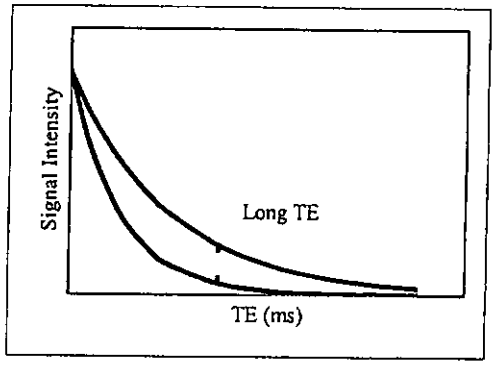

Fig. 1.8 Large T2 difference between tissues shown using long TE.

The eye is an ideal organ for MR imaging because of the wide variation in water content of its various tissues. The water content of vitreous is 98% to 99%, cornea 80%, and the lens 65% to 69% (Mafee et al., 1996). In general, axial and sagittal planes are used to evaluate the globe. MRI orbit images of these two planes are shown in Figures 1.9 and 1.10. In clinical practise, T1-weighted images

usually aim to show anatomical details while T2-weighted images are used to demonstrate pathological conditions.

Fig 1.9. Axial T1-weighted MRI orbit scan

Fig. 1.10. Sagittal T1-weighted MRI orbit scan

Lesions in the superior or inferior portions of the globe are typically well seen on sagittal and coronal images, whereas those located in the lateral or medial aspects usually require axial and coronal sections for adequate visualization. Multiplanar evaluation of the orbital apex and intraconal, intracanalicular, and intracranial portions of the optic nerve is often better achieved with MRI than with CT due to the absence of signals from surrounding bone (Dorfman and Spickler, 1990).

Section thickness generally ranges from 3 mm to 10 mm. Images obtained with either head or surface coils are usually 3 mm to 5 mm in thickness in the axial, sagittal and coronal planes (Dorfman and Spickler, 1990). Interslice gaps approximating 50% of slice thickness are used whenever possible to limit examination time, motion artefacts, and image degradation seen with contiguous sections (Eastwood and Hudgins, 1998, Mafee et al., 1996).

Surface coils improve the detection efficiency of the emitted signal and increase the signal-to-noise ratio, and they improve anatomic details greatly when using on the anterior orbital lesions. (Eastwood and Hudgins, 1998, Nelson and Cartwright, 1992, Weber and Sabates, 1996). However, its disadvantage is that the signal intensity drops off dramatically with increasing depth. The maximum depth that can be imaged with a circular surface coil is equal to the radius of the coil. Image depth must be considered in situations in which evaluation of the orbital apex and intracranial portions of the visual system is important. (Dorfman and Spickler, 1990). Therefore, head coil is usually preferred in such cases. Also, head

coil has high enough signal intensity to allow both eyes to be viewed simultaneously, and it is easier to select the image planes and ensure the proper angle of the image slice. A head coil is usually used when long scanning time is required. It is because images obtained by head coil are less susceptible to degradation caused by ocular movement. Thus head coil is preferred for obtaining T1-weighted images (Bilaniuk and Rapoport, 1994). Apart from the decrease of signal intensity, pronounced motion artifact is another disadvantage using surface coil (Eastwood and Hudgins, 1998, Mafee et al., 1996).

High-resolution thin sections (1 mm) obtained in multiple planes provide excellent anatomic detail of the orbit (e.g. the three ocular layers) and the adjacent regions (Bilaniuk and Rapoport, 1994). High-resolution orbital MRI images are best obtained with surface-coil techniques, which allow thinner scanning sections and improved spatial resolution (Cheng, 1991, Dorfman and Spickler, 1990). However, thin sections have the problem of partial-volume averaging that is generating less signal that may result in a decreased amount of T2 information in later echoes, particularly in rapidly decaying T2 signals (Eastwood and Hudgins, 1998, Mafee et al., 1996).

Conventional T1- and T2-weighted images are usually obtained. T1-weighted images provide excellent anatomical detail, with short acquisition time and so minimize movement artefacts (Duvoisin et al., 1998, Weber and Sabates, 1996). High contrast of the orbital contents and bone can be obtained on T1-weighted images due to high signal to noise ratios. Different structures have

different appearances on MR images. For bony orbit, it is seen as signal void on MR images (Weber and Sabates, 1996). Example of T1-weighted image of the orbit is the bright signal intensity of the orbital fat. Structures of intermediate signal intensity include the extraocular muscles, optic nerve, and iris. Structures of low signal include the lens. The vitreous has a signal intensity that is between the lens and extraocular muscles. The lens capsule has a signal intensity between the fat and extraocular muscles. The T2-weighted image has excellent soft tissue contrast, with long acquisition time and so the spatial resolution is less than the T1-weighted images. T2-weighted image has high signal to noise ratio. Therefore it is good to show pathologic resolution (Dorfman and Spickler, 1990, Duvoisin et al., 1998). Example of T2-weighted image of the orbit is the bright signal intensity of vitreous and cerebrospinal fluid. These intensities of relative structures are reversed on T2-weighted images from T1-weighted images (Weber and Sabates, 1996). Optic nerve is often easier to be observed with T2-weighted image (Daniel and Mitchell, 1999, Dorfman and Spickler, 1990, Duvoisin et al., 1998).

The bright signal intensity of the orbital fat may obscure adjacent structures of lower signal intensity or may silhouette with an adjacent contrast enhancing lesion, obscuring the lesion margin. A solution to these problems is found in the fat suppression technique (Daniel and Mitchell, 1999, Dorfman and Spickler, 1990). Fat suppression provides the best anatomic details, improves the detection of the enhancing lesions, and defines tissue interfaces better without increasing imaging or processing time. Nowadays MRI offer the advantage of fat suppression techniques to prevent mis-registration at the border of fat and water

that cause difficulties in differentiate optic nerve and lacrimal gland (Duvoisin et al., 1998, Mafee et al., 1996, Nelson and Cartwright, 1992, Weber and Sabates, 1996).

Gadolinium is used as a contrast agent in MRI. Pharmacologically, gadolinium is similar to iodinated contrast agents used for CT scan. The use of this contrast has increased the sensitivity of MR imaging by shortening of T1 on short TR/TE images because Gadolinium is a paramagnetic substance (Dorfman and Spickler, 1990). Gadolinium-labeled diethylenetriamine penta-acetic acid (Gd-DTPA) is used for all suspected intraocular and intraorbital masses, infections, and infiltrative processes. It is a T1 contrast agent which enhances T1 image intensity of tissues with increasing vascularity (Cheng, 1991). Also, gadopentetate dimeglumine enhancement is helpful in evaluating intraocular tumors, sinus or intracranial involvement of neoplasms, and the cystic or necrotic nature of lesions (Nelson and Cartwright, 1992). However, sometimes it enhances the lesion to the same intensity as that of retro-orbital fat, and so decreased tumor delineation when the tumor was located within or adjacent to fatty tissue. So fat suppression techniques are needed. Post-contrast T1-weighted fat-suppressed pulse sequences provide the most informative MR images, and should replace conventional T1 imaging after contrast enhancement. Optic nerve involvement and extraocular extension of intraocular tumors are best diagnosed on postcontrast fat-suppressed T1-weighted MR images (Mafee et al., 1996, Nelson and Cartwright, 1992).

MRI is recognised as a powerful aid in the evaluation of the eye and orbit. Its superior soft tissue contrast, multiplanar image reconstruction, and lack of ionising radiation are clear advantages over other modalities such as CT and US (Dorfman and Spickler, 1990). Although MRI is good for soft tissue differentiation, however peripheral orbital vessels are too small to show up on MRI images. Only large vessels (superior ophthalmic vein and ophthalmic artery) are visualized (Duvoisin et al., 1998). The disadvantages of MRI are high motion sensitivity, slightly decreased spatial resolution, high cost, lengthy scanning time, and contraindications of ferromagnetic implants such as surgical clips or pacemakers. Also, patients are advised not to wear eye makeup or else to remove it before the study (Nelson and Cartwright, 1992). Effective way to reduce ocular movement is patient cooperation. Patients are instructed to fix their gaze straight ahead on a single spot during the examination when a surface coil or immobilized them with pressure gauze is used (Bilaniuk and Rapoport, 1994, Cheng, 1991, Dorfman and Spickler, 1990).

1.9.3 Application of MRI orbit scan

MRI remains complementary in the detection of most common pathologies. It is the technique of choice for studying the optic nerve apparatus and visual pathway.

MRI with its superior soft tissue resolution, distinguishes the layers of the globe partially (the sclera is separated from the uvea and retina), which allows visualization of anterior chamber structures not seen on CT, and separates the components of the sheath of the optic nerve (Bilaniuk and Rapoport, 1994, Maya and Heier, 1998, Nelson and Cartwright, 1992). It has the ability to resolve among tumors, adjacent inflammation and associated fluid and provides improved sensitivity in lesion detection. Tumor size, the internal architecture, vascularity, haemorrhage and extrascleral extension can be more accurately assessed, supplying valuable clinical and prognostic information (Bilaniuk and Rapoport, 1994, Dorfman and Spickler, 1990).

Lesions located in the superior orbit may be missed on relatively thick axial images but are very well demonstrated on coronal and sagittal images. Optic nerve lesions require thin contiguous sections. MRI is not the procedure of choice in the evaluation of orbital trauma, not only because it does not provide as much body detail, as does CT, but also because in some instances, there may be unsuspected ferromagnetic foreign bodies. However, MRI is a useful adjunct procedure providing excellent anatomic detail of the eye, orbit, and adjacent brain

(Nelson and Cartwright, 1992). MRI also delineates herniation of fat through fractures better than does CT. Generally CT is the modality of choice for paranasal sinusitis because it best demonstrates bony changes, destruction, or sclerosis. However, if the process has extended beyond the orbit and involves bone marrow, MRI is very useful. In addition, for retinoblastoma, CT is preferable than MRI because CT detects calcification better than MRI (Mafee et al., 1996).

1.10 Volume determination of the orbit and eyeball on images

Apart from using CT and MRI for diagnosis, images from these two modalities are also used for volumetric determination of the orbit and eyeball.

1.10.1 Calibration studies

McGurk et al. (1992) performed a study to determine orbital volume. They reported a method which uses a low-dose CT scan and an off-line computer to calculate orbital volume. They used CT because both osseous and soft-tissue damage in orbital injuries are easier to distinguish. Also low-dose CT reduces radiation exposure to the patient, which is very important because the lens of the eye is particularly sensitive to radiation damage. By using low-dose CT, the surface radiation dose to the orbit was reduced from 105 mSv to 11 mSv, resulting in an estimated lens dose of less than 10 mSv (Bentley et al., 2002, Charteris et al., 1993).

Validation was performed by comparing CT-generated volumes with those obtained by direct orbital measurement. Direct orbital measurement was done on nineteen dried skulls by using alginate to fill directly into each orbit. Alginate is a hydrocolloid with elastic property that regains its shape after deformation and therefore preserves an accurate record after removal from orbit. The orbital foramen was sealed and moistened gauze strips were placed in the medial and

lateral walls of the orbit to aid in withdrawal of the alginate impression before filling. Each orbit was filled with alginate impression to a plane joining the superior and inferior margins of the orbit and the nasomaxillary suture. The volume of the impression was calculated by the Archimede's principle. Their result showed that the mean volume determined by direct impression was around 25.56 – 31.78 cm^3.

Computer generated orbit volume was evaluated on seven skulls. They underwent a 3 mm contiguous transaxial low-dose CT scan (120 kV, 40 mAs). Volumetric measurement was made on the CT console at a fixed window width and level. The radiological boundaries of the orbit were defined anteriorly by a line connecting the anterior surface of the zygomaticofrontal process to the nasomaxillary suture and posteriorly by the optic foramen. The volume of the whole orbit was determined by summating the pixel counts in successive cross-sections and multiplying them by the slice thickness (i.e. 3 mm) through the orbit. Repeatability and inter-observer error were tested too.

Correlation between direct volume measurement and volumes derived from CT scans was with a regression line slope of 0.96. However, there was a consistent volume discrepancy between the two methods with CT under-estimating the alginate volume measurements by 8.7 cm^3 on average for each orbit. Reproducibility was high (CV^2 = 1.3%) and interobserver error was low (CV = 1.6%).

[2] CV= coefficient of variance

The researchers concluded that low-dose CT was successful in producing high quality images for volume measurement, and that the volume discrepancy obtained from these two methods was due to the difference in determining anterior limit to the orbit between dry skulls and CT images. An additional source of under-estimation is partial volume averaging of the orbital content with the bone edge. This source of discrepancy may account for up to one-quarter of the under-estimation. The data indicated that the volumes of the orbits in any one skull are normally within 0.6 cm^3 of each other, which was considered to be an insignificant difference.

Based on the study done by McGurk et al. (1992), Deveci et al. (2000) also tried to use CT to measure orbital volume. The purpose of Deveci's study was to report a simple method for determining orbital volume from spiral CT scans with high accuracy without requiring for additional computing facilities. The method was validated by comparing CT generated volumes with those obtained by direct orbital measurement.

Twenty dried human skulls of various sizes were used to obtain direct orbital measurement. The volume of one orbit of each skull was first directly measured by filling the orbit with putty. Putty is a material with elastic properties that regains its shape after deformation and therefore preserves an accurate record of the orbit after removal. Each orbit was filled with putty to a plane joining the superior and inferior margins of the orbit and the nasomaxillary suture. Before

placement of the paste, the orbital foramina were sealed with wax and the orbital walls were covered with a thin layer of gel to facilitate removal of the paste. Before removal of the paste, axial CT scans of the orbits were obtained. Each scan was displayed in a 512 x 512 matrix. 3D reformations were made from the images. The borders of each orbit were obtained, and the borders of each orbit were traced on all slices of the images by use of PC magnification with a standard window. The radiological boundaries of the orbit were defined anteriorly by a plane connecting the anterior surface of the zygomaticofrontal process to the nasomaxillary suture and posteriorly by the optic foramen. Then the orbital volume of each orbit was calculated by using a 3D software programme in the CT scanner. To determine the accuracy of the method, the orbital volume that obtained from CT scan was compared with the volume of the paste determined by the water displacement method.

The researchers found that the orbital volume ranged from 23.40 cm^3 to 32.48 cm^3. The correlation between the two techniques was high (r = 0.887). The volume discrepancy between these two methods was 0.93 cm^3 only.

Deveci's study achieved a better result than McGurk's study. The volume difference between the CT generated volumes with those obtained by direct orbital measurement was reduced from 8.7cm^3 to 0.93 cm^3. The improvement was due to the use of spiral CT and a different image analysis software used. Spiral CT eliminates the respiratory misregistration artefacts, minimizes motion artefacts .

Heinz et al. (1998) also used CT images to access the effect of buphthalmos on orbital growth in early childhood.

This study involved 8 children less than 6 years old with unilateral or significantly asymmetric buphthalmos. All children underwent a computed axial tomographic scan with 1.5 mm cuts. Volumetric determination of each of the orbital volumes was achieved by tracing in the CT images the bony orbital margins along the medial, posterior and lateral walls of the orbit. The anterior trace was defined by the most anterior aspect of the anterolateral rim of the orbit to the posterior lacrimal crest. All these traces were done manually on an independent display console. The volume was found by integrating the area of each of the tracings on successive slices of each orbit.

The authors found that all patients who had greater orbits also had greater eyes. The difference between the buphthalmic and the nonbuphthalmic orbit found in this study was around 11%. The authors thought that the errors in calculation did not affect the result because their data showed a consistency of the differences in orbital volumes and a small sample size had been used.

1.10.2 Enucleation

Hintschich et al. (2001) used CT images to analyse the extent of bony orbital reduction after early enucleation in humans. They recruited 33 subjects with acquired anophthalmia. These subjects were further divided into 3 groups according to their age of enucleation. All subjects underwent high resolution CT scan to obtain 1.5 mm contiguous slices in the transverse plane. Then 3D reconstruction was performed on these transverse images. The margins of the bony orbit were defined by the orbital walls and the orbital entrance, which was formed by the superior, lateral and inferior orbital rim, the anterior lacrimal crest, and a line joining the anterior lacrimal crest with the superior orbital rim. The optic canal, the nasolacrimal duct, and the pterygopalatine fossa were not considered as part of the bony orbital volume. Volume was then calculated by voxel counting. Interobserver error was tested too.

Hintschich et al. (2001) also validated the volume calculation method on 3D reconstructed orbit by repeating the same on an impression mould of the orbit. From their measurements, the repeated segmentations and volume calculations of the same orbit only showed a variation of ±0.9%. Since the variation was small, they decided that their method was accurate, and it was adopted for orbit volume determination. This study found that the relative volume reduction of the enucleated orbit ranged from 3.8% to 7% compared with the normal orbit.

Another study about orbital growth after enucleation was carried out by Yago and Furuta (2001). They aimed to use CT images to measure the orbital volume for subjects who underwent enucleation without an orbital implant during infancy, and evaluated the growth of their anophthalmic orbits.

Yago and Furuta (2001) recruited 5 subjects. Orbit volume determination of the subjects was performed on reconstructed CT images by a serial of 2 mm-thick coronal images containing the posterior lacrimal crest to the optic canal. The software that was used for measurement was NIH Image. The bony orbit was traced on each image slice. Cross-sectional areas were summed in each image slice to calculate the orbital volume.

The percentage differences in the orbital volumes between the anophtahlmic and normal sides ranged from 9% to 33%. The range obtained was dependent on whether an ocular prosthesis was inserted in the empty orbit or not. The authors commented that the measurement method using serial coronal x-ray reconstruction images might be the most satisfactory one.

1.10.3 Enophthalmos

Bite et al. (1985) investigated changes in the volume of various orbital components in enophthalmos. By the use of late-generation CT scanners and off-line computer image processing, values can be obtained for the volume determination of the bony orbit, total orbital soft-tissue, globe, total fat and total neuro-muscular tissue.

Eleven patients were used in this study. They underwent CT scan of their orbits. Each slice was 1.5 mm thick and adjacent to each other. The mechanism of their software program for calculating volume is first counting the number of voxels in each slice of the desired anatomic structure, and then multiplying the total number of voxels by the volume of one voxel to obtain the total volume of the structure. Region growing, neighbourhood sampling and automatic tracing algorithm techniques were used in these programs.

They found that an increase in bony orbital volume in the enophthalmic orbit when compared to a normal orbit. However, there was no significant difference in the volumes of total soft-tissue, globe, fat and neuromuscular tissue. The authors suggested that the failure in detecting difference in other volumes apart from orbital volume was because the region-growing computer program cannot distinguish among these elements which are of similar radiodensities, and so cannot calculate their volume accurately. It is also possible that soft-tissue differentiation in CT is not sufficiently high to allow ocular soft-tissue recognition.

Schuknecht et al. (1996) also used CT to assess the orbital volume in last post-traumatic enophthalmos. They evaluated 11 subjects with clinical post-traumatic enophthalmos in 1.5 to 6 years ago. CT scan was performed on all subjects with contiguous 2 mm slices in the coronal and axial planes. The orbital volume measurements were obtained by summation of pixel counts, base on density ranges explicitly chosen for each slice by adjusting the Hounsfield Units. Pixel counts were limited to the regions defined by manually tracing the bony boundaries of the orbit on axial slice from the orbital roof to the floor.

Validation was made by measuring the total orbital volume in 3 dried skulls and in 5 control subjects by the same observer who did manual tracing. It was found that the mean orbital volumes of 3 dried skulls and 5 control subjects were 20.4 cm^3 and 25.6 cm^3 respectively. The mean intraindividual side-to-side difference for total orbital volume was 0.6 cm^3 only.

The result of Schuknecht's study showed that the average normal orbital volume was 26.8 cm^3. They commented that the larger orbital volume of the subjects compared with the controls was because of a higher proportion of males in the subjects group who process larger orbits. Comparing the enophthalmic and normal orbit, a mean increase of 17.9% was seen together with an increase in fat volume. Enophthalmos was found to increase with the degree of orbital volume expansion. They also compared their data with those found by other studies and speculated that orbital volume had racial and sex differences. The authors also suggested the discrepancies in total orbital volume calculations among all reported

studies were due to the different interpretation of orbital boundaries, which could be subjective.

Ramieri et al. (2000) performed a study to estimate the dimensions and volumes of the orbit and orbital fat in post-traumatic enophthalmos from 2D and 3D-CT images. In this study, 25 subjects who had operation for various types of facial fractures with severe involvement of the orbits were included. They underwent a post-operative CT scan with contiguous 1 mm thick axial slices. Either 2D or 3D images were used to assess the size of bony changes in the orbit. 3D reconstructed images and volumetric measurements were obtained with Mimics software version 4.0. The contours of the orbital bone and fat were arbitrarily closed tangentially to the orbital rim along a plane from the orbito-zygomatic suture to the anterior lacrimal crest. The contours were traced automatically and volumes were calculated. A repeatability test was performed to evaluate the observer's consistency. The result showed that the fractured non-enophthalmic orbits had increased volumes of up to 18%.

1.10.4 Blowout fractures

Charteris et al. (1993) performed a retrospective analysis to determine whether orbital volume measurement could be a parameter in blowout fracture management.

Thirty-one subjects with a pure blowout fracture of the orbital floor without medial wall involvement were included. Fifteen had surgical exploration and repair and 16 were managed conservatively. All of them attended a low dose CT scan with contiguous 3 mm axial slices taken. Orbital volume was measured by using a cursor to trace the orbital walls and the anterior orbital boundary as defined by a line joining the zygomatico-frontal process. The volume was then calculated by summating the area of the orbit on each section and multiplying by section thickness. A significant difference in orbital volume was found between the surgical (4 cm^3) and non-surgical group (2.22 cm^3).

Lee and Chiu (1993) also used CT images to evaluate orbital volume in blowout fractures. Ten subjects with pure blowout fractures, mid-facial, naso-ethmoidal or zygomatic-malar fractures were recruited. Three of them were operated. There were also 20 controls. Coronal CT scans were performed before and after operation in each case. In each scan, 15 to 20 serial images were obtained from the anterior orbital margin to the optic foramen posteriorly. Image matrix was used 320 x 320. Volumetric determination was done on an off-line computer using software program called Anato®. It generated a pixel count of the

bony sockets for each slice and then added the values from each slice to obtain the total pixel count within the structure. The bony socket was delineated by manually tracing the boundary of the orbit with an electronic stylus. The total number of pixels in the sockets was multiplied by a conversion coefficient to give the volume. There was a significant increase between the average bony orbital volume of the normal control (24.93 cm^3) and that of the injured orbits (27.68 cm^3). Also, enophthalmic subjects showed a larger difference in intraindividual orbital volume than controls.

1.10.5 Growth of the orbit

Furuta (2001) used reconstructed CT images of serial coronal sections retrospectively to measure the orbital volume and study its changes with age.

This study was performed on 109 Japanese subjects. These subjects underwent CT scan because of eye injury and the fellow orbit was normal. The ages of the subjects ranged from 0.2 to 66.8 years. CT reconstruction was based on 2 mm coronal slices from the lacrimal fossa to the optic canal. NIH Image was used for image analysis. For volumetric calculation, the bony orbit was traced on each image. The regions lacking a boundary formed by bone were traced with a straight line. The sectional area of the orbit was measured in each slice by summation of the volumes of the slices

Furuta (2001) reported that the reproducibility of the measurement was good and no laterality of the orbital volume was found. Orbital volume was strongly correlated with height, interlateral orbital rim distance and age. The orbit grew rapidly until the age of 14.9 years in boys and 10.9 years in girl. The mean volume of the mature orbit was 23.6 cm^3 in male and 20.9 cm^3 in female. For the group of subjects who aged over 40 years old, their orbital volume was found to be larger than those aged from 18 to 40 years old. Furuta found that it was probably not encountered as orbit growth, but suggested that difference in generation might bring this difference.

Another study on orbital growth was carried out by Bentley et al. (2002). Their retrospective study aimed to construct a model of change in orbital volume throughout childhood from the age of 1 month to 15 years using MRI images.

There were 67 UK children of different races involved in this study. All of them had undergone MRI scan due to different pathologies but the final findings on MR images were entirely normal. T2-weighted MRI was performed using a 5 mm slice thickness with 2 mm slice intervals. For orbital volume determination, the interface between the bony walls and the soft tissue contents of the orbit was outlined in every slice of the MR images. The posterior limit of the orbit was defined by a line connecting the medial and lateral walls of the optic foramen within the orbit, excluding the optic canal. The anterior boundary was defined by a line extending between the medial and lateral canthi in the appropriate slices, and between the corresponding most anterior bone edges of the medial and lateral orbital walls in the remaining slices. The outlining was done by one operator to ensure consistency between examinations. The volume of each slice was calculated by multiplying the surface of the outline in each slice by the slice thickness. The total volume of the orbit was calculated by adding the volumes of all slices.

It was reported that there was no significant difference in the mean orbital volume between different racial groups. During the first few months of life, the mean orbital volume was 15 cm^3 in male and 13 cm^3 in female infants. The orbits grew to 26 cm^3 in boys and 24 cm^3 in girls by the time at the age of 15 years. By

the age of 5 years, the orbital volume on both sides reached on average 77% of the volume formed at the age of 15 years. There was no significant difference in orbital volume between genders throughout growth.

1.10.6 Eyeball volume measurement

Hahn and Chu (1984) used axial CT images to investigate ocular volume as a function of age and gender.

This retrospectively study was done on 100 subjects with CT axial images from either orbit or head scan. The age of the subjects ranged from 3-days-old to 99 years. The image matrix used was 320 x 320. The slice chosen for ocular measurement was that showing the largest axial plane of the eyeball. The antero-posterior diameter of the eyeball was taken as the distance from the anterior corneal surface to the posterior wall of the choroid, while the coronal diameter was taken as the maximum transverse width of the eyeball. These two dimensions were obtained with the cursor, and used to calculate the total volume of the globe. The eyeball was assumed to be spherical for volume estimation.

Ocular volume was found to increase significantly with age. Ocular volume doubled from birth (3 cm^3) to 24 months of age (6 cm^3). The growth stopped from age 20 to 30 years and at this age, the ocular volume was 9 to 10 cm^3. Male ocular volumes were 0.5 cm^3 larger than those in females.

1.10.7 Shape of the eye

Cheng et al. (1992) used multislice MR images of the eye to calculate ocular dimensions in order to evaluate the shape difference in myopic, hyperopic and emmetropic eyes.

MRI was conducted on 21 subjects with refractive error ranged from +5.5D to –9.5D. MRI was done using a 1.5T scanner with a surface coil. Axial and coronal images were acquired with 8 to 9 mm contiguous slices. Only T1 images were collected. Eye fixation was used during scanning. Measurement of eye size (i.e. the anterior-posterior, equatorial and vertical diameters) and thickness of ocular components were made manually using the built-in metric scale in all MR images.

There was no difference in the shape of hyperopic and emmetropic eyes. Both of them had an equatorial diameter longer than the anterior-posterior and vertical diameters. Myopic eyes were larger than hyperopic eyes with a sphero-elliptical shape. This suggested that during myopic progression, an overall enlargement or a radial volume expansion occurred.

1.11 Summary

From the literature review, it was found that the prevalence of myopia is very high in the young population in Hong Kong. Many of myopes have early onset myopia. At the period that myopia is developing among early onset myopes, the orbit and eyeball are also growing. There is some evidence from a chick study and also from pathology studies in humans that the eyeball size may influence the development of the orbit. There is no literature on how the human myopic eye influences orbital development.

The aims of this study are:

1. to review the accuracy of volume determination from MRI DICOM images.

2. to investigate the development of the orbit in HK Chinese of different ages.

3. to investigate the relationship between eye size and orbit volume in subjects with varying degrees myopia.

Chapter 2 Instrumentation

2.1 Vision examination

The vision examination consisted of two parts. Part 1 consisted of measurements of refractive error using an autorefractor and axial length using a clinical A-scan ultrasound unit. Both measurements were carried out by one registered optometrist at the Optometry clinic of The Hong Kong Polytechnic University. Pupil dilation and cycloplegia were achieved using one drop of Novesine 0.4% and after a few minutes, one drop of cyclopentolate HCL 0.5%. Vision examination started when the subject's near vision was blurred at 33 cm for about 8 hours when viewing a near vision card. Blurred vision usually occurred in 15 to 30 minutes after instillation of cyclopentolate HCL 0.5%.

2.1.1 Axial length measurement of the eyeball

Axial length measurements were obtained using a Mentor Advent™ A/B system. This ultrasound system was a 7MHz system. Totally, 5 internal instrument readings were averaged to give a single reading. The standard deviation rejection level was 0.1mmHg. The system was calibrated before the start of measurement for each subject. Prior to the measurement, one drop of Novesin 0.4% was instilled into each eye. Five readings were recorded, and the mean axial length was calculated. During measurement, the subject was asked to fixate a distant target.

2.1.2 Refractive errors measurement

Cycloplegic refractions were obtained using a Shin-Nippon SRW-5000 infra-red (IR) system autorefractor. The Shin-Nippon SRW-5000 had previously been evaluated on adult and child subjects and was found to be a reliable autorefractor (Chat and Edwards, 2001, Mallen et al., 2001). The measurement method used in this study was the same as described by Chat and Edwards (2001), except the accuracy of the measurement was set to 0.25 D instead of 0.12 D.

2.2 MRI orbit scan

MRI orbit images were obtained from two public hospitals in Hong Kong, Queen Mary Hospital for Study 1 and Queen Elizabeth Hospital for Study 2.

2.2.1 Study 1

A 1.5T MRI scanner was used (Genesis, Signa, GEMS, Milwaukee, WI) for orbit scan. Cases were retrieved by a registered radiographer at the MRI centre in Queen Mary Hospital. This staff member was briefed on the criteria for subject recruitment. Table 2.1 shows the protocol of the T1 and T2 orbit scan used.

Scanning	T1	T2
Protocol name	T1 Axial	T2 OBL Axial FATSAT Orbit T2 Axial STIR T2 Axial FATSAT
Pixel size	0.625 x 0.833 mm^2	
Scan time	3-4 mins	3-4 mins
TR	500-720 ms	2880 - 4760 ms
TE	9-10 ms	31 - 96 ms
Flip angle	90 deg	90 deg
Slice thickness	3 mm	
Spacing between slices	0 or 0.5mm	
Matrix % 100	256 X 192 or 512 X 512	
Field of view (FOV)	16cm	
Rect. FOV	1	
No. Acq	1	
No. Meas	2-3	

Table 2.1 MRI orbit scan protocol of Study 1

2.2.2 Study 2

A 1T MRI scanner was used (Siemens, Magnetom Impact Expert, Erlangen, Germany) for orbit scan. This type of scanner had previously been used in cardiac research, amongst others (Fujimoto et al., 1998, Nakagawa et al., 1998).

The FLASH 3D conventional gradient-echo sequences of T1 and 3D constructive interference in steady state (CISS) T2-weighted were chosen to scan volumetric structure. FLASH sequences use only the longitudinal magnetization in the steady state. The remaining transverse magnetization is destroyed with a so-called 'spoiler'. T1-weighted with FLASH sequence has short TR, short TE and large flip angle. The 3D sequence was used when high resolution and thin contiguous slices are required. In this sequence, there is phase-encoding in the slice-selection direction in addition to the in-plane phase-encoding direction. Because the strength of slice-selection gradients for a given slice thickness can be lower for 3D sequences, thinner slices can be set. No gap is required between the slices. The slices in a 3D data volume are contiguous. 3D CISS sequence was used too because it can produce images thinner than 2mm, with high magnetic field homogeneity and superior contrast with low artifact (Lingawi, 2003).

Table 2.2 shows the details of the protocols used for T1 and T2-weighted scan.

Scanning	T1	T2
Protocol name	CISS T2-weighted sequence	FLASH T1-weighted sequence
Pixel Size	0.98 x 0.98 mm	
Rel S/N ratio	1	
Scan time	7 min 8 sec	8 min 6 sec
TR	16 ms	27 ms
TE	8 ms	5 ms
Flip angle	70 deg	30 deg
No. Slab	1	
Slab thickness	105 mm	105 mm
Eff. thickness	1.5 mm	
No. Paritions	50	70
Shift-mean	-10 mm	
Orientation	Transverse	
Matrix % 100	256 x 256	
FOV	250 mm	
Rect. FOV	8/8	
No. Acq	1	
No. Meas	1	
Coil	CP Head	

Table 2.2 MRI orbit scan protocol of Study 2

2.3 Volumetric determination of the orbit and eyeball

Volumetric determination was done by a computer software called 'OSIRIS'. Osiris is part of a hospital-wide picture archiving and communication system (PACS) under development at the University Hospital of Geneva (Digital Imaging Unit, University Hospital of Geneva, Switzerland). The software can be downloaded from the Internet via the website (http://www.expasy.org/UIN/html1/projects/osiris/osiris.html) free of charge. The version used in this study was OSIRIS 4.0 for Windows. The computer used was an IBM compatible personal computer operating under the WinXP and Win98 platform. OSIRIS has the capability to display MR images and calculate the volumes.

OSIRIS reads images stored in Digital Imaging and Communication in Medicine (DICOM) format. The DICOM format has been adopted as a medical image file format, and used for the communication of medical images. In this study, all images were saved in a recordable compact disc from the MRI scanner directly. All MRI images were in DICOM format, and so were OSIRIS compatible. Step by step procedures of starting OSIRS were described in Appendix 6.

2.3.1 Orbit volume measurement

In this study, orbit volumetric determination was performed on T1-weighted MR images. The orbit volume measurement commenced with the image showing the floor of the orbit and ended with the image showing the roof of the orbit.

When an appropriate image was selected for measurement, the 'Tool' button was clicked on the left hand side and the 'Polygon Region of Interest' (ROI) tool was recalled to draw the region of interest using a mouse or stylus. After drawing the ROI on each image, the volume of the ROI was shown in another dialog called 'Multiple ROI volume'. This dialog gave an interactive 3D representation of the ROI, an outline of the ROI selected, an interactive graphic of the corresponding ROI and some general statistics for the selected ROI. Figure 2.1 shows the information contained in the Multiple ROI volume dialog.

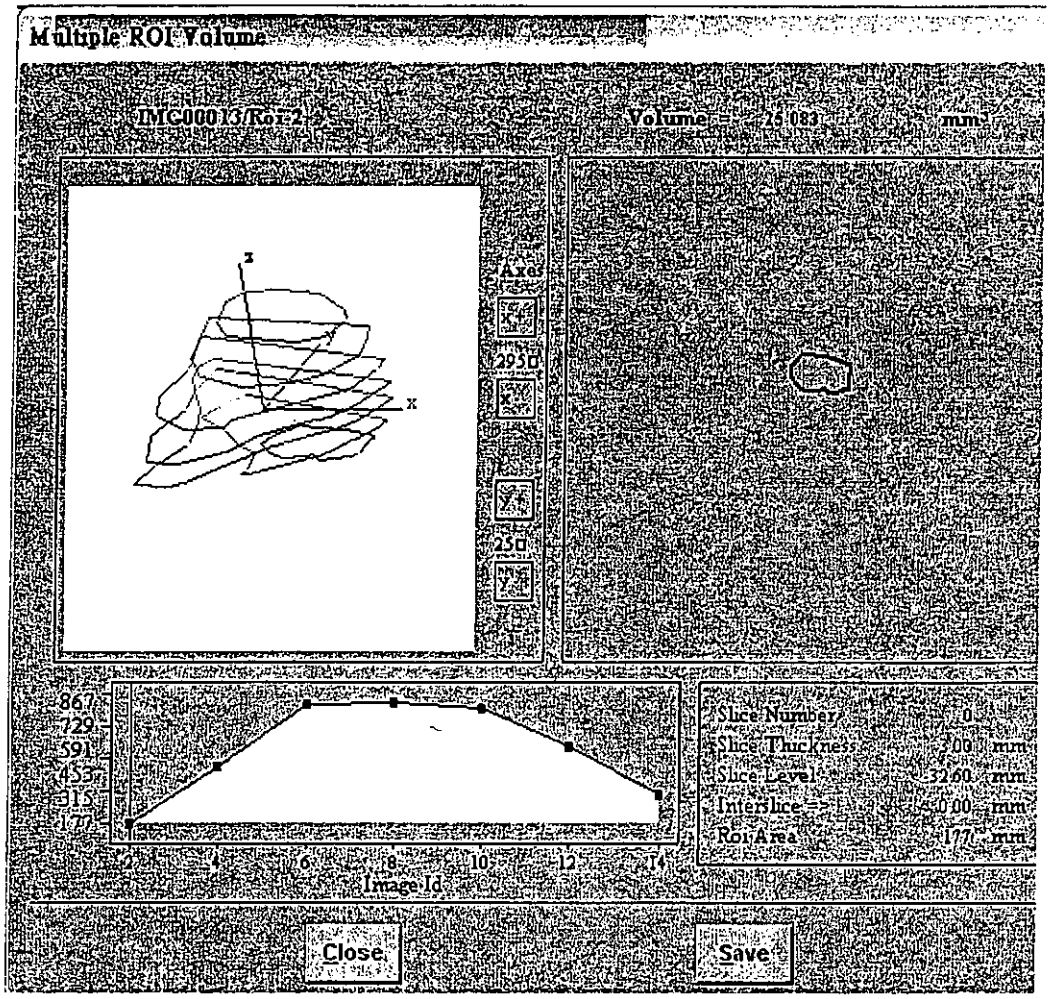

Fig.2.1 Multiple ROI volume dialog

2.3.2. Eyeball volume determination

Eyeball volumetric determination was done on T2-weighted MR images. The T2-weighted image shows a hyper-intensive eyeball.

For eyeball volume measurement, the segmentation technique was used. Segmentation is the process of subdividing an image into regions based on their pictorial characteristics. The segmentation technique that was used in this study was the "region growing" method.

After calling up the segmentation function from OSIRIS, a seed point was planted within the eyeball to grow a region by appending neighbours having similar gray level. After planting a seed, and adjusting the tolerance of the seed (±100 – 250) individually for every image of the subject (Fig. 2.2), a closed polygon that defined the segmented region was generated (Fig. 2.3). The variations in the tolerance indicate the extent of the gray level above and below the gray level of the seed. The ±250 setting included a wider gray level range than ±100, and so generated a larger segmented region (Table 2.3). The decision of the optimum tolerance depended on whether the segmented regions line the eyeball border well and cover all parts of the eyeball image. After completing the segmentation on all eyeball images of each subject, the volume of the segmented region was displayed on another dialog called 'Multiple ROI volume'.

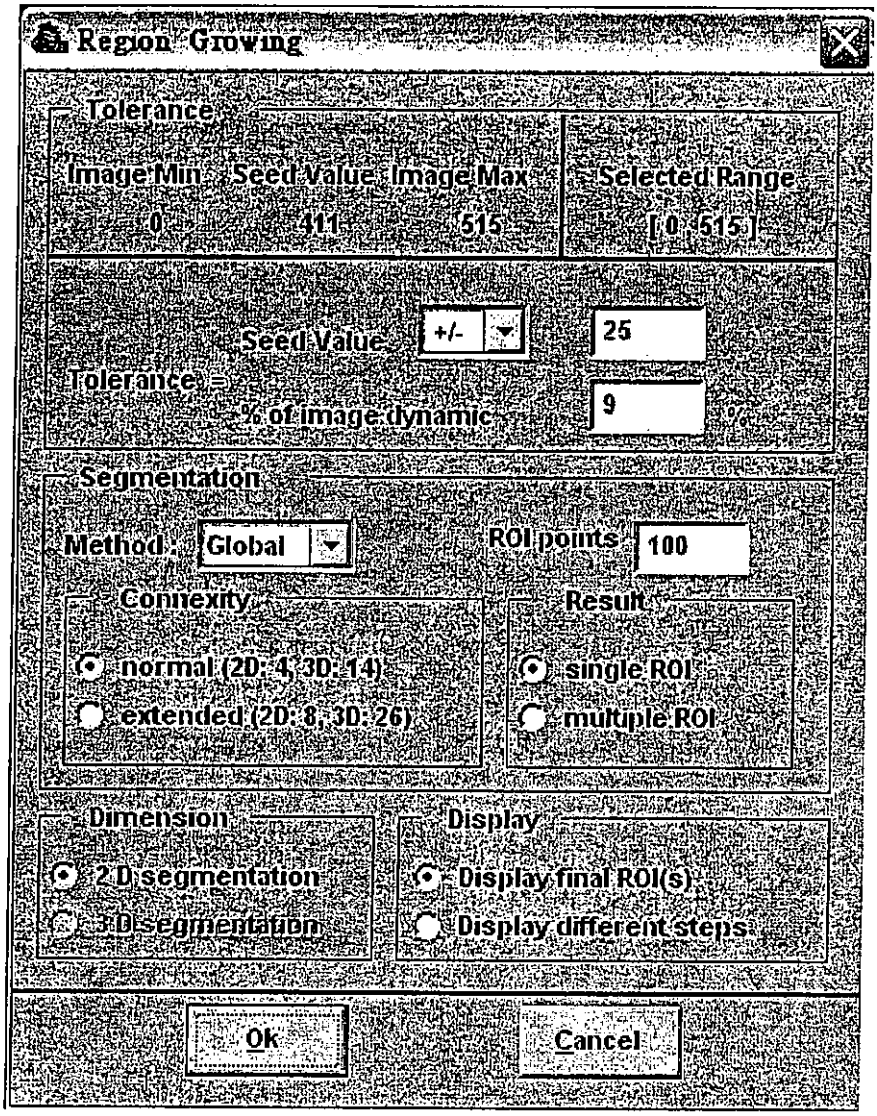

Fig. 2.2 Region growing dialog.

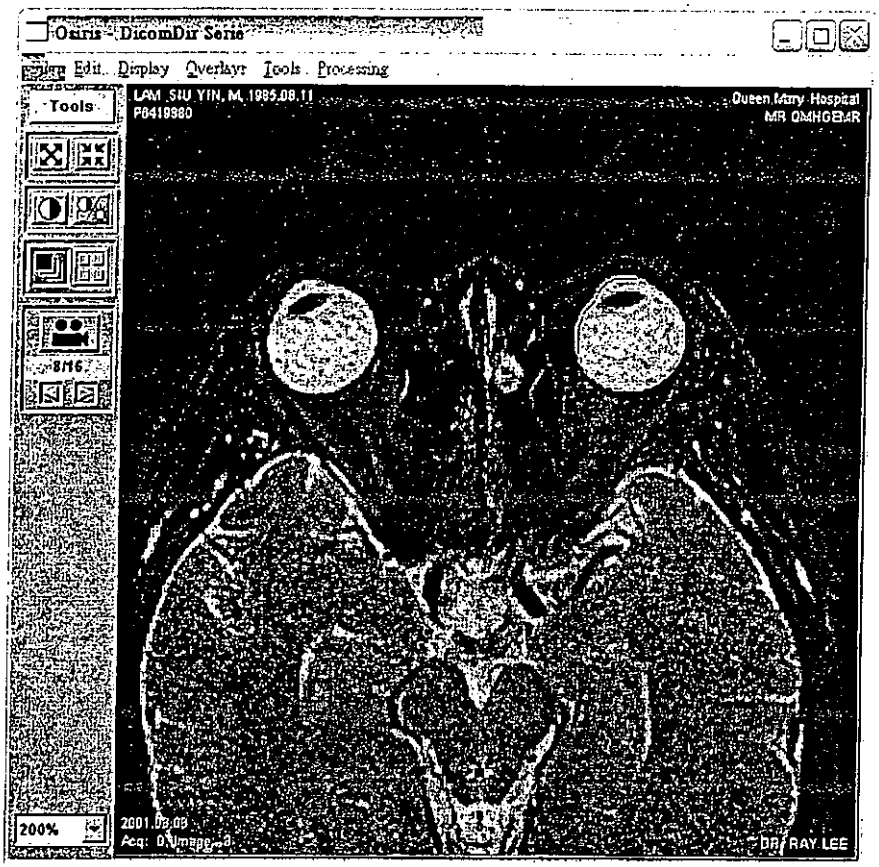

Fig. 2.3 A closed polygon was drawn on the eye by region growing method

		Measurements			
		1	**2**	**3**	**4**
Tolerance	**±100**	5.089	5.042	4.789	6.309
	±150	5.320	5.682	4.973	6.657
	±200	5.440	5.851	5.219	6.880
	±250	5.571	6.219	5.331	6.986

Table 2.3. Changes in volume of eyeball calculated from 4 individuals using different tolerance from ±100 – 250.

2.4 Head dimensions

Head dimensions were measured using a pair of custom-made calipers which had sensitivity of 1 mm. Three dimensions of the head were measured. They were head height, length and breadth. Head height was defined as the distance from the external auditory meatus to the vertex of the head. Head breadth was the intertemporal distance, and the head length was the distance from the glabella and the occipital protuberance of the head.

Chapter 3 Calibration

3.1. Calibration of 1T scanner (QEH)

3.1.1 Introduction

Volumetric measurement is common in clinical diagnosis and treatment planning. Many previous studies have reported the clinical usefulness of volumetric measurements of different body parts (Disler et al., 1994, Duong et al., 1992, Eckstein et al., 1998, Jack et al., 1989, Kohn et al., 1991, Lonn et al., 1999, Qin et al., 1990, Rubin and Phillips, 1991, Scheib et al., 2000).

The absence of radiation and the emergence of higher resolution systems have made MR appear more attractive against CT as a modality for organ volumetric determination. This is particularly so in the case of the eye where concerns about radiation-induced structural changes are very real. Yet, volumetric determination of the eye and orbit may offer new insights in the development of these structures. Against this background, it is reasonable that MR imaging should be studied to determine if it provides acceptable accuracy for eye and orbit volumetric determination.

The easiest way to study the accuracy of the technique to be used for volumetric determination is to conduct a calibration study on phantoms (Disler et al.,

1994, Duong et al., 1992, Lo et al., 2000, Niemczyk et al., 1999, Scheib et al., 2000). Typically, phantoms are made to simulate the structure of interest, for instance the orbit (Deveci et al., 2000, Forbes et al., 1985, McGurk et al., 1992). The phantom is made to a similar shape or size as the structure of interest. The material used to make the phantom varies according to the imaging modality employed. For instance, Iodine-impregnated silicon is used for the phantom when CT imaging is the scanning modality as silicon stands out from other structures on the CT images.

As part of a larger study on the orbit using MR imaging, this report evaluates of the accuracy of orbit and eyeball volumetric determination using MR images. This calibration used tailor-made phantoms that simulated the size and shape of the human orbit and eyeball. To the best of our knowledge, this has not been reported before.

3.1.2 Material and Methods

The eyeball and orbit phantoms were made using techniques previously described (Disler et al., 1994, Duong et al., 1992, Lo et al., 2000, Qin et al., 1990, Rubin and Phillips, 1991).

3.1.2.1 Eyeball phantom

The eyeball phantom consisted of a rectangular plastic tub (measuring 15 x 16 x 9 cm) which was filled with water together with 10 silicon balls. These balls were tailor-made in 10 consecutive diameters ranging from 21 to 30 mm (each differed by 1 mm) to simulate eyeball sizes from infants to adults (Cheng et al., 1992, Curtin, 1985, Day, 1997, Hendicott and Lam, 1991, Morris, 1997, Taylor and Day, 1997). The diameters of the balls were measured using a sliding caliper (Mitutoyo, Japan; with sensitivity of 0.02 mm) and their physical volumes were calculated by mathematical formula: Volume = $4/3\pi(\text{radius})^3$.

3.1.2.2 Orbit mould phantom

The orbit mould phantom consisted of a rectangular plastic tub (measuring 15 x 16 x 9 cm) which was filled with water together with 10 hand-made moulds of high strength silicon mould-making rubber (Silastic® 3841 Base and 81F curing agent, Dow Corning Co., US). Each rubber mould was made by direct impression from an orbit of a dried human skull. Each orbit was filled with the rubber to the plane joining the superior and inferior margins of the orbit and nasomaxillary suture (McGurk et al., 1992). The orbital foramina were sealed before the placement of silicon. The rubber moulds were then removed from the orbits, and weighed using an electronic balance (Precisa XB620M, Swiss). Their physical volumes were found by dividing their weights by density ($1.2 g/cm^3$). Altogether, 10 dried skulls were used.

3.1.2.3 MRI scan

The phantoms were examined in a 1 T MRI scanner (Siemens Magnetom Impact EXPERT, Erlangen, Germany) with a head coil. Contiguous 1.5 mm thick CISS (Constructive interference in steady state, TR/TE=16/8ms) T2-weighted sequence were taken, with matrix 256x256 and slab thickness 105 mm. Each scan took approximately 18 minutes. All images were stored in a compact disc in DICOM format for offline analysis.

3.1.2.4 Volumetric determination

All images were displayed by the OSIRIS software which ran on a personal computer operating under Windows 98. MRI images of the phantoms were shown in Figures 3.1 and 3.2.

Figure 3.1. T2-weighted MRI images of silicon balls (phantom no. B7 to B10, from left to right). Some small air bubbles were seen on ball surfaces.

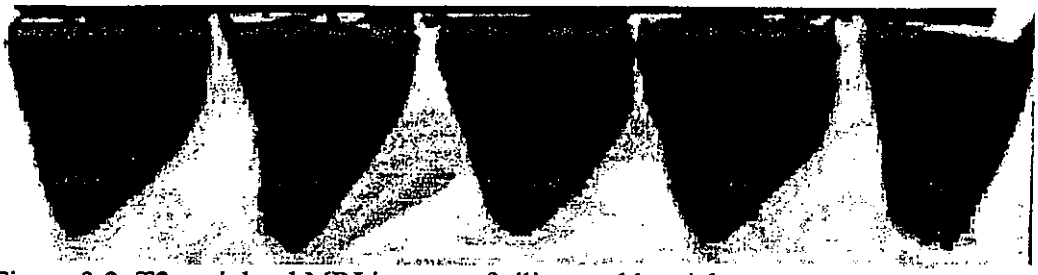

Figure 3.2. T2-weighted MRI images of silicon rubber (phantom no. R1 to R5, from left to right)

The regions of interest (ROIs) were manually drawn around the border of the balls and moulds of the phantom images using a stylus. A dotted line appeared on the screen outlining the selected area. The volumes of the objects were then computed using the 'multiple ROI volume' function of the OSIRIS software. Results were displayed on a separate window, including an interactive three-dimensional representation of the ROI over the set of images. This volume measurement was repeated in the same way on each ball or mould and a total of five computed volume measurements were made. Data collected were analyzed using the paired samples t-test for comparison of the difference between computed and measured physical volumes. All reported significance levels were two-tailed and $p < 0.05$ was considered statistically significant.

3.1.3 Results

Tables 3.1 and 3.2 show the computed volume and physical volume for the eyeball and orbit mould phantoms respectively. In Table 1, B1 to B10 are the 10 silicon balls of physical sizes measured from 3.7 to 11.9 cm^3. In Table 2, R1 to R10 represent 10 silicon orbit moulds of physical sizes measured from 14.7 to 26.6 cm^3. The computed volumes of the silicon balls and moulds ranged from 4.5 to 13.7 cm^3 and 15.7 to 28.5 cm^3 respectively.

Table 3.1. Comparison between the OSIRIS computed and measured physical volumes. B1 to B10 are the silicon balls scanned.

Phantom	Mean Computed vol ± SD (cm^3) (A)	CV (%)	Mean Physical vol ± SD (cm^3) (B)	CV (%)	Difference (B-A)	Error (%) $\frac{(B-A)}{B} \times 100\%$
B1	4.46 ± 0.05	1.01	3.67 ± 0.04	1.14	-0.80	-21.75
B2	5.17 ± 0.07	1.32	4.59 ± 0.08	1.74	-0.58	-12.66
B3	5.91 ± 0.05	0.87	4.97 ± 0.02	0.43	-0.94	-19.00
B4	6.79 ± 0.09	1.36	5.75 ± 0.10	1.82	-1.04	-18.06
B5	7.72 ± 0.09	1.14	6.58 ± 0.10	1.45	-1.14	-17.33
B6	8.64 ± 0.07	0.84	7.42 ± 0.09	1.18	-1.22	-16.43
B7	9.81 ± 0.09	0.89	8.61 ± 0.03	0.39	-1.20	-13.97
B8	11.15 ± 0.08	0.71	9.59 ± 0.05	0.54	-1.57	-16.34
B9	12.03 ± 0.04	0.32	11.01 ± 0.04	0.36	-1.30	-11.79
B10	13.71 ± 0.11	0.81	11.90 ± 0.10	0.87	-1.81	-15.20

Table 3.2. Comparison between the OSIRIS computed and measured physical volumes. R1 to R10 are the silicon moulds scanned using a 1T scanner.

Phantom	Mean computed vol ± SD (cm^3) (A)	CV (%)	Mean physical vol ± SD (cm^3) (B)	CV (%)	Difference (B-A)	Error (%) $\frac{(B-A)}{B}$ X 100%
R1	15.73 ± 0.13	0.83	14.65 ± 0.00	0.01	-1.08	-7.37
R2	20.73 ± 0.09	0.64	18.70 ± 0.00	0.00	-2.03	-10.86
R3	21.45 ± 0.06	0.68	19.44 ± 0.00	0.00	-2.01	-10.34
R4	21.67 ± 0.07	0.46	19.75 ± 0.00	0.01	-1.92	-9.72
R5	21.88 ± 0.15	0.51	20.83 ± 0.00	0.00	-1.05	-5.04
R6	22.74 ± 0.16	0.26	21.31 ± 0.00	0.01	-1.43	-6.71
R7	23.85 ± 0.07	0.25	22.78 ± 0.00	0.01	-1.07	-4.70
R8	24.66 ± 0.13	0.70	22.99 ± 0.00	0.01	-1.67	-7.26
R9	25.31 ± 0.16	0.29	23.33 ± 0.00	0.00	-1.98	-8.49
R10	28.50 ± 0.07	0.33	26.59 ± 0.00	0.01	-1.91	-7.18

For both the eyeball and orbit mould phantoms, there were significant differences between computed volumes and physical volumes (t = 10.063 and 12.184 respectively, pair t-test; $p < 0.05$). The coefficient of variations (CV) for both computed and physical measurements of the ball phantoms were below 1.82%. However, the CV for both computed and physical measurements were lower for the orbit mould phantom (below 0.83%). The percentage errors of the computed volumes of the eyeball and orbit mould phantoms are shown in the last column of Tables 3.1 and 3.2 respectively. Results also show that the CV and percentage error decreased with increasing measured volume.

Figures 3.3 and 3.4 show the correlation between physical volume and computed volume for the eyeball and orbit mould phantoms respectively. There is a high correlation for the eyeball phantom (r = 0.99; $p < 0.05$) and the orbit mould phantom (r = 0.99; $p < 0.05$).

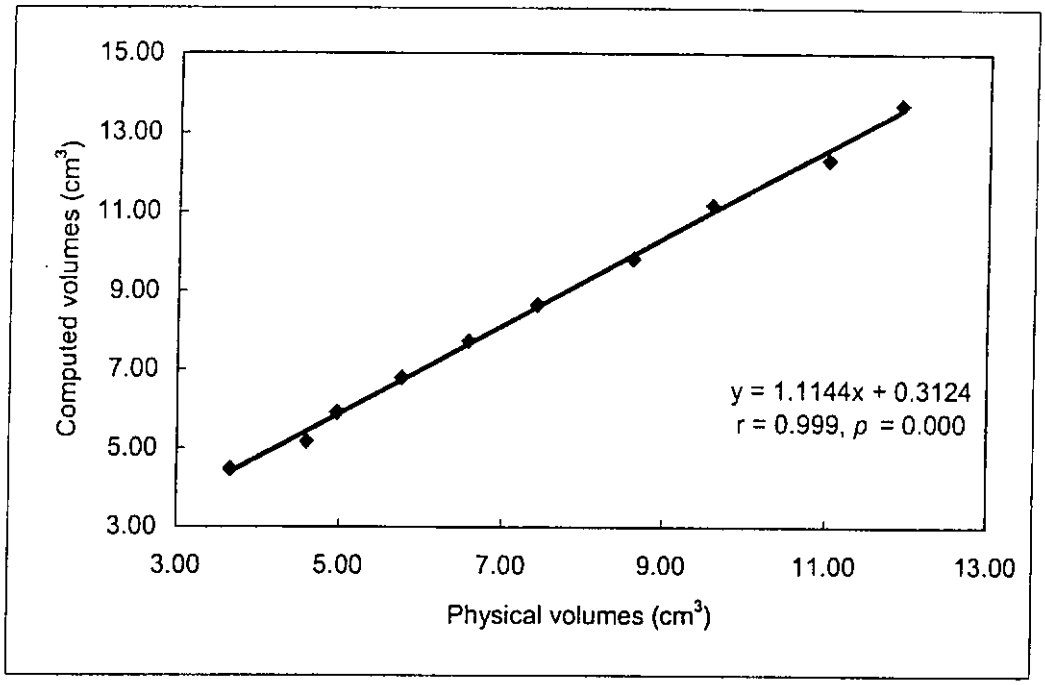

Fig 3.3 Correlation between physical volumes and computed volumes of silicon balls

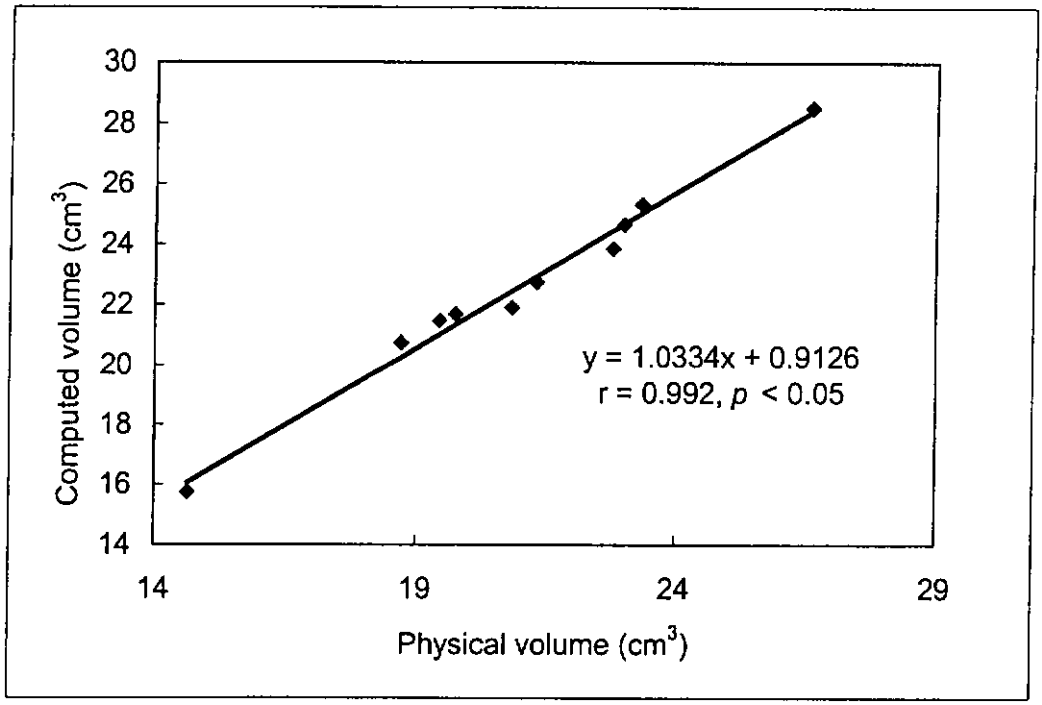

Fig 3.4 Correlations between physical volumes and computed volumes of silicon moulds

Despite the high correlation, the agreement plot in Figure 3.5 shows that with larger object volumes, there is an increase in the difference between the computed and physical volumes. From this plot, a correction factor can be derived for the computed volume so that it will better match the physical volume.

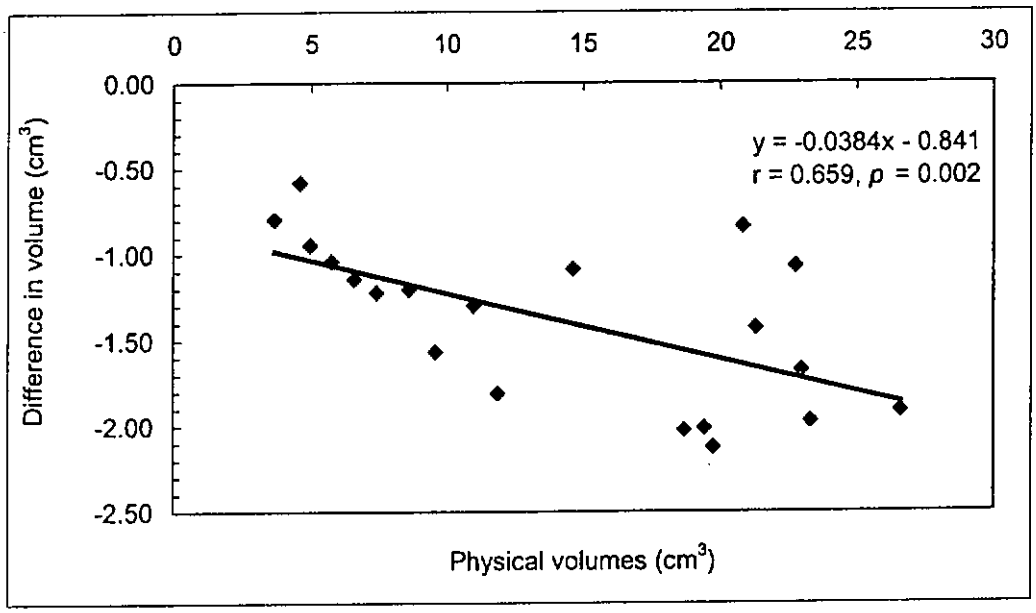

Fig 3.5. Agreement curve of 1 T scanner

3.1.4 Discussion

The orbit is an ideal organ for MR imaging because of the wide variation in water content of its various tissues (Mafee et al., 1996). Apart from orbital volume measurement, orbital soft tissue, extraocular muscle and orbital fat can also be measured using thin MRI slices (Tian et al., 2000).

We are not aware of previous calibration studies focused on orbit and eyeball volumes using MR images. McGurk et al. (1992) and Deveci et al. (2000) have reported two calibration studies on orbit volume using CT. Compared with their studies, our study found a higher correlation between the computed and physical volumes ($r = 0.99$). The reproducibility of the method used for orbital volume determination in our study was also higher (CV = 0.95%) than the one found by McGurk et al (1992) (CV = 1.3%). However, the mean difference between the physical and computed volumes in our study was larger (1.55 ± 0.44 cm^3 and 1.61 ± 0.00 cm^3 for 1.5 T and 1 T scanners respectively) than the one by Deveci et al (2000) (0.93 ± 1.08 mL). The discrepancies in orbital volume found in this study could be attributed to the tracing of the ROI, especially in the identification of the anterior border of the orbit in the MR image.

The accuracy of the computed volume depends on the exact matching of the ROI with the object. The ROI on the displayed image was drawn freehand in our

study. This is one source of error. We minimized this error by repeating the tracing of the ROI several times and averaging the results. We also used thin image slices (1.5 mm) to reduces the partial volume averaging effect in the images (Rubin and Phillips, 1991). Image error due to distortions produced by the process of digitizing hard copies of images were minimized by working with digital images taken directly from the MR workstation and transferred to CD-ROM for offline analysis.

Despite the high correlation between the computed and physical volume, the agreement plot (Figure 3.5) shows a systematic error and the correction formula required to produce a better match between the computed and physical volumes.

To produce a high contrast phantom image, the phantoms are usually immersed in water or a contrast medium (Disler et al., 1994, Duong et al., 1992, Qin et al., 1990, Rubin and Phillips, 1991). However, the immersion of the phantom in fluid may give rise to air bubbles formation (Figure 3.1). These bubbles may attach to the surface of the phantom and create irregular borders. This causes errors in the generation of the ROI, especially when the 'automatic detection' function is used. Manual tracing of the ROI can minimize distortion errors caused by bubbles but in our experience, the tracing error caused by bubbles is still significant, particularly for smaller volumes. Ideally, the bubbles should be removed before scanning is commenced.

Disler et al. (1994) showed in their study that high-contrast images yielded higher accuracy in volume determination. Consequently, for eyeball volume determination, T2-weighted images are better than T1-weighted images because the eyeball image appears bright with a very sharp edge against the surrounding orbital fat and muscles on T2-weighted images in real human subject (Daniel and Mitchell, 1999) . This concurs with our experience. The tracing of the eyeball ROI was easier on T2-weighted images than on T1-weighted images.

3.1.5 Conclusion

We conclude that using MR imaging, it is possible to estimate eyeball and orbit volumes to a degree of accuracy comparable to that of CT imaging.

3.2. Calibration of 1.5T scanner (QMH)

3.2.1. Introduction

Our studies were conducted in two hospitals and these hospitals have different MRI scanners. The previous section discussed, in general, the techniques used for our calibration studies. Results from the 1 T scanner used in Queen Elizabeth Hospital (QEH) were presented. In this section, the results from the 1.5 T scanner used in Queen Mary Hospital (QMH) are presented.

3.2.2 Materials and methods

This calibration used the orbit mould phantom only because the data we obtained from QMH were for the purpose of an orbit volume study (Chapter 4).

3.2.2.1 MRI scan

The orbit mould phantom was examined in a 1.5 T MRI scanner (Siemens Magnetom Impact EXPERT, Erlangen, Germany) with a head coil. Contiguous 3 mm thick T2-weighted sequence (TR/TE = 5960/81.92 ms) was used. The image matrix used was 256x256. All images were stored in a compact disc in DICOM format for offline analysis.

3.2.3 Results

Table 3.3 shows the computed volume and physical volume for the orbit mould phantom. The computed volume and physical volume of the silicon moulds ranged from 13.8 to 24.2 cm^3 and 14.7 to 26.6 cm^3 respectively.

Table 3.3. Comparison between the OSIRIS computed and measured physical volumes. R1 to R10 are the silicon moulds scanned using a 1.5T scanner.

Phantom	Mean computed vol ± SD (cm^3) (A)	CV (%)	Mean physical vol ± SD (cm^3) (B)	CV (%)	Difference (B-A)	Error (%) $\frac{(B-A)}{B}$ X 100%
R1	13.78 ± 0.36	2.65	14.65 ± 0.00	0.01	0.87	5.92
R2	17.32 ± 0.20	1.17	18.70 ± 0.00	0.00	1.38	7.39
R3	17.74 ± 0.20	1.13	19.44 ± 0.00	0.00	1.70	8.74
R4	18.53 ± 0.22	1.20	19.75 ± 0.00	0.01	1.22	6.20
R5	19.21 ± 0.17	0.87	20.83 ± 0.00	0.00	1.62	7.78
R6	19.24 ± 0.18	0.96	21.31 ± 0.00	0.01	2.08	9.74
R7	21.32 ± 0.26	1.23	22.78 ± 0.00	0.01	1.46	6.43
R8	21.77 ± 0.43	2.00	22.99 ± 0.00	0.01	1.22	5.30
R9	21.79 ± 0.32	1.48	23.33 ± 0.00	0.00	1.54	6.61
R10	24.17 ± 0.32	1.33	26.59 ± 0.00	0.01	2.42	9.09

Figure 3.6 shows the correlation between physical volume and computed volume for the orbit mould phantoms ($r = 0.99$, $p < 0.05$).

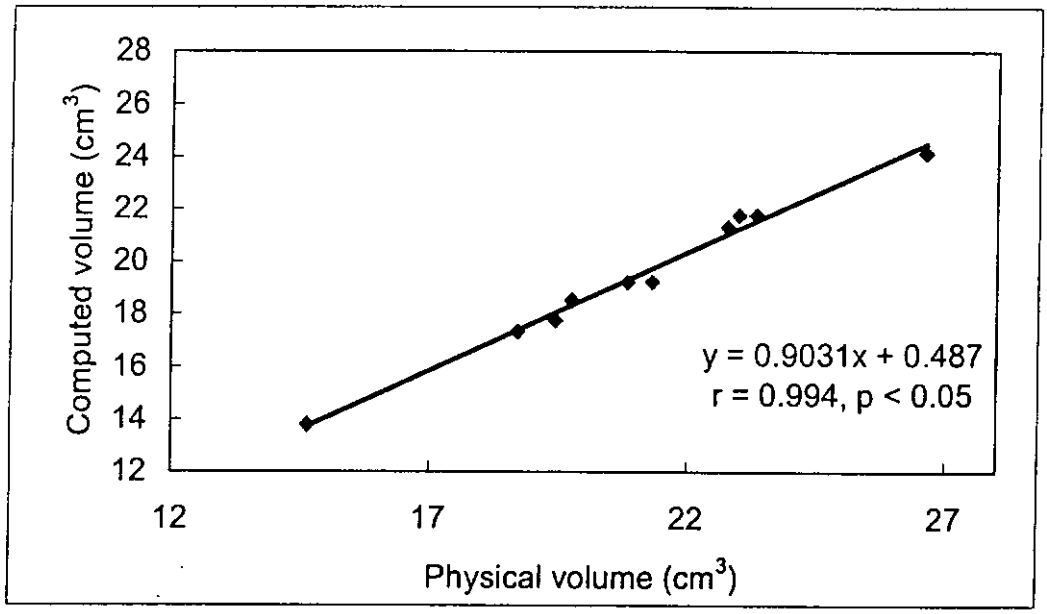

Fig 3.6 Correlations between physical volumes and computed volumes of silicon moulds.

The agreement plot (Fig 3.7) shows that the computed volume was smaller than the physical volume. There is an increase in the difference between the computed and physical volumes when the mould size increased. A correction factor can be derived for the computed volume from this plot.

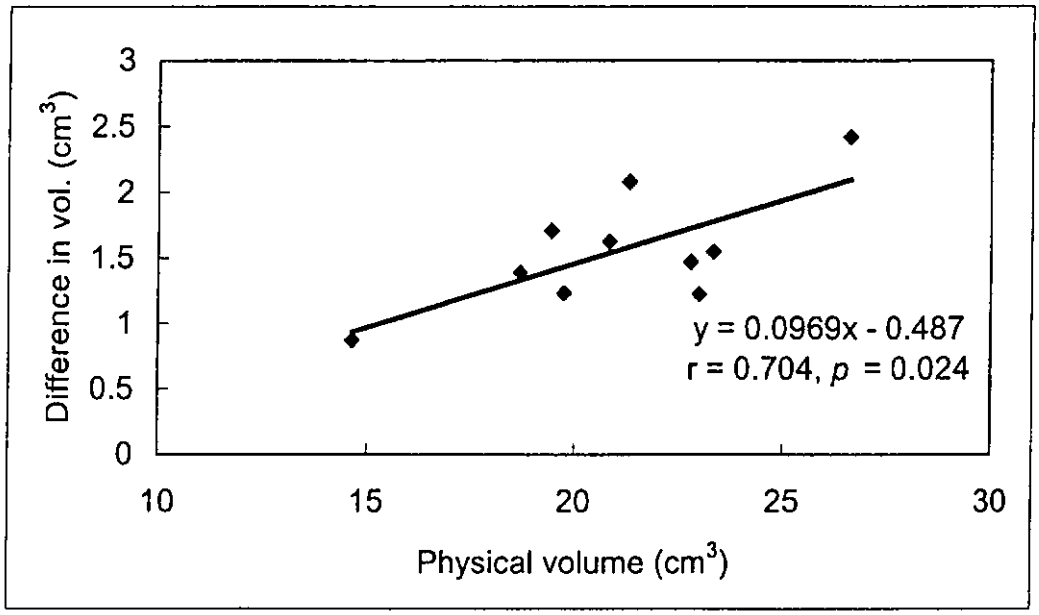

Fig 3.7. Agreement curve of a 1.5 T scanner

3.2.4 Discussion

When we compared the volumes of the orbit mould phantom derived from different scanners, an overestimation of volume was found for the 1 T scanner while an underestimation was found for the 1.5 T scanner. This suggests that using different scanners and scanning protocols could produce variations in volumetric determination. Therefore, a calibration test of individual scanners and scanning protocols is essential to ensure accuracy in volumetric studies.

Chapter 4 Orbital development in Hong Kong Chinese (Study 1)

4.1 Introduction

From birth to adulthood, the orbit is known to enlarge in proportion to the growth of the skull. This enlargement serves the purpose of accommodating a growing eyeball which almost doubles in volume from childhood to adulthood (Curtin, 1985, Day, 1997, Gossman et al., 1999).

Orbit development is very rapid soon after birth. From the first few months of life to the early teens, orbit volume increases almost linearly from about 13 – 15 cm^3 to 24 – 26cm^3 (Bentley et al., 2002). Orbit volume remains fairly constant beyond about 15 to 17 years of age (Furuta, 2001, Waitzman et al., 1992). The female orbits appear to reach adulthood earlier than the male orbit (Furata, 2001). Comparing the data of Furata (2001) and Bentley et al. (2002), orbit volume in Japanese subjects (20 to 23 cm^3) appears smaller than that reported for Caucasian subjects (24 to 26 cm^3). However, differences in the methodology used in the two studies cannot be ruled out as a factor contributing to this possible ethnic difference.

Since there are racial differences in head dimensions, interpupillary distance and palpebral fissure width (Barretto and Mathog, 1999, Quant and Woo, 1993), it is reasonable to expect possible race-related variations in the orbit. However, to the best of our knowledge, there is no literature on the growth of the orbit in Chinese.

The purpose of this study is to examine the development of the orbit in Hong Kong Chinese subjects.

4.2 Materials and methods

4.2.1 Process of data collection

The data collection of this study consisted of two parts, and totally 81 eyes were studied. The first part involved a retrospective review of head MRIs of children subjects who were below 18 years old at the time of their scans. This part was done in collaboration with the Queen Mary Hospital in Hong Kong. For the second part, we used the data from adult subjects who had participated in Study 2 (Chapter 5) of this thesis. No additional scanning was done. The data from this part were analyzed together the data from children.

4.2.2 Entry criteria of children subjects

A retrospective search of the radiological database at Queen Mary Hospital for patients aged below 18 years at the time of their MRI scan was conducted. Patients who had conditions which interfered with the eye and orbit such as thyroid disease or blow-out fractures were excluded. The refractive status of the subjects was unknown.

4.2.3 MRI orbit imaging for child subjects

The MR orbit scan was performed with a head coil on a 1.5 T MRI scanner (Genesis, Signa, GEMS, Milwaukee, WI). Axial images which were 3 mm thick and had 0 to 0.5 mm inter-slice spacing were obtained. Three scans (scout, T1 and T2-weighted) were performed on each subject. T1 (TR/TE = 500 – 720/9.8 – 10 ms) and T2-weighted images (TR/TE = 3200 – 4060/31.6 – 96 ms) were obtained. Each scan took approximately 3.5 minutes. Image resolution of matrix 256 x 192 with 16 cm field of view was set. All images were stored in a compact disc in DICOM format for offline analysis.

4.2.4. Volumetric measurement

Image analysis was conducted using the OSIRIS software (Ligier et al., 1994) which ran on an IBM-compatible personal computer using MS Windows XP with a 15" LCD monitor.

A calibration study was conducted to ensure that the results from the digital images were comparable with physical volumes (see Chapter 3). A correction factor was derived and applied to the computed volumes found.

Orbital volume determination

Using the Polygon Regions of Interest (ROIs) function in OSIRIS, orbital volumes were found by drawing ROI manually on each T1-weighted MR orbit scan with a stylus. The posterior boundary of the orbit was defined by a line connecting the medial and lateral walls of the optic foramen within the orbit. The anterior boundary was defined by a line joining the medial and lateral canthi or the corresponding most anterior bone edges of the medial and lateral orbital walls. The optic canal was excluded during drawing. After defining the orbit areas on a whole series of T1-weighted MR orbit scans, and by the use of multiple ROI volume function in OSIRIS, the volume was generated. Results were displayed on a separate window, including an interactive three-dimensional representation of the ROI over the set of images. Measurement was repeated in the same way a

further four times and the average taken. The left orbit of each subject was chosen to be measured in this study.

4.3 Data analysis

The data collected were processed by the SPSS/ version 10.0.1 statistical software (SPSS Inc. IL). Differences in orbital volumes between gender were analysed using the unpaired t-test. Correlations between different parameters were tested by Pearson's method. All reported significance levels are two-tailed and $p < 0.05$ is considered statistically significant.

4.4. Results

In total, data from 81 subjects, aged from 1 to 42 years (mean age = 15.00 ±10.02 years), were included in this study. Forty-three were females and 38 were males. The orbit volume ranged from 11.56 cm^3 to 25.50 cm^3.

For analysis purposes, those subjects who were aged from 1 to 10 years old were considered as "children" while those who were aged beyond 18 years old were classified as "adults". The remaining subjects were regarded as "teenagers". For the children group, there were 19 girls and 15 boys and their mean ages were 5.21 and 5.18 years old respectively. There was no gender difference in orbit volume ($t = -0.017$, $p > 0.05$, unpaired t-test). For the adult group, there were 18 females and 17 males. The mean age for males and females showed no significant difference (female = 24.78 years, male = 25.35 years) ($t = -0.315$, $p > 0.05$, unpaired t-test) but the mean male orbit volume was significantly larger (2.53 cm^3 larger) than the mean female orbit volume ($t = -3.95$, $p < 0.05$, unpaired t-test). The distribution of "orbit volume" (y) against "age of subjects" (x) is shown in Figure 4.1. In order to show the pattern of orbit development in our subject sample, an S-curve was fitted using a straight line format of y against the normal density function of x. The normal density function of x was calculated using the NORMDIST function in Microsoft Excel spreadsheet.

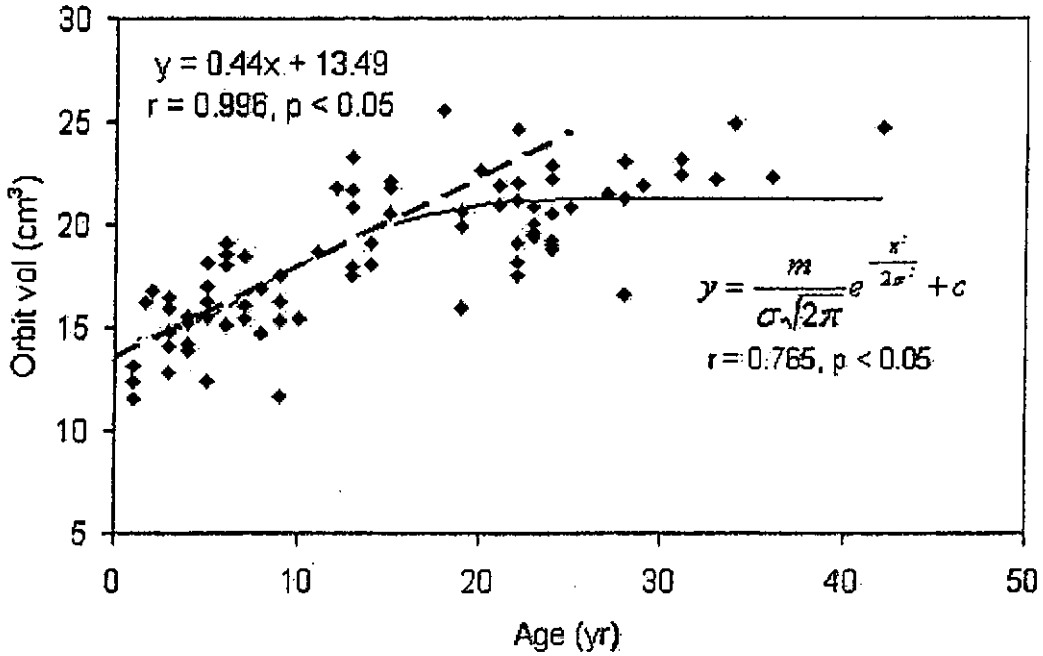

Fig 4.1 Orbit growth pattern of Hong Kong Chinese (where m = -141.8889, c = 21.2749, σ = 512/63)

At 1 year of age, the mean size of the orbit was around 12 cm^3. At the age of 5 years, the volume reached 15.88 cm^3, and at 15 years of age, it was 20.24 cm^3. After the age of 15 years or thereabouts, the rate of orbit development slowed down and reached a steady state at around the age of 20 years. The development of the orbit appeared fairly linear in the first 15 years of life.

Figure 4.2 shows the orbit volumes of our subjects who were aged 15 years and those of a similar age range from Bentley et al (2002)'s study.

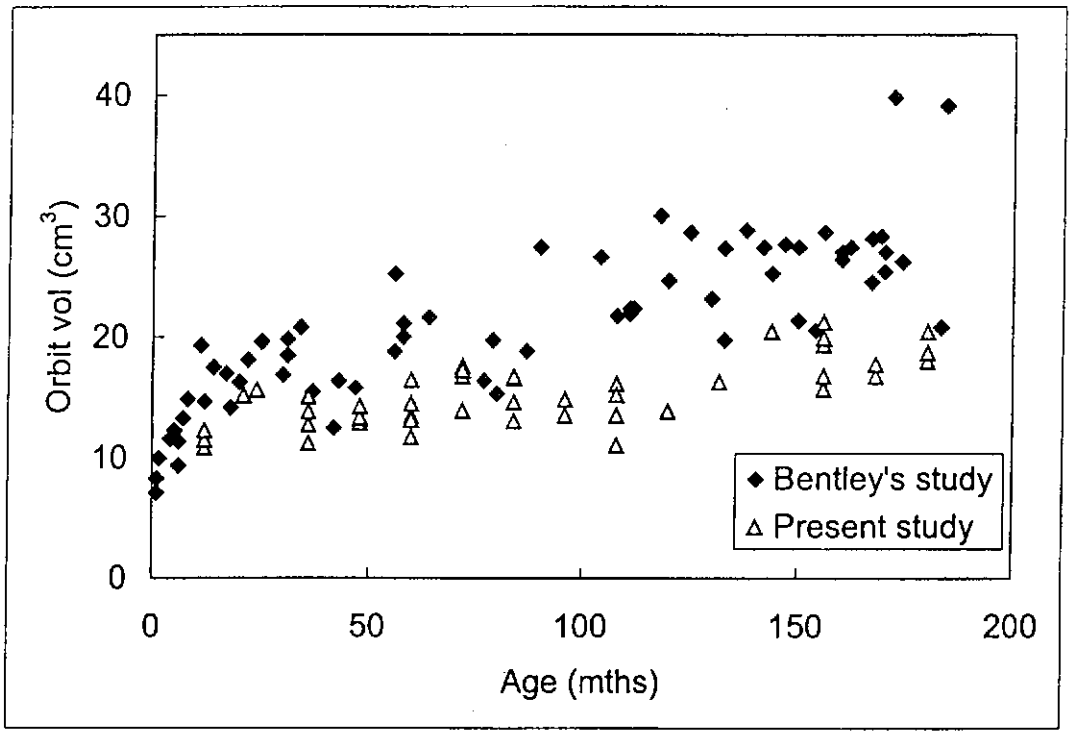

Fig 4.2 Scatter plot showing the orbit volumes found in our study and Bentley (2002)'s study.

In total, there were 46 subjects (20 boys, 26 girls) in our study while there were 38 boys and 29 girl in Bentley et al (2002)'s study. From Figure 4.2, we can see that the orbit volumes of our subjects were, on the whole, lower than those of Bentley et al (2002)'s.

For adult subjects who were aged from 18 to 40 years old, a comparison of their orbit volumes was made with those from Furuta (2001). Since Furuta (2001) did not present raw data, the comparison will be made on averaged data (Table 4.1).

Study	Gender	No. of subjects	Orbit volume±SD (cm3)	Unpaired t-test
Present study	M	16	22.20±1.38	t = 2.4858
Furuta's study		24	23.64±2.02	p < 0.05
Present study	F	18	19.81±2.23	t = 1.3386
Furuta's study		9	20.89±1.28	p > 0.05

Table 4.1 Comparison between the present study and Furuta (2001).

4.5 Discussion

To the best of our knowledge, our study provides a first model of growth of the orbit in Hong Kong Chinese. It shows the trend and rate of the growth of the orbit and also the mean orbital volume for different age groups.

In order to estimate the age of maturity of orbit growth, two straight lines were fitted into Figure 4.3 using the Solver module in Microsoft Excel. We assumed the slope of line in the adult region was zero because it is known that the orbit does not keep growing after maturity. Our results show the age of maturity of orbit growth was 16.1 years old, which is a little older than those suggested by Furuta (2001) (i.e. 10.9 years for females and 14.9 years for males). The pattern of growth of the orbit has a parallel in the inter-pupillary distance (PD) (Figure 4.4). That this is so is not surprising as the PD indirectly reflects the inter-orbit distance and this in turn is related to skull development.

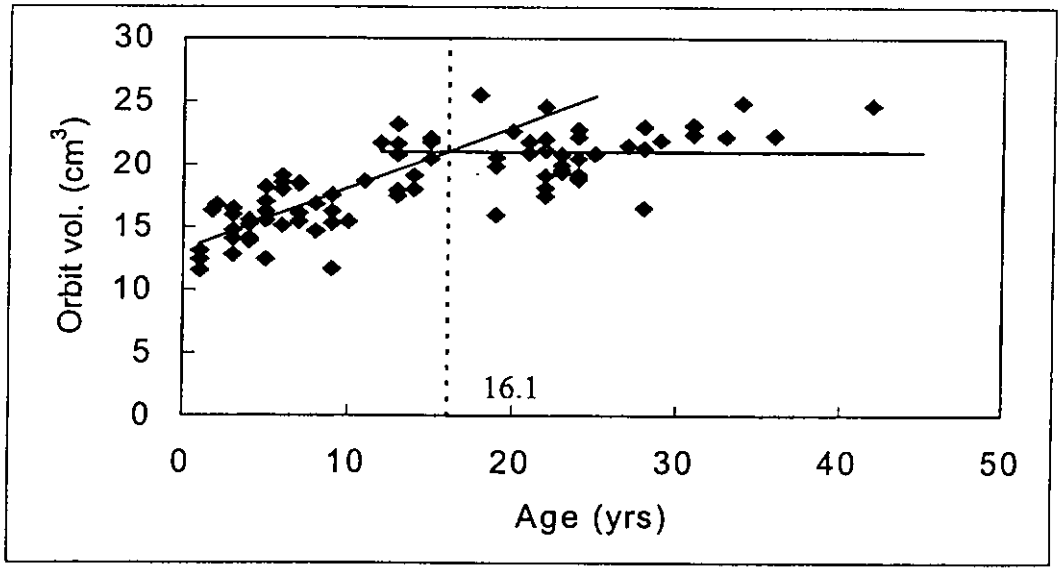

Fig. 4.3 Age of maturity of orbit development found in this study.

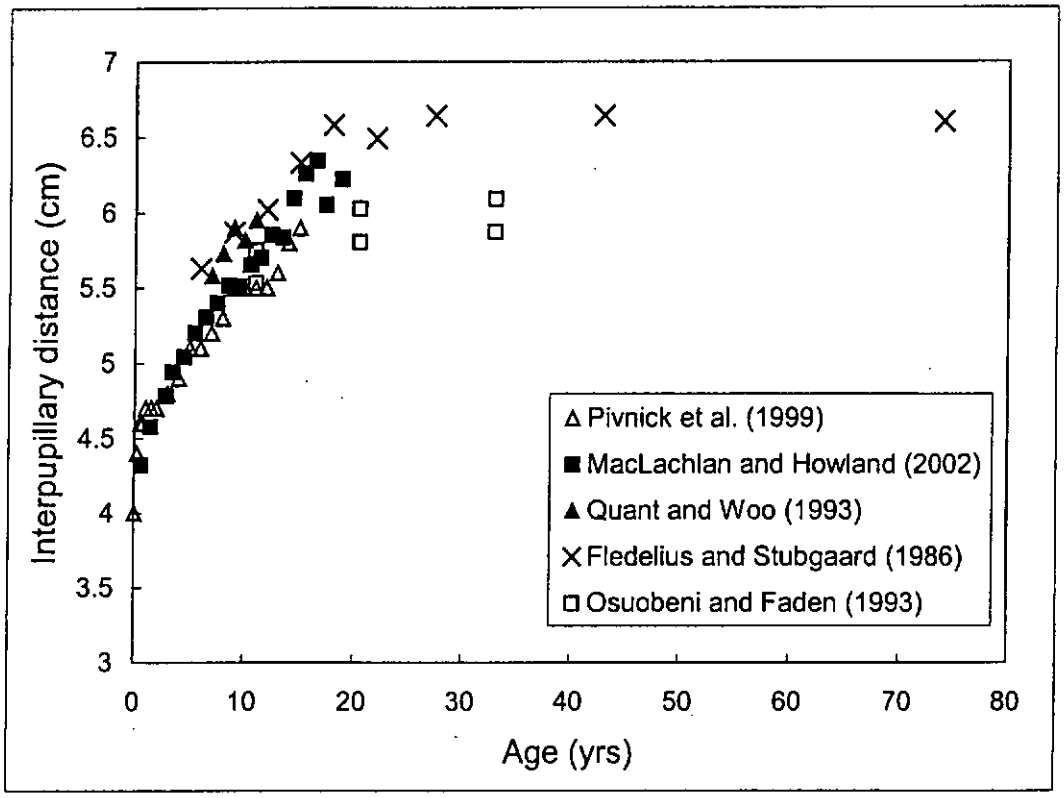

Fig 4.4. Summary of interpupillary distance changes found in other studies.

Compared with the data from Bentley et al (2002) and our study for subjects who were under 15 year olds, it is obvious that the orbit volumes of our subjects were smaller. Since Bentley et al (2002) subjects were mainly Caucasian and our subjects were all Hong Kong Chinese, and the fact that Bentley et al (2002) also used MR images to determine orbit volumes, the difference in orbit volume found could be due to race. However, we cannot rule out other factors such as the image analysis techniques used. In addition, it is unclear whether Bentley et al (2002) calibrated their techniques in the way that we did. Furthermore, for those subjects in our study who were 18 years of age or under, the data we used were retrospective clinical data. These subjects had their MRI scan for clinical reasons. Although our exclusion criteria included conditions

which are known to have an obvious effect of the eye or orbit, some subjects in our final subject pool were referred for MRI scanning because of suspected neurofibromatosis. Although we have excluded confirmed cases, we cannot rule out the possibility that some subjects in our subject pool may go one to develop the condition. Neurofibromatosis is known to have skeletal involvement, including the orbit.

We compared the orbit volume data from our subjects who were aged from 18 to 40 years old with those presented in Furuta (2001)'s study. Male subjects in Furuta (2001)'s study had a significantly larger orbit volume than those in our study but female subjects did not show any significant difference. The orbit volume measurement in Furuta (2001)'s study was done on computed tomography images and no calibration was mentioned in the study. Any difference found should be interpreted in the context of these methodological constraints.

4.6 Conclusion

Orbit volume increases almost linearly from infancy to about the late teens, beyond which it levels off. During this period of development, the orbit doubles in volume.

Chapter 5 Relationship between orbit and eyeball size and myopia (Study 2)

5.1 Introduction

A recent chick study showed that ocular refractive development was associated with orbit development (Wilson et al., 1997). A larger chick eye was associated with a larger orbit. This phenomenon has not been described in humans. However, it is possible that a larger eyeball in early childhood years may influence orbit growth, given that the walls of the orbit are still developing.

It is known that body growth generally reaches a plateau at around the age of 15 years (Bishara, 2000). It has been suggested that orbit growth follows the growth pattern of the whole body skeleton and is related to the growth of the eyeball (Ranly, 2000). Results from a study of 109 Japanese subjects aged from infancy to over 66 years old, showed that orbit growth reached maturity at around the age of 15 years (Furuta, 2001). No difference between the orbit development of boys and girls was found (Bentley et al., 2002, Furuta, 2001).

It is known that orbit volume is increased in buphthalmos and decreased in anophthalmia compared to the fellow orbit with a normal eye (Heinz et al., 1998). Orbit volume decreases after enucleation, presumably due to the absence of intraorbital tissue, but the volume can be maintained by means of orbital implants (Cepela et al., 1992, Eppley et al., 1993, Fountain et al., 1999, Hintschich et al.,

2001, Lo et al., 1990). Changes in orbit volume in response to eye size or absence of the eye were generally more pronounced in children than in adults (Hintschich et al., 2001).

We wanted to find out whether eye size and orbit size in human subjects were related.

5.2 Materials and methods

5.2.1 Subjects

Thirty-three adults aged 19 to 42 years (mean age = 25 ± 5.2years) with SER ranging from +1.00D to -12.75D, who had no pathologic interference of the eyes and orbits, were recruited as subjects. Informed consent was obtained from all subjects.

5.2.2 Methods

5.2.2.1. Ethical Approval

Ethical approval for this study was obtained from the Human Subjects Ethics Subcommittee of The Hong Kong Polytechnic University.

5.2.2.2. Vision examination

All subjects underwent a vision examination by a registered optometrist. Axial length was measured using an ophthalmic ultrasound A-scan unit (Mentor Advent^{TM}, USA). Objective cycloplegic refractions (0.5% Cyclopentolate HCL) were obtained using a Shin-Nippon SRW-5000 open-field IR autorefractor (Shin-Nippon, Tokyo, Japan).

5.2.2.3. MR imaging protocol

The orbits of each subject were examined in a 1 T MRI scanner (Siemens Magnetom Impact EXPERT, Erlangen, Germany) with a head coil. Contiguous unenhanced three dimensional FLASH (Fast low angle shot, TR/TE=27/5ms) T1-weighted sequence and CISS (Constructive interference in steady state, TR/TE=16/8ms) T2-weighted sequence were performed, with matrix 256x256 and slab thickness 105mm. Each scan took approximately 18 minutes. During the scan, subjects were asked to close their eyes in order to minimize eye movements. All images were stored in a compact disc in DICOM format for offline analysis.

5.2.2.4. Head dimension measurement

The head dimensions of subjects were measured using a set of clinical callipers. Skull length, breadth and height were measured.

5.2.2.5. Age of onset of myopia

We asked the "age of onset of myopia" from each subject. This was defined as the age when spectacles were first prescribed to correct distance vision. With the high prevalence of myopia in Hong Kong, it is common for people to know for what purpose their spectacles were prescribed. This method has been found to be a reliable one since the first set of myopia spectacles marks a strong emotional experience (Fledelius, 1995). We defined early-onset myopia as myopia

onset before aged 15 years old (Bullimore et al., 1992, McBrien and Millodot, 1987).

5.2.3 Volumetric measurement

All image analyses were done using the OSIRIS software (Ligier et al., 1994) which ran on an IBM-compatible personal computer using MS Windows 98. The computer was connected to an over-head LCD projector. Images were projected on a screen to a size of 1.2 m x 1.6 m. To check the accuracy of the OSIRIS software, a calibration study was conducted. Spheres of known sizes (range 21 to 30 mm in diameter) and orbit phantoms were scanned using the MR scanner and the resultant images used to determine computed volumes. These computed volumes were then compared to the physical volumes of the spheres and orbit phantoms. A correction factor was derived and applied to the computed volumes found in the rest of this study.

5.2.3.1 Orbit volume determination

Using the Polygon Regions of Interest (ROIs) function in OSIRIS, orbit volumes were found by drawing ROI manually on each T1-weighted MR orbit scan using a stylus on drawing tablet connected to the computer. The posterior boundary of the orbit was defined by a line connecting the medial and lateral walls of the optic foramen within the orbit. The anterior boundary was defined by a line joining the medial and lateral canthi or the corresponding most anterior bone edges of the medial and lateral orbital walls (Bentley et al., 2002, Deveci et al., 2000, Eppley et al., 1993, McGurk et al., 1992). The optic canal was excluded (Fig. 5.1).

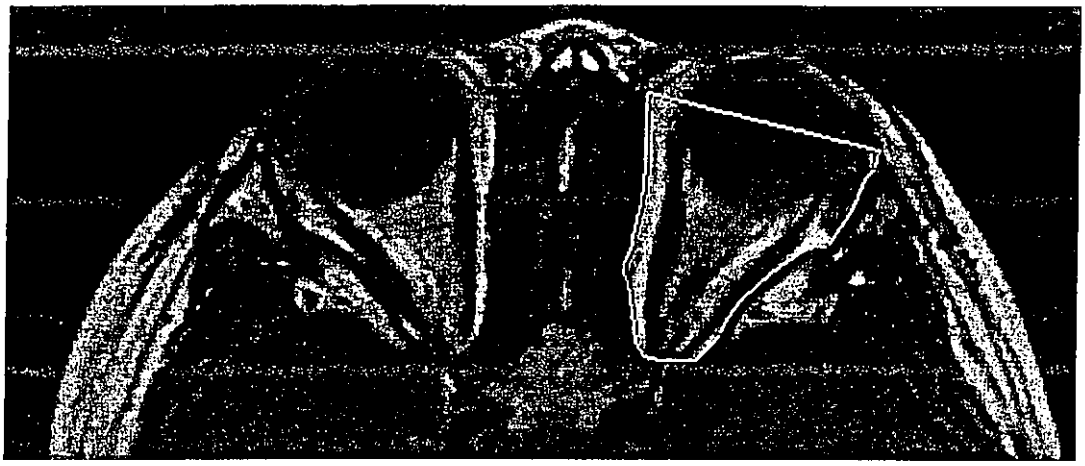

Fig 5.1. ROI was manually drawn around the left orbit border on an axial T1 MRI orbit image.

After defining the orbit areas on a whole series of T1-weighted MR orbit scans, and by the use of the multiple ROI volume function in OSIRIS, the orbit volume was generated. Results were displayed on a separate window, including an interactive three-dimensional representation of the ROI over the set of images. Measurement was repeated in the same way a further four times and the average taken.

5.2.3.2. Eyeball volume determination

The eyeball volume was determined using the image segmentation function in OSIRIS. Segmentation is the process of subdividing an image into regions based on their pictorial characteristics, which helps to define the boundaries of different structures. In this study, the automatic region growing method was used since the eyeball has a well-defined border and its gray values differ from surrounding tissues on T2-weighted images.

The "region growing" segmentation method starts with a seed point, and becomes a region by appending neighbours which have similar properties such as gray level or texture. During measurement, seed planting and tolerance adjustment were done on each T2-weighted MR orbit image. A closed polygon was generated enclosing the eyeball area on each slice (Fig. 5.2).

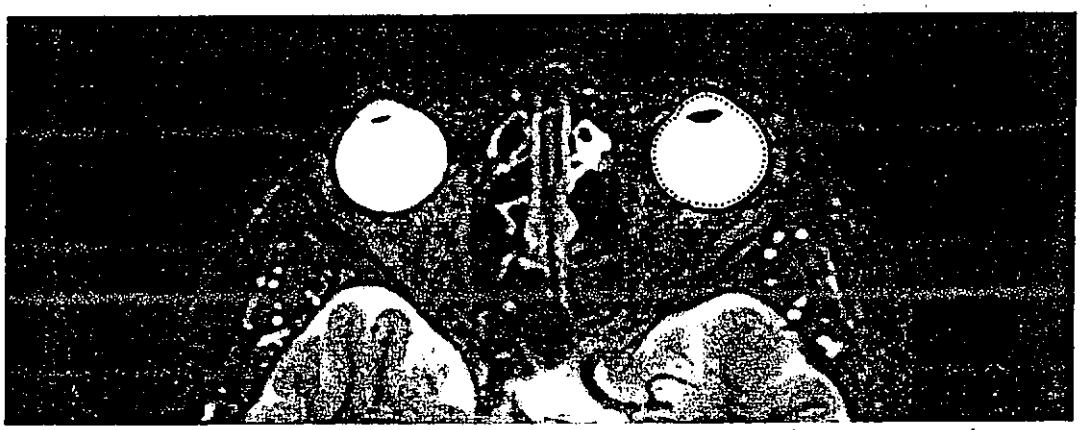

Fig 5.2. ROI was determined automatically by the seed growing segmentation technique on the left eyeball on an axial T2-weighted MRI orbit image.

After defining the eyeball areas on a whole series of T2-weighted MR orbit scans, and by the use of multiple ROI volume function in OSIRIS, the volume was generated. Results were displayed on a separate window, including an interactive three-dimensional representation of the ROI over the set of images. Measurement was repeated four more times and the average found.

5.3 Data analysis

The data collected were processed using the SPSS/ version 10.0.1 statistical software (SPSS Inc. IL). Differences of eyeball and orbit volumes between genders were analysed using the unpaired t-test. Correlations between different parameters were tested by the Pearson's method. All reported significance levels are two-tailed and $p < 0.05$ is considered statistically significant.

5.4 Results

Thirty-three adults completed the study (17 females, 16 males) and results from the left eyes are presented. The spherical equivalent refraction (SER) ranged from +1D to –12.75D. All myopic subjects reported myopia onset before aged 15 years (i.e. early-onset myopes). The age of myopia onset was significantly related to the SER ($r = 0.71$, $p < 0.005$) (Fig. 5.3). Subjects with myopia onset at the age of 4 to 8 years old ($n = 6$) had a mean refractive error of about –9.00D while subjects with myopia onset at the age of 13 to 16 years old ($n = 6$) had a mean refractive error of about –3.00D. Our data support the findings of Fledelius (1995) who first made this observation.

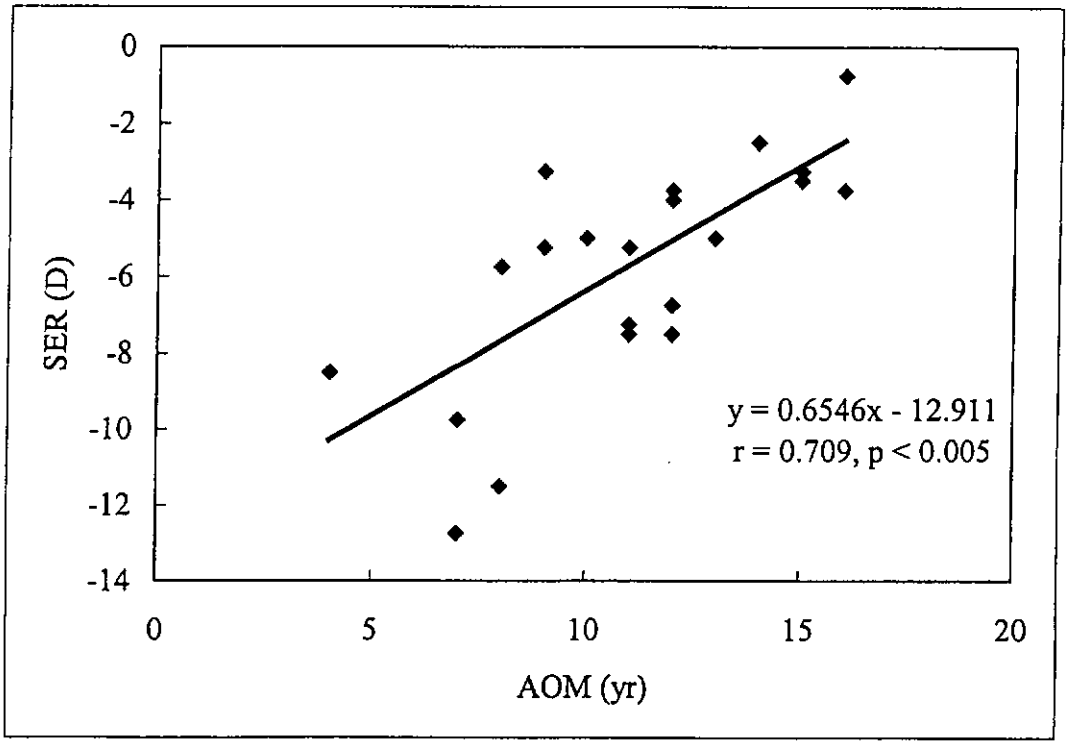

Fig 5.3 The relationship between spherical equivalent refraction (SER) and age of onset of myopia (AOM).

Table 5.1 presents the data for all subjects. The axial lengths and volumes of eyeballs ranged from 22.63 mm to 28.43 mm (mean axial length = 25.34 ± 1.61 mm) and 5.11 cm^3 to 8.83 cm^3 (mean volume = 6.70 ± 0.91 cm^3) respectively. Orbit volumes ranged from 15.96 cm^3 to 24.89 cm^3 (mean volume = 20.94 ± 2.19 cm^3). The axial lengths and volumes of the eyeballs showed no significant gender effects ($p > 0.05$). However, orbit volume was significantly greater in males than females ($t = -3.57$, $p < 0.05$).

Subjects	Gender/ Age	SER (D)	AOM	Axial length (mm)	Eyeball volume ± SD (cm^3)	Orbit volume ± SD (cm^3)	Skull height (cm)	Skull Length (cm)	Skull breadth (cm)
1	F/19	-7.25	11	25.80	6.79±0.02	15.96±0.13	13.45	17.2	15.8
2	F/19	-5.75	8	25.69	7.01±0.00	20.60±0.11	11.9	17.6	15.1
3	F/22	-12.75	7	27.57	7.61±0.02	17.49±0.14	12.4	17.9	15.3
4	F/22	-1.50	N/A	23.34	5.11±0.02	18.11±0.20	13.6	18	15.6
5	F/22	-3.75	12	25.40	6.98±0.01	19.07±0.12	11.15	17.85	15.7
6	F/23	-11.5	8	28.43	7.20±0.02	19.33±0.04	12.4	17.9	16.1
7	F/23	-5.25	11	26.32	7.34±0.00	19.61±0.29	13.4	17.2	15
8	F/24	-2.50	14	25.01	6.22±0.02	18.77±0.12	13.8	18.7	15.2
9	F/24	-5.75	8	24.50	6.78±0.01	18.94±0.16	14.2	18.2	16.1
10	F/24	-7.50	11	27.51	7.33±0.00	19.17±0.15	13.2	18.1	15.6
11	F/24	0.75	N/A	24.22	6.79±0.05	20.48±0.12	13.5	16.5	15.7
12	F/25	-3.50	15	26.39	6.84±0.03	20.85±0.23	13.5	18.9	16.2
13	F/27	-9.75	7	27.19	7.57±0.03	21.49±0.36	9.6	19.1	15.8
14	F/28	-0.50	N/A	23.68	5.54±0.02	16.52±0.18	11.6	17.7	15.5
15	F/31	0.75	NA	23.22	5.58±0.05	23.12±0.18	13.9	17.9	16.5
16	F/34	-0.75	16	24.00	6.70±0.11	24.89±0.12	14	18.2	15.6
17	F/36	-7.50	12	27.22	8.83±0.03	22.30±0.17	15.4	19	15.6
		-4.94		*25.62*	*6.84±0.88*	*19.81±2.3*	*13*	*18.00*	*15.67*
18	M/20	-3.25	9	25.27	6.35±0.01	22.63±0.21	13.5	18.85	16.3
19	M/21	0	N/A	23.20	5.56±0.03	20.93±0.14	10.7	18.6	16.4
20	M/21	-5.00	13	26.55	7.13±0.03	21.82±0.26	15.2	18.3	16.1
21	M/22	0	N/A	23.64	6.00±0.01	21.17±0.41	12.8	19.3	16.6
22	M/22	-5.00	10	26.52	7.40±0.04	22.02±0.16	13.6	20	15.6
23	M/22	-5.25	9	26.66	6.73±0.03	24.57±0.35	14	18.7	16.2
24	M/23	0.25	N/A	22.91	5.54±0.06	19.86±0.21	13	18.4	16.1
25	M/23	1.00	N/A	23.25	5.49±0.01	20.81±0.11	13.8	17.7	15.7
26	M/24	0.25	N/A	22.63	5.39±0.01	22.17±0.08	13	18	15.9
27	M/24	-8.50	4	27.59	8.40±0.01	22.72±0.17	14.5	19.4	16.3
28	M/28	-3.75	16	25.28	7.11±0.02	21.29±0.27	14.8	18	16.4
29	M/28	0	N/A	23.72	5.18±0.02	22.99±0.21	14.9	20.1	16.6
30	M/29	-4.00	12	25.58	6.59±0.03	21.91±0.38	12.8	18.7	16.7
31	M/31	-6.75	12	26.15	7.07±0.03	22.41±0.26	13.4	20	16.5
32	M/33	-3.75	12	26.19	7.53±0.03	22.22±0.47	14.8	19.7	16.2
33	M/42	-3.25	15	25.50	7.27±0.03	24.67±0.15	15.3	21.3	16
		-2.94		*25.04*	*6.55±0.94*	*22.14±1.26*	*13.76*	*19.07*	*16.23*

Table 5.1. Distribution of refractive errors of all subjects with their corresponding age of myopia onset (AOM), axial length, eyeball volume, orbit volume and skull dimensions. Mean values of the measurements of female and male are in italic.

The relationship between SER and axial length ($r = -0.91$, $p < 0.05$) and volume of eyeball ($r = -0.76$, $p < 0.05$) of the subjects can be seen in Figures 5.4a and 5.4b. The correlation between axial length and eyeball volume was 0.86 ($p < 0.05$). However, orbit volume was poorly correlated with eyeball volume ($r = 0.13$, $p > 0.005$) (Fig. 5.5). Orbit volume was also poorly correlated with axial length and SER ($r = -0.11$. $p > 0.05$; $r = 0.201$, $p > 0.05$ respectively).

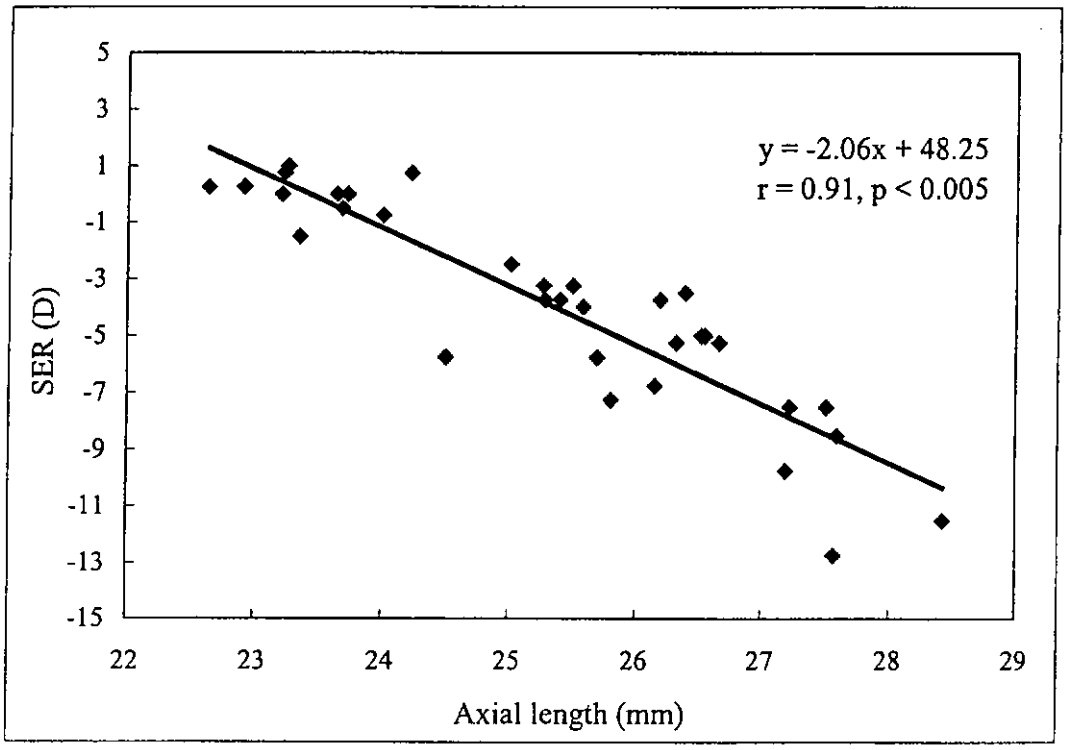

Fig 5.4a. The relationship between SER and axial length.

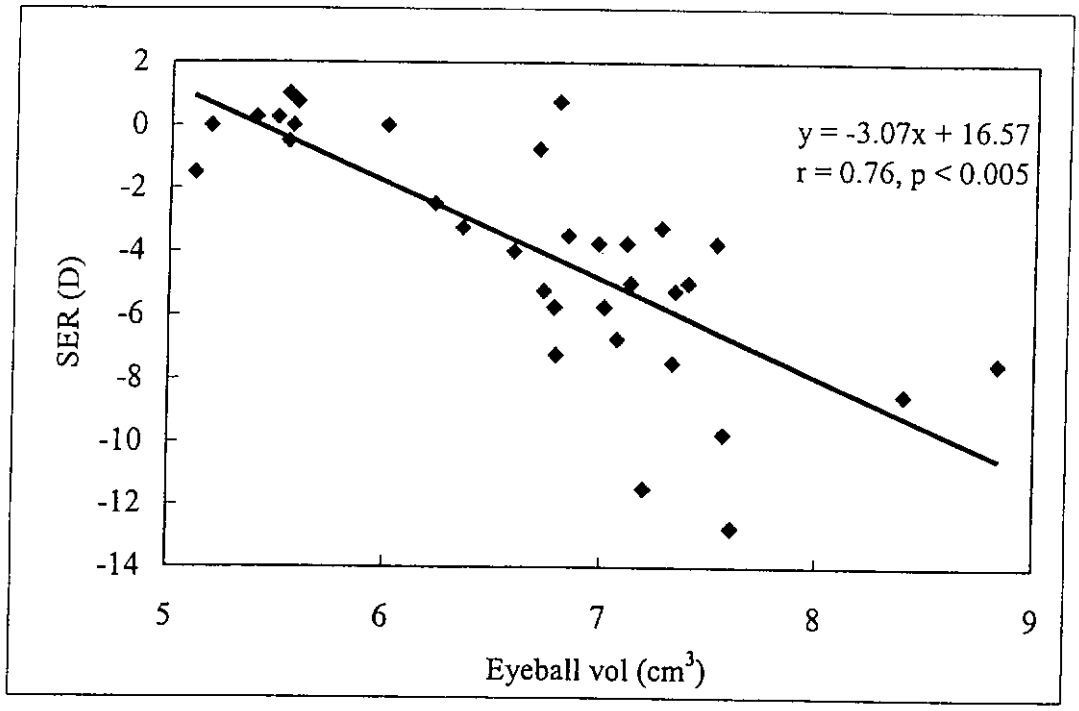

Fig 5.4b. The relationship between SER and volume of eyeball.

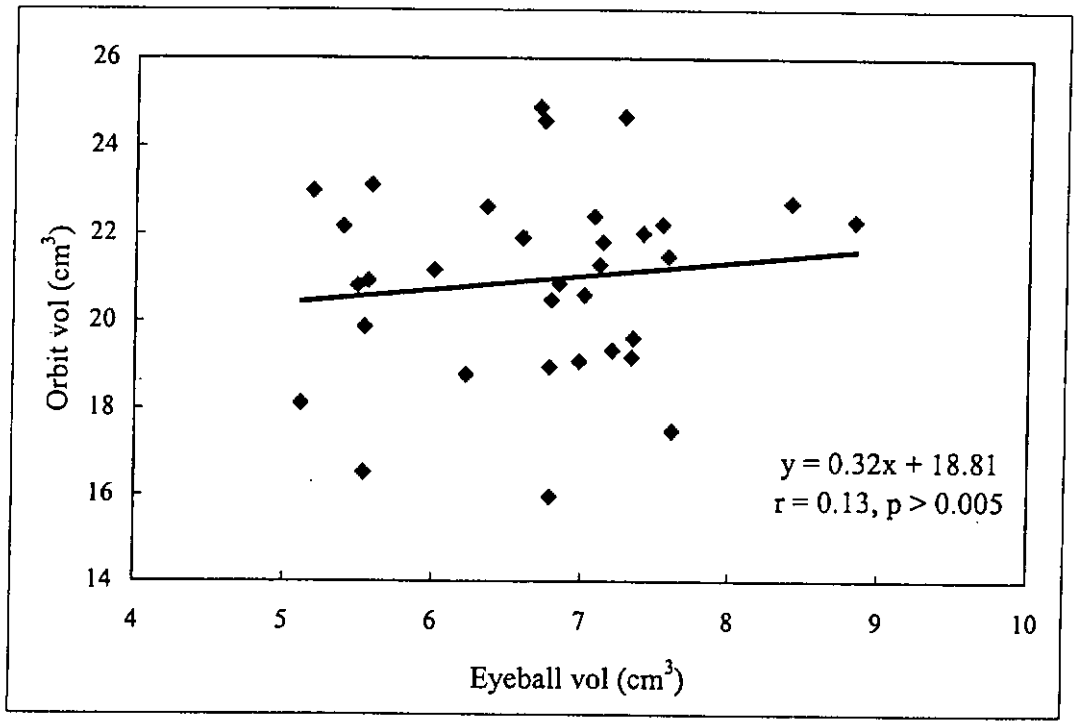

Fig 5.5. The relationship between eyeball volume and orbit volume.

Among the three head dimensions measured, orbit volume showed the strongest correlation with skull length ($r = 0.61$, $p < 0.05$). For the other two parameters, the correlations were 0.50 ($p < 0.05$) (skull breath) and 0.32 ($p > 0.05$) (skull height). The skull dimensions (length and breadth) between male and female subjects were also significantly differently ($t = -3.68$, $p < 0.05$; $t = -4.40$, $p < 0.05$).

5.5 Discussion

Our subjects who reported myopia onset in early childhood become more myopic than those who reported myopia onset later in life. This finding concurs with Fledelius (1995) who also noted this trend and adds further support to early onset myopia as a risk factor for high myopia.

The mean eyeball volume found in this study was 6.70 cm^3 which is smaller than those found by Bite et al. (1985) (mean volume = 8.94 cm^3) and Thaller (1997) (mean volume = 8.15 cm^3). In these other studies, the refractive status of subjects was not known. The methods used were also different. Bite et al (1985) used computed tomography images while Thaller (1997) used water displacement method to find the eyeball volume.

Our subjects' mean orbit volume was 20.94 cm^3. The comparison of the orbit volume with other studies is shown in Table 5.2 (Bite et al., 1985, Deveci et al., 2000, Forbes et al., 1985, Furuta, 2001, McGurk et al., 1992, Schuknecht et al., 1996, Yago and Furuta, 2001). Our mean orbit volume was smaller than those reported in other studies. We note that two major differences between our study and those other studies. First, other studies used images from computed tomography (CT). Bony structures appear better delineated on CT images than on MR images (Duvoisin et al., 1998). Second, our subjects were all Chinese. It is interesting to note that our result was closer to those reported by Furuta (2001) and Yago & Furuta (2001) on Japanese subjects than those studies conducted in the West on presumably Caucasian subjects.

Studies done by	Orbital volume (cm^3)
Our study	20.94
Furuta (2001)	20.90-23.60
Yago and Furuta (2001)	21.66
Bite et al. (1985)	23.20
Schuknecht et al. (1996)	26.80
Deveci et al (2000) (20 dried skulls)	28.00
McGurk et al (1992) (38 dried skulls)	28.67
Forbes et al. (1985)	29.70

Table 5.2 Orbital volume reported by different studies.

Orbit size was reported to be positively associated with eyeball size based on the chick model (Wilson et al., 1997). The chick study showed induced myopic and hyperopic eyes resulted in larger and smaller orbits respectively. In our study, we looked at the orbit volume in subjects with varying degrees of ametropia. Our myopic subjects were early onset myopes. Our conjecture is that if eyeball size influences orbit development, we might be able to see an effect in early onset myopes since it is known that orbit and eyeball volumes do not change much after puberty. Our results showed that orbit volume was not related to myopia. Comparing the most myopic and hyperopic subjects, we found that the most hyperopic subject had an orbit volume 2.37 cm^3 larger than the most myopic subject while the eyeball of the most myopic subject was 1.07 cm^3 larger than that of the most hyperopic subject. In our subjects, we were unable to demonstrate that myopia exerted an extraocular effect on the growth of the orbit.

What could account for the difference between our findings and the chick study findings (Wilson et al., 1997)?

One possible reason for the difference in orbit growth in relation to myopia between chicks and humans may be due to the different anatomical structures of the orbit in the two species. First, the floor of the orbit in the chick is formed by portions of several different bones which do not form a complete orbital floor as found in human (Wilson et al., 1997). Therefore, the orbit floor in chicks could be configured to accommodate eyeball growth. It is difficult to see how this could happen in the human orbit floor. Second, extraocular structures in chicks are proportionately less abundant than in humans. Forbes et al (1985) estimated that the ratio between the volume of the extraocular soft tissues within the orbit (eyeball excluded) to the total volume of the orbit in male subjects was about 0.68. Anecdotal observation suggests this ratio is substantially smaller in chicks. The extraocular fat and muscles in the human orbit may act as a cushion and may be compressed. Apart from the anatomical difference, the difference between the development period of the orbit between chick and human may be another factor. In the chick study, it took 7 days to induce refractive errors after which the chicks were sacrificed to measure orbit volumes. At such a young age (i.e. 14 days), bone remodelling may be feasible. In our human subjects, it is unlikely that eyeball growth due to myopia would have commenced in very early childhood when significant bone remodelling was presumably feasible.

Our study showed that orbit size was unrelated to myopia. This provides further support to the notion that myopia is environmentally-linked. The enlargement of the eyeball in myopia is unrelated to surrounding structures of the eye.

Orbit size was related to head dimensions. People with larger skull lengths also have larger orbits. Waitzman et al. (1992) performed a quantitative survey in craniofacial measurement and found that orbit growth followed the same pattern as cranium growth but they did not indicate the statistical correlation between them. With regard to orbit growth, only the lateral orbital distance and the intertemporal distance continue to increase in size throughout childhood. These two distances are in an equatorial direction with regard to the eyeball. Consequently, the axial length increase in eyeball due to myopia may not have much of an effect on the orbit.

Although myopia does not appear to be related to orbit growth, our results show that in the myopic eye, the vitreous chamber remains largely spherical up to –12.00D. This phenomenon was first noted by Cheng et al. (1992) in an MRI study of a small group of myopic subjects. Gilmartin et al. (2002) also found that the posterior retinal contours for Taiwanese Chinese show that the posterior retinal stretch was symmetrical when comparing to Caucasian. This incidental finding challenges the notion that the eyeball is elongated in myopia, at least within the range of –12.00D.

5.6 Conclusion

A larger eyeball does not appear to be associated with a larger orbit. Orbit size is more closely related to skull length.

Chapter 6 Summary and conclusions

6.1 Summary of all studies

The aim of this research was to explore orbit development in Hong Kong Chinese people. Specifically, we wanted to know if orbit growth and orbit size in Chinese people were similar to other racial groups reported elsewhere. The high prevalence of myopia amongst Hong Kong Chinese also raised the interesting possibility of whether the orbit development might be influenced by the larger eye in myopia.

To shed some light on these issues, we conducted three experiments. Experiment 1 was primarily a calibration exercise. We chose the MR modality to image the orbit because there is no radiation risk compared to CT. From the literature, it was clear that CT offered greater definition, particularly for bony structures such as the orbit. However, we felt the compromise to use MR was reasonable and ethical.

To ensure accuracy was improved, we conducted several calibration exercises. These calibration exercises highlighted the need to calibrate each MR machine used, particularly when volumetric data is desired, to ensure the results are compatible. We speculated on possible sources of errors.

In Study 1, we explored the pattern of orbit volume development using MR data from subjects of different ages. We estimated that orbit volume reaches maturity at around 16 years of age. On the whole, orbit volumes from our subjects were lower than those reported in other studies on mainly Caucasian subjects but similar to the findings on Japanese subjects.

In Study 2, we looked at how orbit volume was influenced by different degrees of myopia. Within the range of about –12.00D, we found no association between orbit volume and myopia.

6.2 Improvements to the present study and possible further work

Studies 1 and 2 were cross-sectional studies. The subject size in some age groups was small. In order to provide a more representative sample, subject size in each age group could be increased to about 30.

In terms of experimental design, a longitudinally study would be more powerful than a cross-sectional study. Data showing eyeball and orbit volumes from infancy to adulthood in individuals would provide the clearest picture of how the growing eyeball is accommodated by the orbit.

In terms of methodology, the orbit scan could be done by a more powerful MRI scanner (e.g. 1.5T scanner) in order to obtain images with better signal-to-noise ratio. Using a surface coil would increase the spatial resolution of the images. The use of thinner and contiguous slices would provide a more accurate measurement in volume.

Up to -12.00D, we found that the eyeball remained largely spherical. However, there is a limit to how large the eyeball can grow and still remain spherical given that the vertical dimension of the orbit is smaller than the horizontal dimension. How large can the eyeball grow to before the orbit becomes a limiting factor?

Appendix 1 Information sheets

INFORMATION SHEET

Investigation of the relationship between orbit volume and eye size in myopia

You are invited to participate in a project conducted by Prof. Maurice Yap, Dr. Karl Fung and Miss Anson Chau, who are staff members and research student of the Department of Optometry and Radiography in The Hong Kong Polytechnic University. This project will form part of Miss Chau's research MPhil study.

The aim of this study is to investigate the relationship between myopia, eyeball size and orbit volume. The study will involve measurement of orbit volume, eyeball size, measurement of head dimensions, and refractive error.

The orbit and eye volumes are determined from a magnetic resonance (MR) scan of your head. The scan will take place in Queen Elizabeth Hospital (QEH). In total, the scan will take approximately 30 minutes. The MR scan used is a standard clinical scanning procedure and has no known radiation risks or side effect except to those people who have electrically, magnetically or mechanically activated implants such as cardiac pacemakers. If you are prone to claustrophobia or are/might be pregnant, you are requested to inform clinician before the scan. Loose foreign objects are prohibited in the examination room (e.g. coins, glasses, jewellery). The clinician performing the scan may refuse to perform the scan on clinical grounds. Earplugs will be provided to you to minimize the disturbance of the noise generated by the scanner during the examination.

During scanning, images of your orbit will be acquired. You will lie on a couch slightly wider than your body and it will slide into the center of a large horizontal cylindrical magnet. You will be asked to lie still during scanning. Soft spongy pads will be put around your face to make your head still. You will wear earplugs during scanning. Inside the magnet, you will be able hear to the research and medical staff. If you find any significant discomfort, you should let us know immediately by pressing the emergency ball, and we will terminate the scanning. You also have right to stop the procedure at any time.

Your eyeball axial length is measured using an ultrasound machine and your refractive error will be determined using an autorefractor. The above measurements will take place at the PolyU Optometry Clinic and will be carried out by a registered optometrist. Prior to the ultrasound measurement, an eye drop will be instilled into each eye. You will be asked to fixate a distant target. Your eyelid will be held apart by the optometrist and an ultrasound probe will be applied to touch your cornea lightly to obtain the measurement. For measuring the refractive error, a cycloplegic eye drop will be instilled. This will result in a temporary blurring of near vision for about 8 hours. Your vision will also appear

brighter than usual and this may cause some discomfort. However, daily activities should not be affected. Thirty to 45 minutes after the eye drop instillation, you will be asked to site in front of the autorefractor and to put your chin on the chin rest and measurement will begin. The whole vision examination will take about an hour.

Finally, your head dimensions will be measured using a set of clinical calipers. Skull length, breadth and height will also be measured.

All measurements are non-invasive and commonly used clinical procedures which are operated within the normal operating parameters. The risks associated with these measurements are minimal. Mild discomfort may come from the noise produced by the MR scanner during examination and photosensitivity and blurring of near vision after applying cycloplegic eye drop.

All information related to you will remain confidential, and will be identifiable by codes only known to researchers of this study. The code key connecting to your name to specific information about you will be kept in a separate and secure place. You will not be identified in any text, photos or video if taken.

You may not gain direct benefits from the above examinations, however your information derived from this study will give us a better understanding of the development of myopia.

You have every right to withdrawn from the study before or during the measurements. Your present and future clinical treatment at QEH and PolyU Optometry Clinic will be unaffected.

If you have any complaints about the conduct of this research study, please do not hesitate to contact Mr Eric Chan, Secretary of the Human Subjects Ethics Sub-Committee of the Hong Kong Polytechnic University in person or in writing (c/o Human Resources Office on 13/F, Lee Ka Shing Tower of the University).

If you would like more information about this study, please contact Prof. Maurice Yap at 2766 or Miss Anson Chau at 9354 .

Thank you for your interest in participating in this study.

Miss Anson Chau
Student investigator

Prof. Maurice Yap, Dr. Karl Fung
Supervisors

參考資料

近視與眼眶及眼球體積調查研究

多謝你參加「近視與眼眶及眼球體積研究」，是次研究是由香港理工大學眼科視光學及放射學學系所籌劃，並由學系職員葉健雄教授和馮家樂博士和學系研究生周卓敏小姐負責。這研究亦是周卓敏小姐哲學碩士課程的一部分。

是次研究目的是分析和調查眼眶及眼球體積與近視的關係。檢查項目包括：量度屈光不正度數、頭顱尺寸、眼球大小和眼眶體積。

我們會利用磁力共振掃描器去顯示眼眶及眼球體積。掃描會於伊利沙伯醫院進行。這研究所採用的是一台達至醫療標準的掃描器，在一般情況下，它不會為閣下帶來副作用；除非閣下體內有金屬移植物如心臟起膊器等。如閣下有幽室恐懼症的傾向或現正或懷疑懷孕，掃描前請通知在場的醫護人員。任何物品〈如錢幣、飾物、眼鏡等〉，均不可帶入掃描室。負責醫生有權基於醫療安全理由，拒絕進行掃描。我們亦會提供一對塞給閣下，以減少檢查時掃描器所產生大量噪音對閣下的干擾。

掃描期間，閣下須安靜地仰臥在床上，然後床會被滑入平放及圓筒形的大磁鐵中。一些軟枕會用來固定閣下的頭顱。在磁鐵中，閣下可聽到我們的聲音。如閣下有任何顯著的不適，請立即按緊急球通知我們。我們有可能止檢查。閣下亦可要求隨時止檢查。

眼科視光師會在香港理工大學眼科視光學診所利用電腦驗眼儀為閣下量度屈光不正度數和利用超聲波量度眼球長度。量度眼球長度前會落眼藥水的。然後閣下須定眼望著一目標，以助眼科視光師將超聲波儀輕放在閣下的角膜上進行量度。同樣，在量度屈光不正度數前，眼科視光師亦會替閣下落麻醉睫肌狀眼藥水。用藥後，會出現近距離視力將會短暫模糊及視覺會較正常為光，導致一些不適，這會維持八小時左右。落藥後三十至四十分鐘，眼科視光師便會替閣下量度度數。整套驗眼檢查需時一小時。

最後，頭顱尺寸括它的長、寬、高將會用彎腳規去量度。

上述的檢查，均為普通非侵害性的臨床程序，而相關的危險亦十分低。閣下所提供的資料將有助我們認識近視的發展。

所有收集的資料將保密和只會作是次研究之用。閣下的名字只會用號來表示，只可由這研究有關的人員得到。研究中包括的拍攝和錄影或日後的文獻出版，閣下均不會被認出。

閣下有權在檢查前或中途退出，而不會受到處罰。閣下在伊利沙伯醫院和香港理工大學眼科視光學診的現有或將來診療均不受影響。

如對上述研究的指引有任何投訴，請致函香港理工大學李嘉誠樓十三樓人力資源部聯絡人類實驗道德委員會秘書長陳先生。

如欲得知上述研究的更多資料，歡迎致電葉健雄教授(2766　　)或周卓敏小姐(9354　　)。

多謝你的參與！

學生研究人員
周卓敏小姐

主研究人員
葉健雄教授
馮家樂博士

啟

Appendix 2 Consent forms

CONSENT TO PARTICIPATE IN RESEARCH

Investigation of the relationship between orbit volume and eye size in myopia

Have you read the information sheet provided? Yes / No

Have you had an opportunity to ask questions and discuss this study? Yes / No

Have you received satisfactory answers to all of your questions? Yes / No

Have you received enough information about the study? Yes / No

Who provided the information / answered your questions

Ms/ Mr/ Dr / Prof _____

Do you understand that participation is entirely voluntary? Yes / No

Do you understand that you are free to withdraw from the study

- At any time Yes / No
- Without having to give a reason Yes / No
- Without affecting your future care (as applicable) Yes / No

Do you agree to take part in this study? Yes / No

Name of participant : _____

Signature of participant : _____

HKID no. of participant : _____( ) D.O.B.: ____/____/____

Name of researcher : _____

Signature of researcher : _____

Date : _____

參加同意書

近視與眼眶及眼球體積調查研究

你有否閱讀參考資料？ 有 / 否

你有否給予機會去發問和討論與這研究有關的事宜？ 有 / 否

你有否得到滿意的答案？ 有 / 否

你有否得到關於這研究的足夠資料？ 有 / 否

誰向你提供這些資料 / 回答問題

_____

你是否明白是次參與乃屬自願性質 是 /否

你是否明白你有自由

- 在任何時間 是 /否
- 不需原因 是 /否
- 在不對你將來的參與有影響下 是 /否

退出這研究？

你是否願意參加這研究？ 是 /否

參加者姓名 : _____

參加者簽署 : _____

參加者身份証號碼 : _____( ) 出生日期 : ____/_____/_____

研究人員姓名 : _____

研究人員簽署 : _____

日期 : _____

Appendix 3 Raw data of calibration studies

Appendix 3.1 1 T scanner (QEH)

	Mould 1	Mould 2	Mould 3	Mould 4	Mould 5	Mould 6	Mould 7	Mould 8	Mould 9	Mould 10
Computed vol/cm^3(c)	15.56	20.76	21.48	21.69	21.65	22.51	23.93	24.54	25.09	28.42
	15.68	20.72	21.47	21.78	21.88	22.81	23.82	24.86	25.39	28.54
	15.91	20.73	21.36	21.59	22.00	22.65	23.75	24.67	25.20	28.43
	15.73	20.58	21.45	21.63	21.85	22.90	23.89	24.59	25.35	28.56
	15.80	20.84	21.49	21.66	22.02	22.85	23.85	24.65	25.51	28.57
Mean vol/ cm^3	15.73	20.73	21.45	21.67	21.88	22.74	23.85	24.66	25.31	28.50
SD	0.13	0.09	0.06	0.07	0.15	0.16	0.07	0.13	0.16	0.07
CV* (%)	0.83	0.46	0.26	0.33	0.68	0.70	0.29	0.51	0.64	0.25
Physical vol/ cm^3 (p)	14.65	18.70	19.44	19.75	20.83	21.31	22.78	22.99	23.33	26.59
	14.65	18.71	19.44	19.75	20.83	21.31	22.77	22.99	23.33	26.59
	14.65	18.70	19.44	19.76	20.83	21.31	22.78	22.99	23.33	26.59
	14.65	18.70	19.44	19.75	20.83	21.32	22.78	22.99	23.33	26.59
	14.65	18.70	19.44	19.75	20.83	21.31	22.77	22.99	23.33	26.59
Mean vol/ cm^3	14.65	18.70	19.44	19.75	20.83	21.31	22.78	22.99	23.33	26.59
SD	0.00	0.00	0.00	0.00	0.00	0.00	0.00	0.00	0.00	0.00
CV (%)	0.01	0.01	0.01	0.01	0.00	0.01	0.00	0.00	0.00	0.01
Difference in vol (p-c)	-1.08	-2.03	-2.01	-1.92	-1.05	-1.43	-1.07	-1.67	-1.98	-1.91
% error (%)	-7.37	-10.86	-10.34	-9.72	-5.04	-6.71	-4.70	-7.26	-8.49	-7.18

*CV = coefficient of variance = SD/mean vol. X 100%

	Ball 1	Ball 2	Ball 3	Ball 4	Ball 5	Ball 6	Ball 7	Ball 8	Ball 9	Ball 10
Computed vol/ cm^3 (c)	4.51	5.06	5.96	6.71	7.73	8.58	9.87	11.12	12.27	13.68
	4.40	5.22	5.83	6.77	7.85	8.76	9.78	11.03	12.37	13.57
	4.44	5.17	5.95	6.77	7.73	8.60	9.89	11.20	12.29	13.85
	4.51	5.19	5.88	6.95	7.70	8.62	9.67	11.20	12.29	13.79
	4.46	5.23	5.93	6.76	7.60	8.66	9.83	11.22	12.29	13.66
Mean vol/ cm^3	4.46	5.17	5.91	6.79	7.72	8.64	9.81	11.15	12.30	13.71
SD	0.05	0.07	0.05	0.09	0.09	0.07	0.09	0.08	0.04	0.11
CV (%)	1.01	1.32	0.87	1.36	1.14	0.84	0.89	0.71	0.32	0.81
Physical vol (p)	3.67	4.46	4.98	5.65	6.47	7.27	8.57	9.56	10.96	12.01
	3.62	4.59	4.96	5.64	6.50	7.44	8.57	9.68	10.97	11.90
	3.64	4.63	4.93	5.80	6.66	7.45	8.62	9.58	11.03	11.75
	3.68	4.63	4.98	5.85	6.69	7.45	8.63	9.56	11.04	11.86
	3.73	4.65	4.98	5.84	6.59	7.50	8.65	9.56	11.04	11.99
Mean vol/ cm^3	3.67	4.59	4.97	5.75	6.58	7.42	8.61	9.59	11.01	11.90
SD	0.04	0.08	0.02	0.10	0.10	0.09	0.03	0.05	0.04	0.10
CV (%)	1.14	1.74	0.43	1.82	1.45	1.18	0.39	0.54	0.36	0.87
Difference in vol (p-c)	-0.80	-0.58	-0.94	-1.04	-1.14	-1.22	-1.20	-1.57	-1.30	-1.81
% error (%)	-21.75	-12.66	-19.00	-18.06	-17.33	-16.43	-13.97	-16.34	-11.79	-15.20

Appendix 3.2 1.5 T scanner (QMH)

	Mould 1	Mould 2	Mould 3	Mould 4	Mould 5	Mould 6	Mould 7	Mould 8	Mould 9	Mould 10
Computed vol/cm^3(c)	13.90	17.3	17.45	18.40	19.24	19.34	21.64	21.90	22.22	23.76
	14.13	17.59	18.00	18.30	19.01	19.09	21.41	22.24	21.78	24.25
	14.07	17.44	17.71	18.51	19.45	19.43	21.13	21.95	21.97	23.97
	13.55	17.19	17.82	18.89	19.26	19.33	21.42	21.65	21.56	24.59
	13.28	17.07	17.73	18.54	19.09	19.00	20.98	21.09	21.41	24.30
Mean vol/ cm^3	13.78	17.32	17.74	18.53	19.21	19.24	21.32	21.77	21.79	24.18
SD	0.36	0.20	0.20	0.22	0.17	0.18	0.26	0.43	0.32	0.32
CV (%)	2.65	1.17	1.13	1.20	0.87	0.96	1.23	2.00	1.48	1.33
Physical vol/ cm^3 (p)	14.65	18.70	19.44	19.75	20.83	21.31	22.78	22.99	23.33	26.59
	14.65	18.71	19.44	19.75	20.83	21.31	22.77	22.99	23.33	26.59
	14.65	18.70	19.44	19.76	20.83	21.31	22.78	22.99	23.33	26.59
	14.65	18.70	19.44	19.75	20.83	21.32	22.78	22.99	23.33	26.59
	14.65	18.70	19.44	19.75	20.83	21.31	22.77	22.99	23.33	26.59
Mean vol/ cm^3	14.65	18.70	19.44	19.75	20.83	21.31	22.78	22.99	23.33	26.59
SD	0.00	0.00	0.00	0.00	0.00	0.00	0.00	0.00	0.00	0.00
CV (%)	0.01	0.01	0.01	0.01	0.00	0.01	0.00	0.00	0.00	0.01
Difference in vol (p-c)	0.87	1.38	1.70	1.22	1.62	2.08	1.46	1.22	1.54	2.42
% error (%)	5.92	7.39	8.74	6.20	7.78	9.74	6.43	5.30	6.61	9.09

Appendix 4 Corrected raw data of Study 1

Subject No.	Age	Sex	Left orbit measurements/cm^3						True physical vol/cm^3
			1	2	3	4	5	Mean vol	
1	1	F	10.85	11.23	11.03	10.70	10.80	10.92	11.56
2	1	F	12.23	11.37	11.96	11.54	11.49	11.72	12.44
3	1	M	12.09	12.40	12.46	11.86	12.71	12.30	13.09
4	1.75	M	15.26	15.08	15.27	15.28	15.15	15.21	16.30
5	2	M	15.23	15.79	15.45	15.77	16.02	15.65	16.79
6	3	F	11.69	11.80	11.90	12.71	12.21	12.06	12.81
7	3	F	12.85	13.31	13.56	13.24	12.98	13.19	14.06
8	3	M	15.21	14.94	14.74	14.92	14.67	14.90	15.96
9	3	F	14.89	15.59	15.32	15.75	15.34	15.38	16.49
10	3	F	12.33	13.87	13.09	14.97	14.85	13.82	14.77
11	4	F	13.29	12.36	13.17	13.16	13.13	13.03	13.89
12	4	M	13.49	13.42	13.11	13.08	13.20	13.26	14.14
13	4	M	14.22	13.96	14.46	14.20	14.26	14.22	15.21
14	4	M	14.57	14.70	14.34	14.80	14.35	14.55	15.57
15	5	F	11.37	11.63	12.00	11.78	11.85	11.73	12.45
16	5	F	14.47	14.45	14.70	14.67	14.20	14.50	15.52
17	5	M	15.91	15.73	15.86	16.08	15.70	15.85	17.02
18	5	F	17.19	17.33	16.70	16.58	16.69	16.90	18.17
19	5	F	14.98	15.11	15.31	15.20	15.12	15.14	16.23
20	6	M	15.99	15.95	16.16	18.11	17.48	16.74	18.00
21	6	F	17.26	17.43	18.28	17.83	17.74	17.71	19.07
22	6	M	13.49	14.51	14.76	14.08	13.87	14.14	15.12
23	6	F	16.52	17.20	17.56	17.52	17.39	17.24	18.55
24	7	F	13.34	14.23	14.77	14.53	15.25	14.42	15.43
25	7	F	14.31	14.63	14.76	15.81	15.52	15.01	16.08
26	7	M	17.50	16.41	17.27	17.42	17.31	17.18	18.49
27	7	F	16.71	16.80	17.42	17.17	17.44	17.11	18.40
28	8	M	13.62	13.66	14.01	13.64	13.86	13.76	14.70
29	8	M	16.02	15.26	15.84	15.63	15.69	15.69	16.84
30	9	M	14.48	14.22	14.19	14.50	14.16	14.31	15.30
31	9	F	16.35	16.16	16.47	16.31	16.39	16.33	17.55
32	9	M	10.96	11.19	11.46	11.03	10.63	11.05	11.70
33	9	F	15.08	15.46	15.07	15.16	15.02	15.16	16.24
34	10	F	14.57	14.58	14.04	14.40	14.60	14.44	15.44

35	11	F	15.71	16.73	17.79	18.09	18.43	17.35	18.67
36	12	M	20.21	20.01	19.87	20.01	20.43	20.11	21.72
37	13	F	16.57	16.50	16.50	15.83	16.00	16.28	17.49
38	13	F	16.70	16.66	16.43	16.87	16.68	16.67	17.92
39	13	M	19.19	18.96	19.58	19.45	19.16	19.27	20.80
40	13	M	20.77	19.95	19.91	19.67	19.85	20.03	21.63
41	13	M	21.20	21.72	21.64	21.61	20.98	21.43	23.19
42	14	F	15.76	16.42	17.91	16.86	16.82	16.75	18.01
43	14	F	18.35	17.97	17.50	17.46	17.47	17.75	19.11
44	15	F	19.18	19.35	18.59	18.81	19.04	18.99	20.49
45	15	M	20.26	19.91	20.34	20.37	19.93	20.16	21.79
46	15	M	20.14	20.44	21.22	20.33	20.07	20.44	22.10
47	18	M	23.68	23.21	23.41	23.75	23.53	23.52	25.50
48	19	F	17.45	17.57	17.69	17.69	17.41	17.56	15.96
49	19	F	19.07	18.35	18.34	18.15	18.22	18.43	19.86
50	19	F	21.99	22.21	22.21	22.03	22.20	22.13	20.60
51	20	M	24.77	24.28	24.28	24.33	24.30	24.39	22.63
52	21	M	22.52	22.62	22.35	22.72	22.54	22.55	20.93
53	21	M	23.26	23.44	23.89	23.78	23.46	23.57	21.82
54	22	F	19.36	19.03	19.11	19.16	18.99	19.13	17.49
55	22	F	19.67	19.94	19.52	19.96	19.63	19.74	18.11
56	22	F	20.80	20.50	20.62	20.50	20.62	20.61	19.07
57	22	M	22.20	22.18	22.85	23.10	22.79	22.62	21.17
58	22	M	23.80	23.63	24.03	23.84	23.67	23.79	22.02
59	22	M	25.95	26.81	26.76	26.38	26.30	26.44	24.57
60	23	F	20.81	20.86	20.79	20.81	20.89	20.83	19.33
61	23	F	20.81	21.48	21.55	21.27	21.18	21.26	19.61
62	23	M	21.43	21.67	21.09	21.50	21.53	21.44	19.96
63	23	M	22.20	22.32	22.15	22.36	22.42	22.29	20.81
64	24	F	20.17	20.34	20.52	20.31	20.31	20.33	18.77
65	24	F	20.18	20.15	20.38	20.45	20.48	20.33	18.94
66	24	F	20.51	20.92	20.65	20.65	20.72	20.69	19.17
67	24	F	21.94	21.91	21.81	22.10	22.07	21.97	20.48
68	24	M	23.96	23.92	23.76	23.86	23.83	23.87	22.17
69	24	M	24.78	24.52	24.55	24.32	24.44	24.52	22.77
70	25	F	22.12	22.10	22.59	22.11	22.46	22.28	20.85
71	27	F	22.95	22.34	22.68	22.32	23.13	22.68	21.49
72	28	F	18.31	17.96	17.82	18.09	17.99	18.03	16.52
73	28	M	22.78	23.24	23.36	22.77	22.92	23.01	21.29
74	28	M	25.14	24.79	24.88	24.60	24.68	24.82	22.99

75	29	M	22.52	23.00	23.11	23.21	23.56	23.08	21.91
76	31	M	24.32	24.63	24.47	24.58	24.80	24.56	23.12
77	31	F	23.96	24.25	24.02	23.54	24.07	23.97	22.41
78	33	M	23.59	24.53	24.75	24.27	23.88	24.20	22.22
79	34	F	26.43	26.45	26.42	26.68	26.63	26.52	24.89
80	36	F	23.97	23.66	23.95	24.15	23.96	23.94	22.30
81	42	M	26.62	26.52	26.26	26.29	26.41	26.42	24.67

Explanation:
Corrected raw date means the volumes presented in the above table were corrected to true physical volume by using the equation derived from the calibration study.

Subject no. 49 to 81: Equation for orbit volume correction is: $c = 1.0334p + 0.9126$;
Subject no. 1 to 48: Equation for orbit volume correction is: $c = 0.9031p + 0.487$,
c = computed volume; p = physical volume

Clinical history of children subject of Study 1

Subject No.	Age	Sex	Clinical history
1	1	F	Periorbital haematoma
2	1	F	Periorbital cellulitis
3	1	M	Retinoblastoma of Lt. Eye
4	1.75	M	Retinoblastoma
5	2	M	Neck Plexiform Neurofibroma
6	3	F	Lt optic nerve coloboma
7	3	F	Cerebral infract
8	3	M	Neuroblastoma
9	3	F	Neurofibrosis
10	3	F	Neurofibromatosis
11	4	F	Congenital cataract & bilateral optic atrophy
12	4	M	Neurofibromatosis
13	4	M	Neurofibromatosis
14	4	M	Neurofibromatosis
15	5	F	Neurofibromatosis
16	5	F	Poor vision
17	5	M	Neurofibromatosis
18	5	F	CNS Pathology or Optic Neuritis
19	5	F	Optic neuraglioma
20	6	M	?Muscle tumor, ? Intramuscular abscess of Lt. Orbit
21	6	F	Neurofibromatosis
22	6	M	Persistent Lt. Ptosis
23	6	F	Neurofibroma
24	7	F	R/O multiple sclerosis
25	7	F	Neurofibromatosis
26	7	M	Neurofibromatosis
27	7	F	Noonau's syndrome with Lt. VI nerve palsy
28	8	M	Neurofibromatosis
29	8	M	Neurofibromatosis
30	9	M	Optic atrophy for investigation
31	9	F	Lt. Eye proptosis
32	9	M	Retinoblastoma
33	9	F	Optic disease
34	10	F	? Intracranial lesion
35	11	F	Opthalmoplegia
36	12	M	? Intracranial lymphoma
37	13	F	? Infiltrative ophthalmopathy

38	13	F	CNS Relapse
39	13	M	Neurofibromatosis
40	13	M	Neurofibromatosis
41	13	M	Neurofibromatosis
42	14	F	Rt. Orbital haemangioma, for reassessment
43	14	F	Rt. Blind eye
44	15	F	Rt hemianopia
45	15	M	Rt. Optic atrophy
46	15	M	Neurofibromatosis
47	18	M	Lt. Ciliary body thickening
48	19	F	Rt. Eye proplosis

Appendix 5 Corrected Raw data of Study 2

Subject No.	Sex	Age (year)	AOM* (year)	SER# (D)	AL▲ (mm)	Head height (cm)	Head length (cm)	Head breadth (cm)	Orbit vol (cm^3)	SD	Eyeball vol (cm^3)	SD
1	F	19	11	-7.25	25.8	13.45	17.2	15.8	15.96	0.13	6.79	0.02
2	F	19	8	-5.75	25.69	11.9	17.6	15.1	20.6	0.11	7.01	0
3	M	20	9	-3.25	25.27	13.5	18.85	16.3	22.63	0.21	6.35	0.01
4	M	21	13	-5	26.55	10.7	18.6	16.4	21.82	0.26	7.13	0.03
5	M	21	N/A	0	23.2	15.2	18.3	16.1	20.93	0.14	5.56	0.03
6	F	22	7	-12.75	27.57	12.4	17.9	15.3	17.49	0.14	7.61	0.02
7	F	22	12	-3.75	25.4	13.6	18	15.6	19.07	0.12	6.98	0.01
8	F	22	N/A	-1.5	23.34	11.15	17.85	15.7	18.11	0.2	5.11	0.02
9	M	22	9	-5.25	26.66	12.8	19.3	16.6	24.57	0.35	6.73	0.03
10	M	22	10	-5	26.52	13.6	20	15.6	22.02	0.16	7.4	0.04
11	M	22	N/A	0	23.64	14	18.7	16.2	21.17	0.41	6	0.01
12	F	23	8	-11.5	28.43	12.4	17.9	16.1	19.33	0.04	7.2	0.02
13	F	23	11	-5.25	26.32	13.4	17.2	15	19.61	0.29	7.34	0
14	M	23	N/A	0.25	22.91	13	18.4	16.1	20.81	0.11	5.49	0.01
15	M	23	N/A	1	23.25	13.8	17.7	15.7	19.86	0.21	5.54	0.06
16	F	24	11	-7.5	27.51	13.8	18.7	15.2	19.17	0.15	7.33	0
17	F	24	8	-5.75	24.5	14.2	18.2	16.1	18.94	0.16	6.78	0.01
18	F	24	14	-2.5	25.01	13.2	18.1	15.6	18.77	0.12	6.22	0.02
19	F	24	N/A	0.75	24.22	13.5	16.5	15.7	20.48	0.12	6.79	0.05

20	M	24	4	-8.5	27.59	13	18	15.9	22.72	0.17	8.4	0.01
21	M	24	N/A	0.25	22.63	14.5	19.4	16.3	22.17	0.08	5.39	0.01
22	F	25	15	-3.5	26.39	13.5	18.9	16.2	20.85	0.23	6.84	0.03
23	F	27	7	-9.75	27.19	9.6	19.1	15.8	21.49	0.36	7.57	0.03
24	F	28	N/A	-0.5	23.68	11.6	17.7	15.5	16.52	0.18	5.54	0.02
25	M	28	16	-3.75	25.28	14.8	18	16.4	21.29	0.27	7.11	0.02
26	M	28	N/A	0	23.72	14.9	20.1	16.6	22.99	0.21	5.18	0.02
27	M	29	12	-4	25.58	12.8	18.7	16.7	21.91	0.38	6.59	0.03
28	F	31	NA	0.75	23.22	13.9	17.9	16.5	23.12	0.18	5.58	0.05
29	M	31	12	-6.75	26.15	13.4	20	16.5	22.41	0.26	7.07	0.03
30	M	33	12	-3.75	26.19	14.8	19.7	16.2	22.22	0.47	7.53	0.03
31	F	34	16	-0.75	24	14	18.2	15.6	24.89	0.12	6.7	0.11
32	F	36	12	-7.5	27.22	15.4	19	15.6	22.3	0.17	8.83	0.03
33	M	42	15	-3.25	25.5	15.3	21.3	16	24.67	0.15	7.27	0.03

Remarks:
Equation for orbit volume correction is: $c = 1.0334p + 0.9126$;
Equation for eyeball volume correction is : $c = 1.1144p + 0.3214$; c = computed volume, p = physical volume

* = Age of onset of myopia
# = Spherical equivalent refraction
▲ = Axial length of eyeball

Appendix 6 Starting OSIRIS

Open OSIRIS was opened when the CD-R was placed in the CD-ROM, then a Get File dialog appeared on the screen. The appropriate drive was chosen and it will show the number of folders in the CD-R in the Directories box. One of the folders was selected to see the number of subfolders in it and also number of images in such subfolders. Figure 6.1 shows the Get file dialog, figures 6.2 and 6.3 shows the details of the dialog.

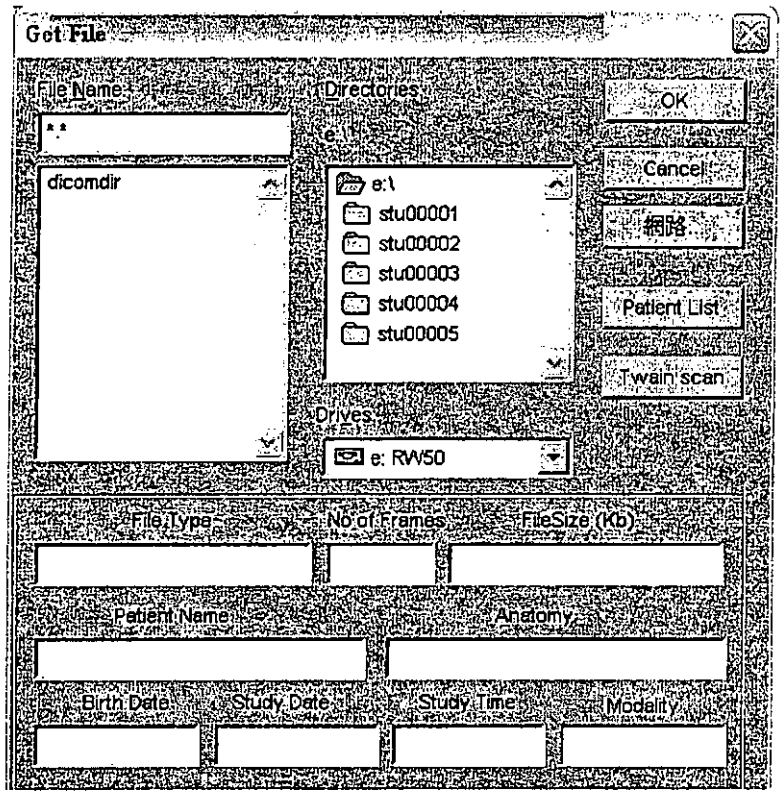

Fig 6.1 Get file dialog

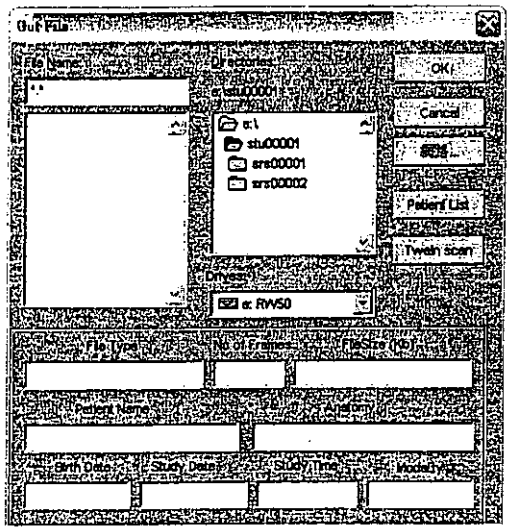

Fig.6.2 Number of subfolders can be shown in the dialog

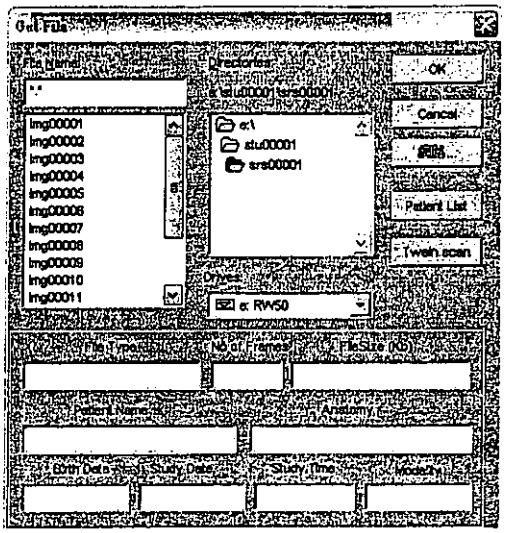

Fig. 6.3 Number of images in the selected subfolder can also be shown

After choosing the right subfolder that contained images for measurement. 'Patient List' button was clicked on the left hand side. OSIRIS then loaded the images from the CD-R and a DICOMDIR dialog was appeared. This dialog showed the name of the subject, which the subfolder belongs to, the name of the study, and number of images. The bottom part of the dialog displayed all the images in form of minified icons. The whole set of images were opened by clicking an 'Open' button on the right hand side.

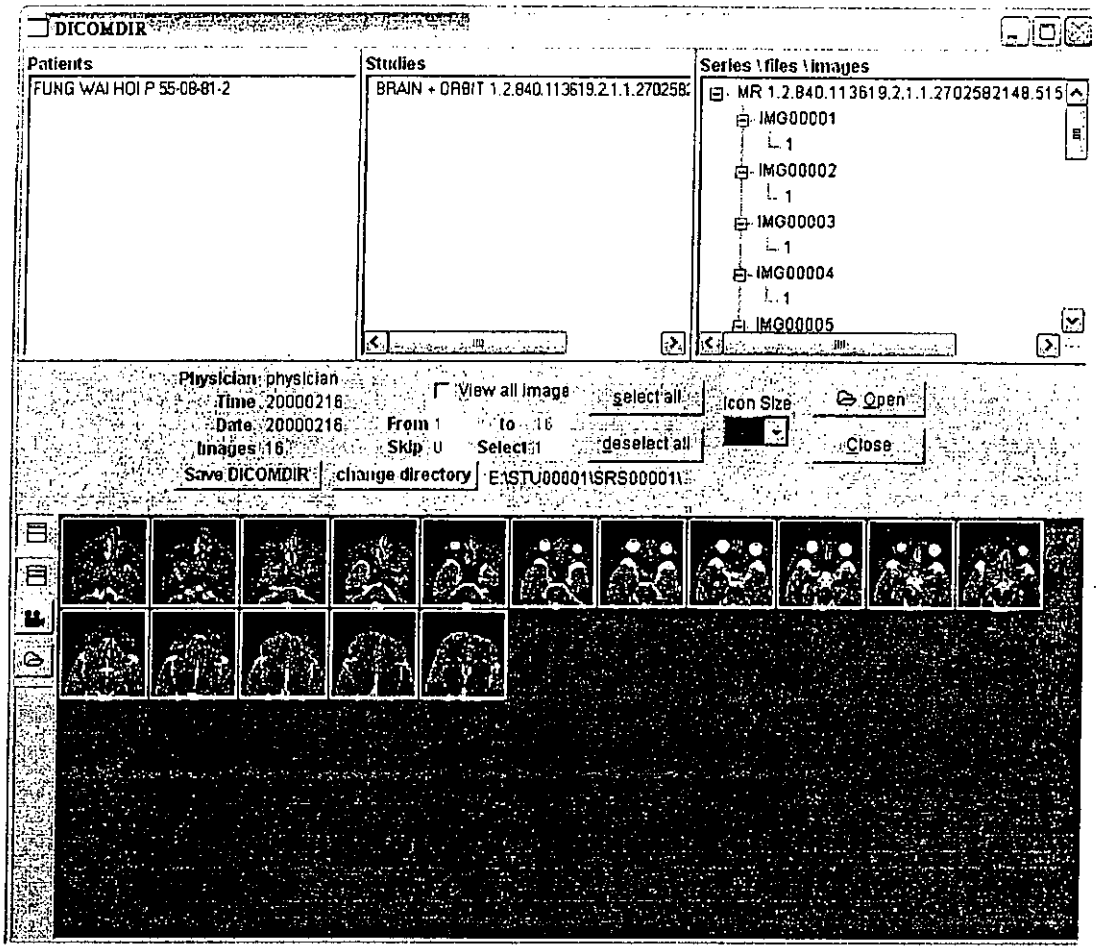

Fig. 6.4 DICOMDIR dialog was shown after clicking the 'Patient List' button

A DicomDir Serie dialog that consisted of the image and the toolbar was shown. The images were in stack mode, and they could be switched between each other by clicking the arrows on the left hand side. All of the images were magnified to 4 times of the original for volumetric measurement. In this dialog, we could view the study and image information, for example the patient's name, sex, age, history, and details of scanning protocol, etc. Figures 6.4 and 6.5 show the DICOMDIR and DicomDir Serie dialogs. Figures 6.6 and 6.7 show the detail information of the study and image.

Fig. 6.5 DicomDir Serie dialog

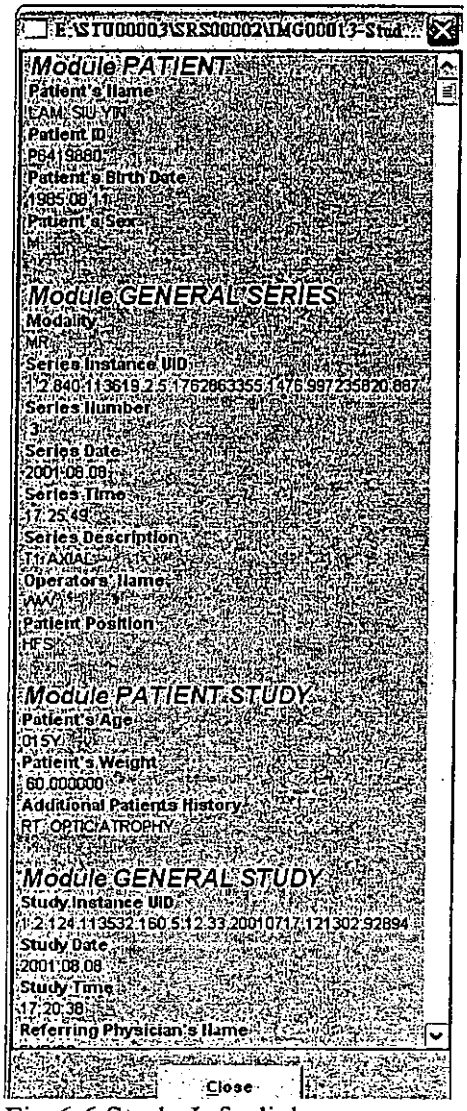

Fig.6.6 Study Info dialog

Fig.6.7 Image Info dialog

References

Adams AJ. Axial length elongation, not corneal curvature, as a basis of adult onset myopia. Am J Optom Physiol Opt 1987;64(2):150-2.

Adams AJ, Baldwin WR, Biederman I, et al. Myopia : prevalence and progression. Washington: National Academy Press; 1989.

Barretto RL, Mathog RH. Orbital measurement in black and white populations. Laryngoscope 1999;109(7 Pt 1):1051-4.

Bentley RP, Sgouros S, Natarajan K, Dover MS, Hockley AD. Normal changes in orbital volume during childhood. J Neurosurg 2002;96(4):742-6.

Bilaniuk LT, Rapoport RJ. Magnetic resonance imaging of the orbit. Top Magn Reson Imaging 1994;6(3):167-81.

Bishara SE. Facial and dental changes in adolescents and their clinical implications. Angle Orthod 2000;70(6):471-83.

Bite U, Jackson IT, Forbes GS, Gehring DG. Orbital volume measurements in enophthalmos using three-dimensional CT imaging. Plast Reconstr Surg 1985;75(4):502-508.

Buchman SR, Bartlett SP, Wornom IL, 3rd, Whitaker LA. The role of pressure on regulation of craniofacial bone growth. J Craniofac Surg 1994;5(1):2-10.

Bullimore MA, Gilmartin B, Royston JM. Steady-state accommodation and ocular biometry in late-onset myopia. Doc Ophthalmol 1992;80(2):143-55.

Cepela MA, Nunery WR, Martin RT. Stimulation of orbital growth by the use of expandable implants in the anophthalmic cat orbit. Ophthal Plast Reconstr Surg 1992;8(3):157-67; discussion 168-9.

Chan JHM. MRI : principles & applications. 2 ed. Hong Kong: Lippincott Williams & Wilkins Asia Ltd; 2000.

Chan OY, Edwards M. Comparison of cycloplegic and noncycloplegic retinoscopy in Chinese pre-school children. Optom Vis Sci 1994;71(5):312-8.

Charteris DG, Chan CH, Whitehouse RW, Noble JL. Orbital volume measurement in the management of pure blowout fractures of the orbital floor. Br J Ophthalmol 1993;77(2):100-2.

Chat SW, Edwards MH. Clinical evaluation of the Shin-Nippon SRW-5000 autorefractor in children. Ophthalmic Physiol Opt 2001;21(2):87-100.

Cheng HM. Magnetic resonance imaging of the human eye in vivo. Optom Vis Sci 1991;68(12):976-80.

Cheng HM, Singh OS, Kwong KK, et al. Shape of the myopic eye as seen with high-resolution magnetic resonance imaging. Optom Vis Sci 1992;69(9):698-701.

Curtin BJ. The development of refraction. In: The Myopias. Basic Science and Clinical Management. Philadelphia: Harper & Row, Publishers; 1985.

Daniel GB, Mitchell SK. The eye and orbit. Clin Tech Small Anim Pract 1999;14(3):160-9.

Day S. Normal and abnormal visual development. In: Talyor D, editor. Paediatric Ophthalmology. Oxford: Blackwell Science; 1997; 13-28.

Deveci M, Ozturk S, Sengezer M, Pabuscu Y. Measurement of orbital volume by a 3-dimensional software program: an experimental study. J Oral Maxillofac Surg 2000;58(6):645-8.

Disler DG, Marr DS, Rosenthal DI. Accuracy of volume measurements of computed tomography and magnetic resonance imaging phantoms by three-dimensional reconstruction and preliminary clinical application. Invest Radiol 1994;29(8):739-45.

Dorfman RE, Spickler EM. Current status of magnetic resonance imaging of the orbit. Top Magn Reson Imaging 1990;2(4):17-26.

Duong DH, Rostomily RC, Haynor DR, Keles GE, Berger MS. Measurement of tumor resection volumes from computerized images. Technical note. J Neurosurg 1992;77(1):151-4.

Duvoisin B, Zanella FE, Sievers KW. Imaging of the normal and pathological orbit. Eur Radiol 1998;8(2):175-88.

Eastwood JD, Hudgins PA. New techniques in magnetic resonance imaging. Curr Opin Ophthalmol 1998;9(6):54-60.

Eckstein F, Schnier M, Haubner M, et al. Accuracy of cartilage volume and thickness measurements with magnetic resonance imaging. Clin Orthop 1998(352):137-48.

Edwards M. The refractive status of Hong Kong Chinese infants. Ophthalmic Physiol Opt 1991;11(4):297-303.

Edwards MH. The development of myopia in Hong Kong children between the ages of 7 and 12 years: a five-year longitudinal study. Ophthalmic Physiol Opt 1999;19(4):286-94.

Edwards MH, Shing FC. Is refraction in early infancy a predictor of myopia at the age of 7 to 8 years? The relationship between cycloplegic refraction at 11 weeks and the manifest refraction at age 7 to 8 years in Chinese children. Optom Vis Sci 1999;76(5):272-4.

Eppley BL, Holley S, Sadove AM. Experimental effects of intraorbital tissue expansion on orbitomaxillary growth in anophthalmos. Ann Plast Surg 1993;31(1):19-26; discussion 26-7.

Fledelius HC. Adult onset myopia--oculometric features. Acta Ophthalmol Scand 1995;73(5):397-401.

Forbes G, Gehring DG, Gorman CA, Brennan MD, Jackson IT. Volume measurements of normal orbital structures by computed tomographic analysis. AJR Am J Roentgenol 1985;145(1):149-54.

Fountain TR, Goldberger S, Murphree AL. Orbital development after enucleation in early childhood. Ophthal Plast Reconstr Surg 1999;15(1):32-36.

Fujimoto S, Mizuno R, Nakagawa Y, Dohi K, Nakano H. Estimation of the right ventricular volume and ejection fraction by transthoracic three-dimensional echocardiography. A validation study using magnetic resonance imaging. Int J Card Imaging 1998;14(6):385-90.

Furuta M. Measurement of orbital volume by computed tomography: especially on the growth of the orbit. Jpn J Ophthalmol 2001;45(6):600-6.

Gentry LR. Anatomy of the orbit. Neuroimaging Clin N Am 1998;8(1):171-94.

Gilmartin B, Logan NS, Wildsoet CF. Posterior retinal contours in Taiwanese Chinese and Caucasian anisomyopia. 9th International Conference on Myopia; 2002;24

Goh WS, Lam C. A visual survey of school children in Hong Kong. Clin Exp Optom 1993;76(3):101-108.

Goh WS, Lam CS. Changes in refractive trends and optical components of Hong Kong Chinese aged 19-39 years. Ophthalmic Physiol Opt 1994;14(4):378-82.

Goldschmidt E, Lam CS, Opper S. The development of myopia in Hong Kong children. Acta Ophthalmol Scand 2001;79(3):228-32.

Goose DH, Appleton J. Human dentofacial growth. Oxford: Pergamon; 1982.

Goss DA, Cox VD, Herrin-Lawson GA, Nielsen ED, Dolton WA. Refractive error, axial length, and height as a function of age in young myopes. Optom Vis Sci 1990;67(5):332-8.

Gossman MD, Mohay J, Roberts DM. Expansion of the human microphthalmic orbit. Ophthalmology 1999;106(10):2005-9.

Gottlieb MD, Fugate-Wentzek LA, Wallman J. Different visual deprivations produce different ametropias and different eye shapes. IOVS 1987;28(8):1225-35.

Grosvenor T. A review and a suggested classification system for myopia on the basis of age-related prevalence and age of onset. Am J Optom Physiol Opt 1987;64(7):545-54.

Grosvenor T, Goss DA. Clincial management of myopia. Boston: Butterworth Heinemann; 1999.

Grosvenor T, Scott R. Comparison of refractive components in youth-onset and early adult-onset myopia. Optom Vis Sci 1991;68(3):204-9.

Hahn FJ, Chu WK. Ocular volume measured by CT scans. Neuroradiology 1984;26(6):419-20.

Hass J, Kahle G, Draf W. The topography of the orbit as demonstrated by High-resolution Computed Tomography and multiplanar reconstructions. In: The Orbit and the visual pathway: anatomical and pathological aspects and detailed clinical accounts. Berlin,New York: W. de Gruyter; 1994; 41-49.

Heinz GW, Clunie DA, Mullaney PB. The effect of buphthalmos on orbital growth in early childhood: increased orbital soft tissue volume strongly correlates with increased orbital volume. J Aapos 1998;2(1):39-42.

Hendicott P, Lam C. Myopic crescent, refractive error and axial length in Chinese eyes. Clin Exp Optom 1991;74(5):168-74.

Hintschich C, Zonneveld F, Baldeschi L, Bunce C, Koornneef L. Bony orbital development after early enucleation in humans. Br J Ophthalmol 2001;85(2):205-8.

Ho PCP, Lo PI, Lau JTF. Myopia among Chinese university students-a study of ocular refration and its optical components. In: Chew, S.J., Weintraub, J., eds. Proceedings of the 5th International Conference on Myopia, 1994. Singapore: Myopia International Research Foundation Inc. 1995;75.

Jack CR, Jr., Twomey CK, Zinsmeister AR, et al. Anterior temporal lobes and hippocampal formations: normative volumetric measurements from MR images in young adults. Radiology 1989;172(2):549-54.

Jiang BC, Woessner WM. Vitreous chamber elongation is responsible for myopia development in a young adult. Optom Vis Sci 1996;73(4):231-4.

Johnston GR, Feeney DA. Radiology in ophthalmic diagnosis. Vet Clin North Am Small Anim Pract 1980;10(2):317-37.

Kennedy RE. Effects of enucleation on socket anatomy. Journal of Ophthalmic Prosthetics 1997;243-6.

Kohn MI, Tanna NK, Herman GT, et al. Analysis of brain and cerebrospinal fluid volumes with MR imaging. Part I. Methods, reliability, and validation. Radiology 1991;178(1):115-22.

Lam CS, Edwards M, Millodot M, Goh WS. A 2-year longitudinal study of myopia progression and optical component changes among Hong Kong schoolchildren. Optom Vis Sci 1999;76(6):370-80.

Lam CS, Goh WS, Tang YK, et al. Changes in refractive trends and optical components of Hong Kong Chinese aged over 40 years. Ophthalmic Physiol Opt 1994;14(4):383-8.

Lam CS, Yap M. Ocular dimensions and refraction in Chinese Orientals. Proc Int Soc Eye Res 1990;6:121.

Lam CSY, Goh WSH. The incidence of refractive errors among school children in Hong Kong and its relationship with the optical components. Clin Exp Optom 1991;79:97-103.

Larsen JS. The sagittal growth of the eye. 3. Ultrasonic measurement of the posterior segment (axial length of the vitreous) from birth to puberty. Acta Ophthalmol (Copenh) 1971;49(3):441-53.

Larsen JS. The sagittal growth of the eye. II. Ultrasonic measurement of the axial diameter of the lens and the anterior segment from birth to puberty. Acta Ophthalmol (Copenh) 1971;49(3):427-40.

Lee JW, Chiu HY. Quantitative computed tomography for evaluation of orbital volume change in blow-out fractures. J Formos Med Assoc 1993;92(4):349-55.

Leung JT, Brown B. Progression of myopia in Hong Kong Chinese schoolchildren is slowed by wearing progressive lenses. Optom Vis Sci 1999;76(6):346-54.

Ligier Y, Ratib O, Logean M, Girard C. Osiris: a medical image-manipulation system. MD Comput 1994;11(4):212-8.

Lin LL, Chen CJ, Hung PT, Ko LS. Nation-wide survey of myopia among schoolchildren in Taiwan, 1986. Acta Ophthalmol Suppl 1988;185:29-33.

Lingawi SS. Identification of cranial nerve impingement using 3-dimensional constructive interference in steady state sequence. Journal of Hong Kong College of Radiologist 2003;6:25-27.

Lo AK, Colcleugh RG, Allen L, Van Wyck L, Bite U. The role of tissue expanders in an anophthalmic animal model. Plast Reconstr Surg 1990;86(3):399-408.

Lo LJ, Lin WY, Wong HF, Lu KT, Chen YR. Quantitative measurement on three-dimensional computed tomography: an experimental validation using phantom objects. Changgeng Yi Xue Za Zhi 2000;23(6):354-9.

Lo PI, Ho PC, Lau JT, et al. Relationship between myopia and optical components--a study among Chinese Hong Kong student population. Yan Ke Xue Bao 1996;12(3):121-5.

Lonn L, Starck G, Alpsten M, Ekholm S, Sjostrom L. Determination of tissue volumes. A comparison between CT and MR imaging. Acta Radiol 1999;40(3):314-21.

MacLachlan C, Howland HC. Normal values and standard deviations for pupil diameter and interpupillary distance in subjects aged 1 month to 19 years. Ophthalmic Physiol Opt 2002;22(3):175-82.

Mafee MF, Inoue Y, Mafee RF. Ocular and orbital imaging. Neuroimaging Clin N Am 1996;6(2):291-318.

Mallen EA, Wolffsohn JS, Gilmartin B, Tsujimura S. Clinical evaluation of the Shin-Nippon SRW-5000 autorefractor in adults. Ophthalmic Physiol Opt 2001;21(2):101-7.

Maya MM, Heier LA. Orbital CT. Current use in the MR era. Neuroimaging Clin N Am 1998;8(3):651-83.

McBrien NA, Adams DW. A longitudinal investigation of adult-onset and adult-progression of myopia in an occupational group. Refractive and biometric findings. Invest Ophthalmol Vis Sci 1997;38(2):321-33.

McBrien NA, Millodot M. A biometric investigation of late onset myopic eyes. Acta Ophthalmol (Copenh) 1987;65(4):461-8.

McGurk M, Whitehouse RW, Taylor PM, Swinson B. Orbital volume measured by a low-dose CT scanning technique. Dentomaxillofac Radiol 1992;21(2):70-2.

Moller HU. Milestones and normative data. In: Talyor D, editor. Paediatric Ophthalmolgy. Oxford: Blackwell Science; 1997; 42-56.

Morris R. Strabismus surgery. In: Talyor D, editor. Paediatrics Ophthalmolgy. Oxford: Blackwell Science; 1997; 969-1020.

Nakagawa Y, Fujimoto S, Nakano H, et al. Magnetic resonance velocity mapping of transtricuspid velocity profiles in dilated cardiomyopathy. Heart Vessels 1998;13(5):241-5.

Nelson CC, Cartwright MJ. Orbital diagnosis and imaging. Curr Opin Ophthalmol 1992;3(5):623-31.

Niemczyk K, Vaneecloo FM, Lemaitre L, et al. The growth of acoustic neuromas in volumetric radiologic assessment. Am J Otol 1999;20(2):244-8.

Osborne D, Hadden OB, Deeming LW. Orbital growth after childhood enucleation. Am J Ophthalmol 1974;77(5):756-9.

Osuobeni EP, Faden FK. Interpupillary distance of females of Arab origin. Optom Vis Sci 1993;70(3):244-7.

Parsons GS, Mathog RH. Orbital wall and volume relationships. Arch Otolaryngol Head Neck Surg 1988;114(7):743-7.

Pivnick EK, Rivas ML, Tolley EA, Smith SD, Presbury GJ. Interpupillary distance in a normal black population. Clin Genet 1999;55(3):182-91.

Qin YF, Van Cauteren M, Osteaux M, Willems G. Determination of liver volume in vivo in rats using MRI. Eur J Radiol 1990;11(3):191-5.

Quant JR, Woo GC. Normal values of eye position and head size in Chinese children from Hong Kong. Optom Vis Sci 1993;70(8):668-71.

Ramieri G, Spada MC, Bianchi SD, Berrone S. Dimensions and volumes of the orbit and orbital fat in posttraumatic enophthalmos. Dentomaxillofac Radiol 2000;29(5):302-11.

Ranly DM. Craniofacial growth. Dent Clin North Am 2000;44(3):457-70, v.

Reedy BK, Pan F, Kim WS, Bartlett SP. The direct effect of intraorbital pressure on orbital growth in the anophthalmic piglet. Plast Reconstr Surg 1999;104(3):713-8.

Romans LE. Basic Principles of Computed Tomography. In: Introduction to Computed Tomography. Baltimore: Williams & Wilkins; 1995; 6.

Rootman J. Basic anatomic considerations. In: Rootman J, editor. Diseases of the Orbit. Philadelphia: J.B. Lippincott Company; 1988; 3-17.

Rubin RT, Phillips JJ. Adrenal gland volume determination by computed tomography and magnetic resonance imaging in normal subjects. Invest Radiol 1991;26(5):465-9.

Scheib SG, Gianolini S, Haller D, Wellis GN, Siegfried J. VOLUMESERIES: a software tool for target volume follow-up studies with computerized tomography and magnetic resonance imaging. Technical note. J Neurosurg 2000;93 Suppl 3203-7.

Schuknecht B, Carls F, Valavanis A, Sailer HF. CT assessment of orbital volume in late post-traumatic enophthalmos. Neuroradiology 1996;38(5):470-5.

Seeram E. Physical principles of Computed Tomography. In: Computed tomography : physical principles, clinical applications, and quality control. 2 ed. Philadelphia: W.B. Saunders; 2001; 66.

Sorsby A, Benjamin B, Sheridan M, Stone J, Leary GA. Refraction and its components during the growth of the eye from the age of three. Medical Research Councial Special Report Series 19611-67.

Sorsby A, Leary GA. A longitudinal study of refraction and its components during growth. Spec Rep Ser Med Res Counc (G B) 1969;3091-41.

Thaller VT. Enucleation volume measurement. Ophthal Plast Reconstr Surg 1997;13(1):18-20.

Taylor D, Day S. Disorders of the eye as a whole. In: Talyor D, editor. Paediatric Ophthalmology. 2 ed. Oxford: Blackwell Science; 1997; 205-213.

Tian S, Nishida Y, Isberg B, Lennerstrand G. MRI measurements of normal extraocular muscles and other orbital structures. Graefes Arch Clin Exp Ophthalmol 2000;238(5):393-404.

Waitzman AA, Posnick JC, Armstrong DC, Pron GE. Craniofacial skeletal measurements based on computed tomography: Part II. Normal values and growth trends. Cleft Palate Craniofac J 1992;29(2):118-28.

Weber AL, Sabates NR. Survey of CT and MR imaging of the orbit. Eur J Radiol 1996;22(1):42-52.

Westbrook C. MRI at a glance. Oxford: Blackwell Science;2002

Willi K. Principles of Computed Tomography. In: Computed tomography : fundamentals, system technology, image quality, applications. Munich: MCD Verlag; 2000; 29.

Wilson KT, Sivak JG, Callender MG. Induced refractive anomalies affect chick orbital bone structure. Exp Eye Res 1997;64(5):675-82.

Wojno TH. Orbital trauma and fractures. In: Tenzel RR, editor. Orbit and Oculoplastics: Gower Medical Publishing; 1991; 9.1-9.10.

Wong TY, Foster PJ, Ng TP, et al. Variations in ocular biometry in an adult Chinese population in Singapore: the Tanjong Pagar Survey. Invest Ophthalmol Vis Sci 2001;42(1):73-80.

Woung LC, Ukai K, Tsuchiya K, Ishikawa S. Accommodative adaptation and age of onset of myopia. Ophthalmic Physiol Opt 1993;13(4):366-70.

Yago K, Furuta M. Orbital growth after unilateral enucleation in infancy without an orbital implant. Jpn J Ophthalmol 2001;45(6):648-52.

Yap M, Wu M, Liu ZM, Lee FL, Wang SH. Role of heredity in the genesis of myopia. Ophthalmic Physiol Opt 1993;13(3):316-319.

Zadnik K, Manny RE, Yu JA, Mitchell GL, Cotter SA, Quiralte JC, Shipp MD, Friedman NE, Kleinstein RN, Walker TW, Jones LA, Moeschberger ML, Mutti DO, CLEERE study group. Ocular component data in schoolchildren as a function of age and gender. Optom Vis Sci 2003;80(3):226-36